

## **3.4 Cooperative Phenomena in Complex Macroscopic Systems**

## Super-solidity in 2D Bose Systems

Yoshihiko HIRANO, Yuichi MOTOYAMA, and Naoki KAWASHIMA

*Institute for Solid State Physics,*

*The University of Tokyo, Kashiwa-no-ha, Kashiwa, Chiba 277-8581*

Motivated by recent experiments on the He-4 atoms adsorbed on graphite surfaces, we studied Bosonic models in two dimensions. We considered two models: (i) a simple model (the hard-core Bose gas on a honeycomb lattice with nearest-neighbor repulsion), and (ii) a realistic model (the Bose particles interacting with each other by Aziz potential in the periodic potential mimicking the effect of the graphite substrate). Using the computational resources allocated to the present proposal, we mainly carried out calculations of (i), for which we summarize in the following what we achieved in the project. For calculations of (ii), one of the present authors (Y.M.) writes a separate report.

We considered the hard-core boson system on the honeycomb lattice with the nearest neighbor repulsion and the periodic potential that forms triangular super-lattice. Specifically, the model is described by the following Hamiltonian:

$$H = -t \sum_{\langle ij \rangle} (a_i^\dagger a_j + \text{h.c.}) + V \sum_{\langle ij \rangle} n_i n_j - \mu \sum_i n_i + \sum_i \varepsilon_i n_i. \quad (\varepsilon_i = 0, \varepsilon)$$

This Hamiltonian naturally interpolates between the honeycomb lattice ( $\varepsilon = 0$ ) and the

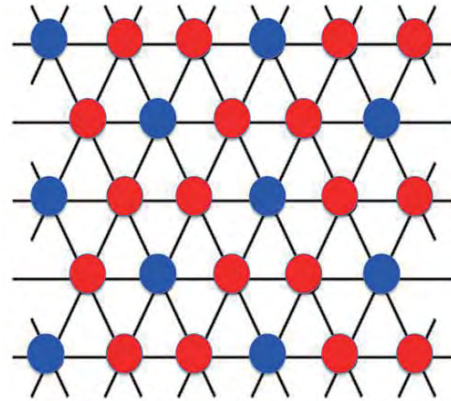


**Fig. 1:** The honeycomb lattice with periodic potential. ( $\varepsilon_i = 0$  on the red sites whereas  $\varepsilon_i = \varepsilon > 0$  on the blue.)

triangular lattice ( $\varepsilon = \infty$ ). In the former case, the model is equivalent to the  $S = 1/2$  ferromagnetic Heisenberg model showing with uniform magnetic field and show only uniformly ordered states.

For the computation, we used our own code based on DSQSS, the program package based on the worm algorithm for the world-line quantum Monte Carlo simulation. The package is an open-source software, available through GitHub under the GPU license.

For the present model, we computed three quantities: the density, the

superfluid density and the static structure factor, as functions of the chemical potential. In these calculations, we fixed the value of  $t/V$  as  $t/V = 0.1$ , and varied  $\varepsilon/V$  as  $\varepsilon/V = 0.0, 0.1, 0.2, 0.5$  and  $1.0$ .

Our calculation revealed the following. Near  $\mu/V = 3$ , and at all values of  $\varepsilon/V$ , the system is in the super fluid phase where the super current is carried by particles that mainly reside easy sites (red sites in Fig.1). Increase in the chemical potential brings the system into the  $2/3$ -filling incompressible solid state through a second order phase transition. In this solid state, nearly all easy sites are occupied and red ones are mostly empty. The superfluid density is

negligibly small. Further increase of the chemical potential does not change the system until it reaches a discontinuous phase transition to the second superfluid phase. This phase persists up to the final phase transition to the fully occupied state.

Our results are still in the preliminary stage, and will need further investigation before we report our results in full details. However, our aim is to systematically modify the discrete lattice model to closer proximity to the realistic model for the helium-on-graphite system that is defined in continuous space, thereby obtaining information complementary to the continuous space simulation.

# Novel phases in frustrated spin systems

Tsuyoshi OKUBO

*Institute for Solid State Physics, University of Tokyo  
Kashiwa-no-ha, Kashiwa, Chiba 277-8581*

The kagome lattice Heisenberg antiferromagnet is a typical example of the two-dimensional frustrated spin systems. Due to strong quantum fluctuations, the ground state of the  $S = 1/2$  quantum spin kagome lattice Heisenberg model is expected to be a spin-liquid state without any magnetic long-range orders. Under magnetic fields, it has been proposed that several magnetization plateaus at  $1/9, 1/3, 5/9$ , and  $7/9$  of the saturation magnetization appear in the magnetization curve based on a density matrix renormalization group (DMRG) calculation [1]. Recently, a tensor network calculation has also shown the existence of these magnetization plateaus [2]. On the other hand, based on the exact diagonalization (ED) up to 42 sites, Nakano and Sakai proposed that the expected  $1/3$  plateau has peculiar critical exponents compared to other two-dimensional systems such as the triangular lattice Heisenberg antiferromagnets [3, 4].

In this year project, we have investigated the ground state properties of  $S = 1/2$  kagome lattice Heisenberg antiferromagnet under external magnetic fields using a infinite Projected Entangled Pair State (iPEPS) tensor network method. In this iPEPS method, we represent the ground state wave-function as the two-dimensional network of tensors (Fig. 1). By optimizing each tensor so as to minimize the energy, we obtained wave-functions close to the ground state under magnetic fields. The magnetization curve obtained by iPEPS contains clear  $1/9, 1/3, 5/9$  and  $7/9$  plateaus that are consistent with the previous calculations. We

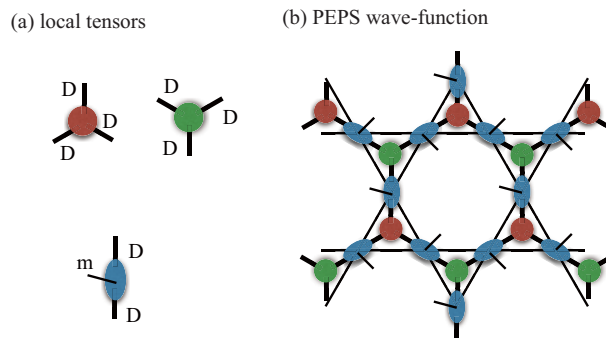


Figure 1: Tensor network representation of the ground state wave-function for the kagome lattice Heisenberg antiferromagnet.

also investigated effects of the Dzyaloshinskii-Moriya (DM) interaction, which exists in real kagome lattice compounds. Our calculation shows that the plateau width becomes smaller when we increase the amplitude of the DM interaction and the plateaus disappear for  $D_z/J \gtrsim 0.1$ .

## References

- [1] S. Nishimoto, N. Shibata, and C. Hotta, *Nat. Commun.* **4**, 2287 (2013).
- [2] T. Picot, M. Ziegler, R. Orus, and D. Poilblanc, arXiv:1508.07189.
- [3] H. Nakano and T. Sakai, *J.Phys.Soc.Jpn.* **79**, 053707 (2010).
- [4] H. Nakano and T. Sakai, *J.Phys.Soc.Jpn.* **83**, 104710 (2014).

# Structure formation of biomembranes

Koh M. NAKAGAWA<sup>a</sup>, Hayato SHIBA<sup>a,b</sup>, J.-B. FOURNIER<sup>c</sup>, and Hiroshi NOGUCHI<sup>a</sup>

<sup>a</sup> *Institute for Solid State Physics, University of Tokyo, Kashiwa, Chiba 277-8581*

<sup>b</sup> *Institute for Materials Research, Tohoku University 2-1-1 Sendai 980-8577*

<sup>c</sup> *Laboratoire Matière et Systèmes Complexes (MSC), UMR 7057 CNRS, Université Paris, Diderot, F-75205, Paris, France*

We have studied the following three phenomena using ISSP super computer this year.

## 1 Vesicle dynamics induced by chemical reaction

Some softmatter systems exhibit various shape transformations induced by chemical reactions, for example, self-beating gel, self-reproducing vesicle, and cell-division. Recently we studied shape transformations of an oil droplet induced by dehydrocondensation reaction using dissipative particle dynamics simulations [1]. Various types of shape transformations are found such as a spherical oil to a tubular vesicle and toroidal vesicle. Multiple daughter vesicles generation from the oil droplet is found during the shape transformation, and this process is also found in the experimental observations.

To investigate chemical-reaction-induced shape transformations further, we examine shape transformations of vesicle induced by hydrolysis reaction. The hydrolysis reaction are modeled as a stochastic process. A forward chemical reaction (bond breaking) and inverse chemical reaction (bond binding) are included in this chemical reaction model. Hydrolysis reaction changes the number difference of amphiphile molecules between two monolayers of the vesicle, resulting in various shape transformations such as budding and bilayer protrusion into inside of the vesicle (Fig. 1 (a) bilayer protrusions and (b) budding). We also found that these shape transformation pathways strongly depend on a spatial inhomogeneity of reaction products and stress relaxation time scale, which depends on the bilayer elastic

modulus and solvent shear viscosity.

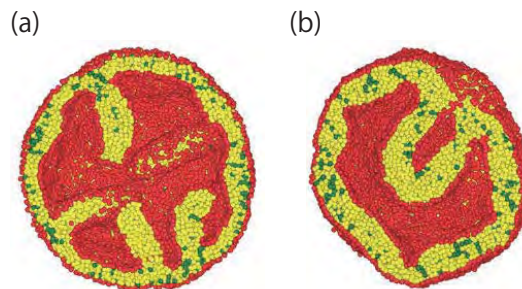


Figure 1: Two snapshots of typical shape transformations. (a) bilayer protrusions and (b) budding.

## 2 Relation between three membrane surface tensions

Three types of the surface tensions can be defined for lipid membranes: internal tension  $\sigma$  conjugated to real membrane area, mechanical frame tension  $\tau$  conjugated to the projected area, and “fluctuation tension”,  $r$ , obtained from the fluctuation spectrum of the membrane height. We studied the relation of these surface tensions using the Monte-Carlo simulation technique for a lattice membrane defined by a Monge gauge, where the membrane surface is described as a function of height [2]. It involves the exact, nonlinear, Helfrich Hamiltonian and a measure correction for excess entropy of the Monge gauge.

Our results for the relation between  $\sigma$  and  $\tau$  corresponds very well to the previous theoretical prediction based on a Gaussian approximation. The fluctuation tension  $r$  coin-

sides with the frame tension with an accuracy of our simulation. We checked that our conclusions are valid for an different ensemble in which the membrane area is controlled.

### 3 Shape transformation induced by banana-shaped proteins

In living cells, membrane morphology is regulated by various proteins. Many membrane reshaping proteins contain a Bin/Amphiphysin/Rvs (BAR) domain, which consists of a banana-shaped rod. The BAR domain bends the biomembrane along the rod axis and the features of this anisotropic bending have recently been studied. We study as to how such a local anisotropic curvature induces effective interaction between proteins and changes the global shape of vesicles and membrane tubes using meshless membrane simulations. The proteins are modeled as banana-shaped rods strongly adhered to the membrane.

As reported last year, the rod assembly occurs separately in parallel and perpendicular directions with coupled membrane shape deformation at low rod density. This year, we revealed that polyhedral vesicles and polygonal tubes are stabilized at high rod densities [3]. The discrete shape transition between triangular and buckled discoidal tubes and between polyhedral shapes are obtained. As line tension of the membrane edge is reduced, the protein adhesion induces membrane rupture leading to high-genus vesicle formation and vesicle inversion [4]. These shape transformations and assemblies are not obtained by isotropic inclusions.

We also studied the effects of the spontaneous (side) curvature perpendicular to the rod, which can be generated by protein-protein and membrane-protein interactions [5]. We revealed that the perpendicular curvature can drastically alter the tubulation dynamics from a flat membrane at high protein density whereas no significant difference is obtained at low density. A percolated network is intermediately formed depending on the perpen-

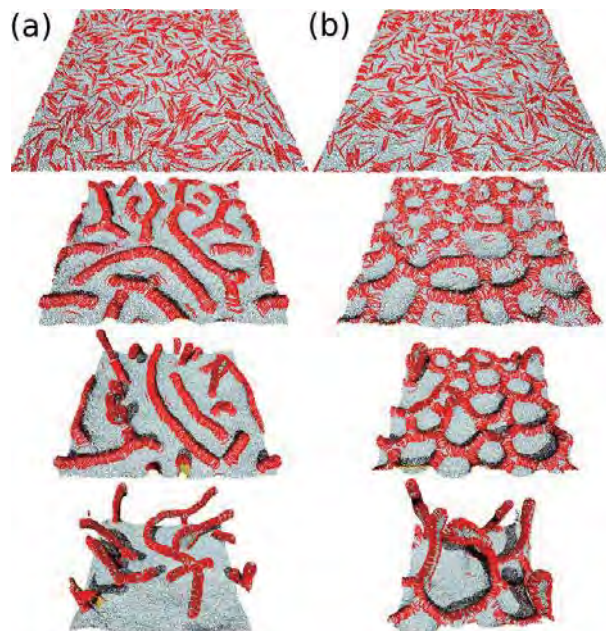


Figure 2: Sequential snapshots of tabulation from a flat membrane induced by protein rods. (a) Positive perpendicular rod curvature. (b) Negative perpendicular rod curvature.

dicular curvature (see Fig.2). This network suppresses tubule protrusion. The stability of network structures can be explained by a simple geometric model. Positive surface tensions and the vesicle membrane curvature can stabilize this network structure by suppressing the tubulation. It is known that tubulation dynamics can be different even for proteins consisting of the same BAR domains. Our finding suggests that the interactions between the rest parts of the proteins can give significant effects.

### References

- [1] K. M. Nakagawa and H. Noguchi: *Soft Matter* **11**, 1403 (2015).
- [2] H. Shiba, H. Noguchi, and J.-B. Fournier: *Soft Matter* **12**, 2373 (2016).
- [3] Noguchi: *J. Chem. Phys.* **143**, 243109 (2015).
- [4] Noguchi: *Phys. Rev. E* **93**, 052404 (2016).
- [5] Noguchi: *Sci. Rep.* **6**, 20935 (2016).

# Dynamical properties and thermal properties of Kitaev-Heisenberg models on a honeycomb lattice

Takafumi SUZUKI

*Graduate school of Engineering,*

*University of Hyogo, Shosha 2167, Himeji, Hyogo 670-2520*

In this project, we studied dynamical properties and thermal properties of Kitaev-Heisenberg models on a honeycomb lattice.

Magnetic properties of 4d and 5d transition metal compounds have attracted much attention in condensed matter physics. In some materials, the energy scales of spin-orbit interactions, on-site coulomb interactions, and crystal fields compete with each other and such competition can produce an interesting phase, namely the Kitaev's spin liquid.  $\text{Na}_2\text{IrO}_3$ , for instance, is considered as a candidate for realization of the Kitaev's spin liquid. In  $\text{Na}_2\text{IrO}_3$ , each  $\text{Ir}^{4+}$  ion constituting the honeycomb-lattice network carries a total angular momentum  $J_{\text{eff}} = 1/2$ . Since  $\text{IrO}_6$  octahedrons are connected by sharing the oxygen atoms on the edges making the Ir-O-Ir bond angle nearly  $90^\circ$ , three kinds of anisotropic interactions are expected between the transition metal ions depending on the bonding direction. Thus, considering the direct interactions via overlap of 5d orbitals,  $\text{Na}_2\text{IrO}_3$  is expected to be described by the Kitaev-Heisenberg model [1] on the honeycomb lattice.

$\text{Na}_2\text{IrO}_3$  shows an antiferromagnetic zigzag order below  $T_N \sim 15$  [K]. In a typical Kitaev-

Heisenberg model, where ferromagnetic Kitaev and antiferromagnetic Heisenberg interactions are summed for nearest neighbor pairs, the zigzag order is not stabilized. Thus, several magnetic effective models have been proposed to explain the zigzag order.

In order to discuss the proper model for  $\text{Na}_2\text{IrO}_3$ , we evaluated the dynamical properties of five models proposed in Refs. [2-6]. By using exact diagonalization method, we calculated dynamical structure factor (DSF) up to  $N=32$  site cluster. First, we compared the numerical results for the candidate models [2-6] and the inelastic neutron scattering results [2]. We found that the model proposed in the Ref. [5] can explain the experimental results well. Next, we calculated the linearized spin-wave dispersion to discuss the characteristics of the low-lying magnetic excitations. The obtained results indicated that the spin-wave excitations in the magnetic ordered phases fail to explain the low-lying excitations of the DSFs, when the system is located in the vicinity of the Kitaev's spin liquid phase. In contrast, if the system is placed in the depth of the magnetic ordered phase, the low-lying excitation can be

successfully explained by the spin-wave excitation. We also studied the temperature dependence of the specific heat. If the system is located in the vicinity of the Kitaev's spin liquid phase, where the spin-wave picture for the low-lying magnetic excitations is broken down, we observe a clear two-peak structure in the temperature dependence of the specific heat that is also observed in the Kitaev's spin liquid phase. The origin of the two-peak structure in the specific heat is associated with the fractionalization of quantum spins, emergence of two Majorana fermions. Therefore, the obtained result implies that the two-peak structure of the specific heat becomes a good indicator for the closeness to the Kitaev's spin liquid phase [8].

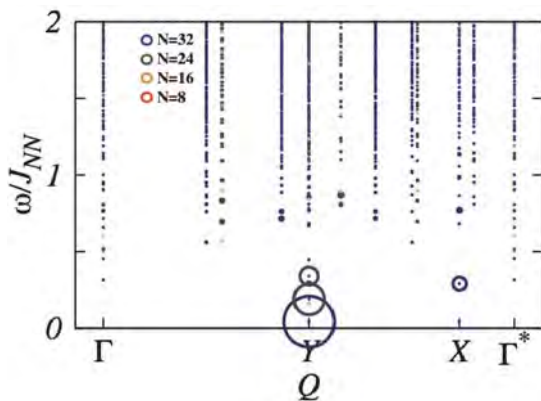


Fig 1. Dynamical structure factor of the effective model for  $\text{Na}_2\text{IrO}_3$

proposed in Ref. [5]. Area of circles corresponds to the scattering intensity.  $J_{\text{NN}}$  the nearest-neighbor Heisenberg interaction and  $J_{\text{NN}} \sim 4.17$  [meV].

## References

- [1] G. Jackeli and G. Khaliullin, Phys. Rev. Lett. **102**, 017205 (2009).
- [2] S. K. Choi, R. Coldea, A. N. Kolomojorov, T. Lancaster, I. I. Mazin, S. J. Blundell, P. G. Radealli, Y. Singh, P. Gegenwart, K. R. Choi, et al., Phys. Rev. Lett. **108**, 127204 (2012).
- [3] J. Chaloupka, G. Jackeli, and G. Khaliullin, Phys. Rev. Lett. **110**, 097204 (2013).
- [4] V. M. Katukuri, S. Nishimoto, V. Yushankhai, A. Stroyanova, H. Kandpal, S. Choi, R. Coldea, I. Rousochatzakis, L. Hozoi, and J. van den Brink, New J. Phys. **16**, 013056 (2014).
- [5] Y. Yamaji, Y. Nomura, M. Kurita, R. Arita, and M. Imada, Phys. Rev. Lett. **113**, 107201 (2014).
- [6] Y. Sizyuk, C. Price, P. Wolfe, and N. B. Perkins, Phys. Rev. B **90**, 155126 (2014).
- [7] T. Suzuki, Y. Takuto, Y. Yamaji, and S. Suga, Phys. Rev. B **92**, 184411 (2015).
- [8] Y. Yamaji, T. Suzuki, Y. Yamada, S. Suga, N. Kawashima, and M. Imada, arXiv:1601.

# Development of Quantum Monte Carlo Algorithm and Application to Hardcore Bose System

Akiko Masaki-Kato

*Riken,*

*Hirosawa, Wako, Saitama 351-0105*

The worm algorithm for quantum Monte Carlo methods based on the Feynman's path integral is capable of global updates of the worldline configuration and has a broader range of applicability for quantum lattice model without the negative sign problem. However parallelization of the worm algorithm is nontrivial because of the event-driven process of updates by single moving-worm. We have developed the parallelized multi-worm algorithm (PMWA) and, in last year, we presented the numerical recipe of this algorithm which is described to be applicable for general quantum lattice model in Ref. [1]. PMWA is implemented on the directed loop algorithm (DLA) [2], a kind of the worm algorithm. In PMWA we execute to measure physical quantities in configuration space including many worms introduced by the additional source field to the Hamiltonian. After the simulation, we extrapolate the source field to 0 to obtain values without the source field.

This year, we developed the method of measuring various physical quantities, especially G-sector measurement i.e. off-diagonal quantities. Besides we investigated extrapolation rules of the various quantities. To

give practical arguments, we focus on hardcore boson model. We first determined the 3D phase diagram of the ground state of this model under the source field (Fig.1) in order to make use of extrapolation. This phase diagram can be mapped to  $S=1/2$  spin model under the both transvers and longitudinal field as shown in Fig. 1. We accurately explored the phase boundary by finite size scaling with the different system size up to  $L=576$  and the inverse temperature  $\beta = L/2$ . To calculate large size we impose the nontrivial parallelization with domain decomposition of the configuration space and the trivial parallelization to calculate statistical error with 1728 cores of F144 queue. Then we measure the various quantities of hardcore boson with/without random potential. We find that integrated quantities, e.g. the compressibility and the xx-susceptibility, rapidly change by small source field, therefore it is difficult to extrapolate. To improve this problem we use the modified definition of these quantities. The modified quantities coincide the original quantities at 0 limit of the source field and change relatively slow for the source field[3].

Moreover, this year, we have opened our

source codes on a github repository[4] as an application named “DSQSS” which consist of not only DLA for serial or trivial-parallel simulations but also PMWA for nontrivial parallel simulation. We prepare the manual and tutorial for calculating Heisenberg models. For a future work we are planning to unify the DLA code and the PMWA cod and provide various tutorials.

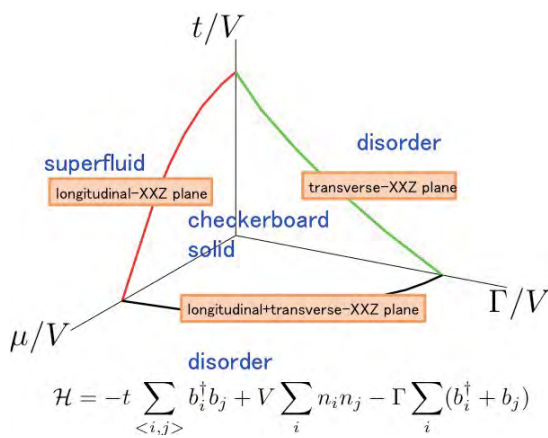


Fig. 1: The phase diagram of the ground state of

the hardcore boson.

## References

- [1] A. Masaki-Kato, T. Suzuki, K. Harada, S. Todo, N. Kawashima, Phys. Rev. Lett., 112, 140603 (2014).
- [3] A. Masaki-Kato and N. Kawashima, in preparation.
- [4] <https://github.com/qmc/dsqss/wiki>.

# Equilibrium and dynamical properties in glassy systems

Koji HUKUSHIMA

*Department of Basic Science, University of Tokyo  
3-8-1 Komaba, Meguro-ku, Tokyo 153-8902*

Frustration is a key concept in condensed matter physics. In particular, the frustration in classical magnetism caused by competing interactions provides us novel critical and ordering phenomena such as re-entrant transition. In many-particle systems, a competition between local-packing patterns and global crystallization can lead to frustration. Such frustration plays also an important role in structural glass transition.

In this project, we studied an effect of geometrical constraints in a lattice glass model. More specifically, hard rigid rods with  $k$  successive occupied sites are put on a three-dimensional lattice. This system has no interaction except for hard-core repulsion and a possible phase transition is entropy driven. This rigid-rods system in two dimensions has been studied by Ghosh and Dhar. They found that an orientational long range order occurs at finite mean coverage of rods in the system for  $k \geq 7$ . The transition of the orientational transition is of second order and its universality class depending on the lattice structure belongs to two-dimensional Ising model for a square lattice. In our work, we use the exchange MC method for accelerating equilibrium process, which allows us to achieve equilibration of the system for large sizes. It is found that, in contrast to the two dimensions, the system even with  $k = 6$  in a simple cubic lattice exhibits the second-order orientational phase transition. No explicit interaction between any two layers is there in the system. Therefore, the order-parameter distribution has a different structure between the systems with  $k = 6$  and  $k \geq 7$ . However, finite-size scaling analysis reveals that the systems share a common universality class, independent of the value of  $k$ , which belongs to three-dimensional three-state

antiferromagnetic Potts model.

Another topic is a development of Markov-chain Monte Carlo (MCMC) algorithms. Some simple algorithms with local updates including the original Metropolis algorithm frequently suffer from difficulties of slow relaxation. The cluster algorithms are one of the promising ways for overcoming the slow relaxation, but unfortunately they do not work in frustrated spin systems. Recently, another type of algorithms has attracted great interests, which does not rely on the detailed balance condition. The event-chain Monte Carlo (ECMC) algorithm is one of such algorithms breaking the detailed balance condition. ECMC is proposed originally for hard-sphere systems and is subsequently generalized for more general particle systems such as soft-sphere and Lennard–Jones particles and continuous spin systems such as  $XY$  and Heisenberg spin models[1]. We applied ECMC to a Heisenberg ferromagnetic model in three dimensions and found that it enables to reduce the dynamical exponent from a conventional value  $z = 2$ [1]. Furthermore, using a large scale simulation with ECMC, phase transitions in a Heisenberg spin model of a chiral helimagnet with the Dzyaloshinskii–Moriya interaction in three dimensions are studied. In the presence of a magnetic field perpendicular to the axis of the helical structure, it is found that there exists a critical point on the temperature and magnetic-field phase diagram and that above the critical point the system exhibits a phase transition with strong divergence of the specific heat and the uniform magnetic susceptibility[2].

[1] Y. Nishikawa, M. Michel, W. Krauth, K. Hukushima: Phys. Rev. E **92**, 063306 (2015).

[2] Y Nishikawa, K Hukushima: arXiv preprint arXiv:1603.04200

# Entanglement and Quantum Phase Transition in Quantum Spin Systems

Synge Todo

*Department of Physics, University of Tokyo, Tokyo 113-0033, Japan*

*Institute for Solid State Physics, University of Tokyo, Kashiwa, 277-8581, Japan*

Quantum phase transitions are phase transitions between two different ground states that are triggered by quantum fluctuations at absolute zero temperature. We develop various novel and powerful techniques to tackle various exotic quantum critical phenomena observed in quantum spin systems and performed large-scale and high-precision simulations on the ISSP supercomputer system.

**Critical Phenomena of quantum systems with strong spatial and temporal anisotropy:** we have developed a generic method that can automatically optimize the aspect ratio of the system by the combination of the quantum Monte Carlo method and the machine learning technique, and applied to the two-dimensional Bose-Hubbard model with dynamical exponent  $z > 1$  [1]. We also extended our method to systems with quenched randomness and studied the dynamical property of the Superfluid-Bose-Glass transition.

**Analysis of quantum phases and quantum phase transitions by local  $Z_N$  Berry phase:** we have developed a new quantum Monte Carlo technique for calculating the overlap of two wave functions (including phase factor), and applied it to the local  $Z_N$  Berry phase that is a topological order parameter for low-dimensional quantum magnets.

**Critical phenomena of long-range interacting spin model:** using the  $O(N)$  cluster algorithm, we have precisely studied the critical exponents and critical amplitudes of

the long-range interacting spin model on the square lattice, and established the non-trivial dependence of the critical exponents on the exponent of interaction  $\sigma$ .

**QMC level spectroscopy:** It is hard to estimate the gap precisely in the quantum Monte Carlo simulations because it is not simply expressed by an average with respect to the Boltzmann distribution. We devised an unbiased and reliable gap-estimation method in the worldline quantum Monte Carlo simulations [2]. It was shown that the criticality of the spin-phonon model is described by the Wess-Zumino-Witten model and the quantum nature of the lattice degrees of freedom is essential to the one-dimensional quantum spin or spinless fermion systems.

The programs used in the present research projects have been developed based on the open-source libraries: ALPS [3], ALPS/looper [4], BCL [5], worms [6], etc.

## References

- [1] S. Yasuda, H. Suwa, and S. Todo: Phys. Rev. B **92** (2015) 104411.
- [2] H. Suwa and S. Todo: Phys. Rev. Lett. **115** (2015) 080601.
- [3] <http://alps.comp-phys.org/>.
- [4] <http://wistaria.comp-phys.org/alps-looper/>.
- [5] <http://github.com/cmsi/bcl>.
- [6] <http://github.com/wistaria/worms>.

# Estimation of spin-spin interactions from magnetization process by Bayesian inference

Ryo TAMURA

*Computational Materials Science Unit, National Institute for Materials Science,  
1-1 Namiki, Tsukuba, Ibaraki, 305-0044*

The importance of data-driven technique using the machine learning has been well recognized in both academic and industrial fields. By using the machine learning, we can estimate an appropriate governing equation by finite observable data sets. In the condensed matter physics, the machine learning techniques have been used for such as interpolating Density Functional Theory (DFT)[1] and Dynamical Mean-Field Theory (DMFT)[2] calculations, and for model selection of strongly correlated systems[3] and the Ginzburg-Landau equation[4].

We developed a method for estimating spin-spin interactions in the Hamiltonian from a given magnetization process by the machine learning based on the Bayesian statistics[5]. In the estimation method, plausible spin-spin interactions that explain the given magnetization process are determined by maximizing the posterior distribution. It is obtained as the conditional probability of the spin-spin interactions for a given magnetization process with observation noise.

The efficiency of the estimation method was tested for a case of synthetic magnetization process data obtained by the classical Heisenberg model. In this research, we used the Markov chain Monte Carlo (MC) method and the exchange MC method to analyze the posterior distribution. The combination of Markov chain MC and exchange MC methods makes a significant contribution to finding the global maximum of the posterior distribution in sys-

tems where many local maxima exist. Results showed that the developed estimation method enables estimation of the spin-spin interactions with high accuracy and, in particular, the relevant terms of the spin-spin interactions are successfully selected from among redundant interaction candidates by using  $l_1$  regularization in the prior distribution:

$$P(\mathbf{x}) \propto \exp\left(-\lambda \sum_{k=1}^K |x_k|\right), \quad (1)$$

where  $\{x_k\}$  denotes the set of spin-spin interactions and  $K$  is the number of spin-spin interactions we consider. The inference scheme using the prior distribution is called Least Absolute Shrinkage and Selection Operator (LASSO)[6] and the value of  $\lambda$  controls the strength of regularization. We would like to emphasize that the framework of our estimation method can be used not only for magnetization processes but also for any measured data as the input data.

This work was done in collaboration with Koji Hukushima (The University of Tokyo).

## References

- [1] Z. Li, J. R. Kermode, and A. D. Vita, Phys. Rev. Lett. **114** (2015) 096405.
- [2] L.-F. Arsenault, A. Lopez-Bezanilla, O. A. Lilienfeld, and A. J. Millis: Phys. Rev. B **90** (2014) 155136.

- [3] H. Takenaka, K. Nagata, T. Mizokawa, and M. Okada: J. Phys. Soc. Jpn. **83** (2014) 124706.
- [4] S. Taverniers, T. S. Haut, K. Barros, F. J. Alexander, and T. Lookman: Phys. Rev. E **92** (2015) 053301.
- [5] R. Tamura and K. Hukushima: in preparation.
- [6] R. Tibshirani: J. Royal. Statist. Soc. B. **58** (1996) 267.

# Impurity effect on magnetocaloric effect in Gadolinium alloy

Ryo TAMURA

*Computational Materials Science Unit, National Institute for Materials Science,  
1-1 Namiki, Tsukuba, Ibaraki, 305-0044*

Cooling phenomena are widely used in everyday applications, such as food storage and medical treatment, and also in technology for next-generation electronics, such as hydrogen-fuel cells and quantum information processing. Thus, high-performance cooling technology has been actively developed for many fields. Magnetic refrigeration is a promising candidate for next-generation cooling technology that can solve environmental and noise problems. The key to the magnetic refrigeration is the change of magnetic entropy in magnetic materials under different magnetic fields, which is known as the magnetocaloric effect [1, 2, 3].

The Active Magnetic Regeneration Refrigeration (AMRR) cycle is a typical cycle to perform magnetic refrigeration. In this cycle, the multiple magnetic materials are used. In each magnetic material, the temperature exhibiting the maximum magnetic entropy change is different. Then, to change the temperature at which the magnetic entropy change becomes maximum is important for practical applications of magnetic refrigeration with various temperature range. In order to control this temperature, the impurity effect has been often considered. In general, the maximum magnetic entropy change is realized around the phase transition temperature in each magnetic material. Thus, using the impurity effect, the phase transition temperature can be changed. We studied the impurity effect on the magnetocaloric effect for the Gadolinium alloy [4].

Gadolinium alloy is a ferromagnetic material with the Curie temperature which is around the room temperature and is a typical magnetocaloric material. In order to clarify the impurity effect in Gadolinium alloy, we considered that some of the Gd ions are substituted for non-magnetic ions. By using Monte Carlo simulations, we calculated, depending on the concentration of non-magnetic ions, specific heat and magnetic entropy change of the  $S = 7/2$  Ising model as an effective model of Gadolinium alloys. The obtained results were compared with experimental results in the Gd-R alloy (R = Y, Zr). The results showed that the Curie temperature linearly decreases with the concentration of non-magnetic ions in the effective model, which was observed in the Gd-R alloy.

This work was done in collaboration with R. Arai (Chiba University), H. Fukuda (Chiba University), J. Li (Chiba University), A. T. Saito (Toshiba Corporation), S. Kaji (Toshiba Corporation), H. Nakagome (Chiba University), and T. Numazawa (NIMS).

## References

- [1] R. Tamura, T. Ohno, and H. Kitazawa: *Appl. Phys. Lett.* **104** (2014) 052415.
- [2] R. Tamura, S. Tanaka, T. Ohno, and H. Kitazawa: *J. Appl. Phys.* **116** (2014) 053908.

- [3] S. Toyozumi, H. Kitazawa, Y. Kawamura, H. Mamiya, N. Terada, R. Tamura, A. Dönni, K. Morita, and A. Tamaki: *J. Appl. Phys.* **117** (2015) 17D101.
  
- [4] R. Arai, R. Tamura, H. Fukuda, J. Li, A. T. Saito, S. Kaji, H. Nakagome, and T. Numazawa: *IOP Conf. Ser.: Materials Science and Engineering* **101** (2015) 012118.

## Randomness-induced quantum spin-liquid behaviors in the frustrated spin-1/2 Heisenberg antiferromagnets on two-dimensional lattices

Hikaru Kawamura, Kazuki Uematsu and Tokuro Shimokawa

*Graduate School of Science, Osaka University, Toyonaka 560-0043*

The quantum spin-liquid (QSL) state possibly realized in certain  $S=1/2$  frustrated magnets has attracted interest of researchers. After a long experimental quest, several candidate materials were recently reported in certain geometrically frustrated magnets, including both the triangular-lattice and the kagome-lattice antiferromagnets (AFs).

In our 2013 and 2014's project, with examples of triangular-lattice  $S=1/2$  organic salts such as  $\kappa$ -(ET)<sub>2</sub>Cu<sub>2</sub>(CN)<sub>3</sub> and EtMe<sub>3</sub>Sb[Pd(dmit)<sub>2</sub>]<sub>2</sub> and the kagome-lattice AF herbertsmithite CuZn<sub>3</sub>(OH)<sub>6</sub>Cl<sub>2</sub> in mind, we investigated the properties of the bond-random  $S=1/2$  AF Heisenberg model on the triangular and the kagome lattices by means of an exact diagonalization (ED) method. The Hamiltonian is given by  $\sum_{\langle ij \rangle} J_{ij} S_i S_j$  where the nearest-neighbor exchange coupling  $J_{ij}$  is assumed to obey the bond-independent uniform distribution between  $[(1-\Delta)J, (1+\Delta)J]$  with the mean  $J$ . The parameter  $\Delta$  represents the extent of the randomness.

We then found that the model exhibited a randomness-induced gapless QSL behavior at low temperatures [1,2]. This "random singlet"

state explains many of the experimental features observed in the triangular organic salts and the kagome herbertsmithite.

In this year's project, we extend these calculations for the AF bond-random  $S=1/2$  Heisenberg models in three directions. First, in order to get further detailed information on the nature of spin correlations in the random-singlet state, we newly compute static and dynamical spin structure factors  $S(q)$  and  $S(q, \omega)$  by the ED method both for the triangular and the kagome models [3]. As an example, we show in Fig.1 the computed static spin structure factor  $S(q)$  of the random kagome-lattice model of  $\Delta=1$ .

Second, we newly computed several finite-temperature properties of both the random triangular and kagome models by means of the TPQ (thermal pure quantum state) method for lattices considerably larger than those obtained by the standard ED method. The obtained new data have confirmed and strengthened our earlier conclusions about the gapless nature of the random-singlet state, including the  $T$ -linear low- $T$  specific heat and the gapless behavior of the susceptibility with a Curie tail, also

revealing some new features [4].

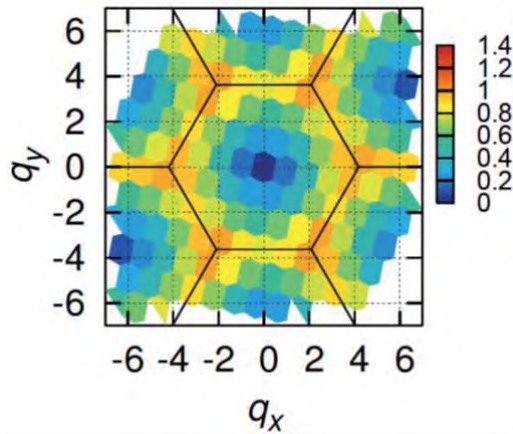


Fig. 1: The ground-state spin structure factor  $S(q)$  in the  $(q_x, q_y)$  plane in the random singlet state of the random kagome model with  $\Delta=1$ . The system size is  $N=30$ .

Third, in order to get a wider view on the generality of the random-singlet state, and especially, to understand how frustration and randomness cooperate to realize the phase, we also studied the properties of the  $S=1/2$  random Heisenberg model on the *honeycomb lattice* with the next-nearest-neighbor interaction ( $J_1$ - $J_2$  model) in comparison with those of the triangular and the kagome lattices [5]. Honeycomb lattice might be interesting because of its potential to sustain enhanced fluctuations originating from the weak connectivity of the lattice (small number of nearest neighbors,  $z=3$ ). We draw a  $T=0$  phase

diagram in the plane of frustration ( $J_2$ ) and randomness ( $\Delta$ ) plane by means of the ED method, and the result is shown in Fig.2. One sees that the random-singlet phase appears in a wide region of the phase diagram.

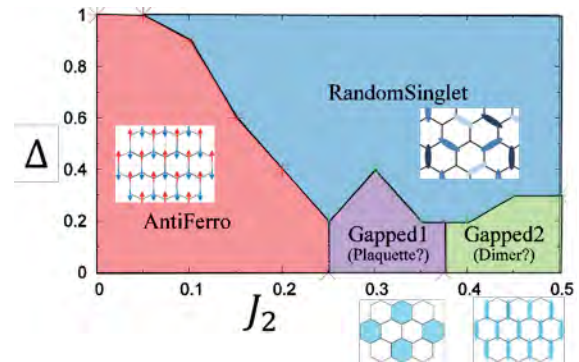


Fig. 2: The ground-state phase diagram of the  $J_1$ - $J_2$  random kagome model in the frustration ( $J_2$ ) vs. randomness ( $\Delta$ ) plane.

- [1] K. Watanabe, H. Kawamura, H. Nakano and T. Sakai, J. Phys. Soc. Jpn. **83**, 034714 (2014).
- [2] H. Kawamura, K. Watanabe, and T. Shimokawa, J. Phys. Soc. Jpn. **83**, 103704 (2014)
- [3] T. Shimokawa and H. Kawamura, Phys. Rev. B **92**, 134407 (2015).
- [4] T. Shimokawa and H. Kawamura, in preparation.
- [5] K. Uematsu and H. Kawamura, in preparation.

# Effects of inhomogeneity in the one-dimensional Burridge-Knopoff model of earthquakes

Hikaru Kawamura and Jun Akutagawa

Graduate School of Science, Osaka University, Toyonaka, Osaka 560-0043

An earthquake is a stick-slip dynamical instability of a pre-existing fault driven by the motion of a tectonic plate. Numerical simulations of earthquakes based on a simplified statistical model, the so-called Burridge-Knopoff (BK) model, has been popular in statistical physics and provided much information about statistical properties of earthquakes. Some of the properties of the BK model was reviewed in Ref.[1].

Earthquake, not doubt, is quite a complex phenomenon. One fundamental question is where its complexity is originated from. In one view, complexity of earthquakes is originated from the complexity or the heterogeneity of the fault, including the complexity of material properties such as the elastic and the frictional properties, or the complexity of the shape and geometry of the fault, *etc.* In the other view, the apparent complexity of earthquakes is self-generated even from simple uniform parameters via its nonlinear dynamics. It would be very important to understand which of these two contrasting views is appropriate or dominant in real earthquakes. In this year's project, we take the first step toward the understanding of the role of inhomogeneity in

earthquake occurrence.

The model studied is the one-dimensional BK model under the rate-and-state friction law, where the step-type inhomogeneity is assumed in the frictional parameter  $b$ , i.e., the  $b$  parameter in the left half is taken smaller than that in the right half,  $b_{left} < b_{right}$ . In Fig.1, we show the probability that a given block becoming an epicenter for each type of events including 1) small events, 2) large unilateral events propagating left, 3) those propagating right, and 4) large events propagating to both sides. One sees that seismicity here is quite anisotropic.

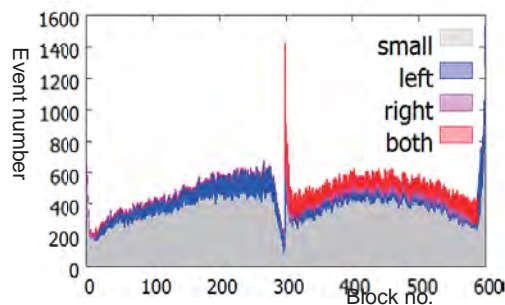


Fig.1 The number of events plotted versus the epicenter-block number of the event.

## References

- [1] For review, see, H. Kawamura, T. Hatano, N. Kato, S. Biswas and B.K. Chakrabarti, *Rev. Mod. Phys.* 84, 839-884 (2012).

# Entanglement in A Solvable Quantum System

## – A Generalized Cluster-Ising Model –

Shu TANAKA

*Waseda Institute for Advanced Study, Waseda University  
1-6-1, Nishi-Waseda, Shinjuku-ku, Tokyo, 169-8050 Japan*

Entanglement is an important concept in quantum information science, statistical physics, and condensed matter physics. Entanglement can be quantified by the entanglement entropy and entanglement spectrum. The entanglement entropy is obtained by the reduced density matrix which is calculated by tracing out the degree of freedom in a part of a system we consider. The entanglement entropy diverges logarithmically with the system size when the system is a one-dimensional critical system. On the contrary, the entanglement entropy converges to a particular value when the system is gapped. The entanglement spectrum is also obtained by the reduced density matrix, which characterizes topological properties of quantum systems.

We proposed a new one-dimensional topological model called a generalized cluster-Ising model [1] whose Hamiltonian is given by

$$\begin{aligned} \mathcal{H} = & -J^{XZX} \sum_i \sigma_i^x \sigma_{i+1}^z \sigma_{i+2}^x \\ & -J^{YY} \sum_i \sigma_i^y \sigma_{i+1}^y \\ & -J^{YZY} \sum_i \sigma_i^y \sigma_{i+1}^z \sigma_{i+2}^y. \end{aligned} \quad (1)$$

In this model, topological phase transitions appear depending on the parameters. The phase boundaries can be determined analytically since the above model can be transformed into a free fermion model[1, 2]. We identified each phase by some order parameters obtained by the time-evolving block decimation method for infinite systems (iTEBD).

Entanglement properties of the model were also investigated by the exact diagonalization method. We found that the number of degenerated ground states corresponds to the number of the lowest eigenvalues of the reduced density matrix.

Next, we studied the dynamic behavior of the model under the sweep dynamics in which an interaction parameter changes with a finite speed. We found that the topological blocking phenomenon occurs at the topological phase transition point.

We expected that the obtained results are related to the quantum information processing based on the Ising model.

This work was done in collaboration with Takumi Ohta (YITP, Kyoto University), Ipei Danshita (YITP, Kyoto University), and Keisuke Totsuka (YITP, Kyoto University).

## References

- [1] T. Ohta, S. Tanaka, I. Danshita, and K. Totsuka: J. Phys. Soc. Jpn. **84** (2015) 063001.
- [2] T. Ohta, S. Tanaka, I. Danshita, and K. Totsuka: Phys. Rev. B **93** (2016) 165423.

# Quantum Phase Transition of the Spin Nanotubes

Tôru SAKAI<sup>1,2,3</sup>, Hiroki NAKANO<sup>1,2</sup>, and Tokuro SHIMOKAWA<sup>3</sup>,

<sup>1</sup>*Graduate School of Material Science, University of Hyogo,  
Kouto, Kamigori, Hyogo 678-1297, Japan*

<sup>2</sup>*Research Center for New Functional Materials, University of Hyogo,  
Kouto, Kamigori, Hyogo 678-1297, Japan*

<sup>3</sup>*Synchrotron Radiation Research Center, Kansai Photon Science Institute,  
Quantum Beam Science Research Directorate,  
National Institute for Quantum and Radiological Science and Technology (QST)  
SPring-8, Kouto, Sayo, Hyogo 679-5148, Japan*

<sup>4</sup>*Department of Physics, Osaka University, Toyonaka, Osaka 560-0043, Japan*

Recently some quantum spin systems on tube lattices, to called spin nanotubes, have been synthesized. They are expected to be interesting low-dimensional systems like the carbon nanotubes. As the first step of theoretical study on the spin nanotube, we investigate the  $S=1/2$  three-leg spin tube, which is the simplest one, using the density matrix renormalization group (DMRG) and the numerical exact diagonalization (ED), combined with a precise finite-size scaling analysis named level spectroscopy[1]. The spin gap, which is one of the most interesting macroscopic quantum effects, was revealed to be open due to frustration for sufficiently strong rung exchange couplings, in contrast to the three-leg spin ladder system which is gapless. The critical point of a quantum phase transition between the gapped and gapless phases was estimated. It is consistent with the previous effective Hamiltonian approach[1]. We also found a new quantum phase transition to another spin-gap phase caused by the ring exchange interaction. In addition we theoretically predicted some new field-induced quantum phase transitions. A chirality-mediated novel superconductivity mechanism is also proposed[2, 3].

The recent numerical diagonalization and finite size scaling analyses on the  $S=1/2$

three-leg spin tube indicated a new quantum phase transition between the  $1/3$  magnetization phase and the plateauless one, with respect to the coupling anisotropy. The phase diagram at  $1/3$  of the saturation magnetization was presented[4].

## References

- [1] T. Sakai et al., Phys. Rev. B 78 (2008) 184415.
- [2] T. Sakai et al., J. Phys.: Condens. Matter 22 (2010) 403201.
- [3] K. Okunishi et al., Phys. Rev. B 85 (2012) 054416.
- [4] T. Sakai and H. Nakano, Physics Procedia 75 (2015) 369.

# Field-Induced Quantum Phase Transition in the Kagome-Lattice Antiferromagnet

Tôru SAKAI<sup>1,2,3</sup>, Hiroki NAKANO<sup>1,2</sup>, and Tokuro SHIMOKAWA<sup>3</sup>,

<sup>1</sup>*Graduate School of Material Science, University of Hyogo,  
Kouto, Kamigori, Hyogo 678-1297, Japan*

<sup>2</sup>*Research Center for New Functional Materials, University of Hyogo,  
Kouto, Kamigori, Hyogo 678-1297, Japan*

<sup>3</sup>*Synchrotron Radiation Research Center, Kansai Photon Science Institute,  
Quantum Beam Science Research Directorate,  
National Institute for Quantum and Radiological Science and Technology (QST)  
SPring-8, Kouto, Sayo, Hyogo 679-5148, Japan*

<sup>4</sup>*Department of Physics, Osaka University, Toyonaka, Osaka 560-0043, Japan*

The kagome-lattice antiferromagnets have attracted a lot of interest in the field of the low-temperature physics. It exhibits some exotic field-induced phenomena, like a magnetization plateau, jump etc. Our previous large-scale numerical exact diagonalization study on the  $S=1/2$  kagome-lattice antiferromagnet revealed that a novel field-induced phenomenon, "the magnetization ramp", occurs at  $1/3$  of the saturation magnetization[1]. It is characterized by different critical exponents between the lower-field and higher-field sides of the magnetization curve[2]. In order to clarify unconventional properties around the  $1/3$  magnetization, we considered some extended lattice models; a distorted kagome lattice and distorted triangular lattice etc[3]. The ground-state magnetization curve recently obtained by the numerical exact diagonalization up to 42-spin clusters is also presented to estimate the shape in the thermodynamic limit. Our numerical exact diagonalization study also indicates that the ground state of the kagome-lattice antiferromagnet is gapless quantum spin liquid.

The recent critical exponent analysis up to 42-spin cluster still confirmed the unconventional magnetization behavior around the  $1/3$

magnetization plateau-like anomaly; the field derivative is infinite at the low-field side, while it is zero at the high-field side[4].

## References

- [1] H. Nakano and T. Sakai, J. Phys. Soc. Jpn. 79 (2010) 053707.
- [2] T. Sakai and H. Nakano, Phys. Rev. B 83 (2011) 100405(R).
- [3] H. Nakano and T. Sakai, J. Phys. Soc. Jpn. 83 (2014) 104710.
- [4] T. Sakai and H. Nakano, Physics Procedia 75 (2015) 821.

# Protein-folding Simulations by Efficient Sampling Algorithms

Yasuteru Shigeta

*Center for Computational Sciences,*

*University of Tsukuba, 1-1-1 Tennodai, Tsukuba, Ibaraki 305-8577*

In recent progress in protein-folding simulations, force fields for the all-atom model have been updated extensively. Although further refinements might still be needed to improve accuracy, most current force fields are capable of folding proteins in good agreement with experimental data, indicating that semiempirical atomic force fields are accurate enough to simulate protein folding. However, it is expensive computationally to produce statistically reliable trajectories of protein folding to reach a typical folding time scale, i.e., milliseconds, because the time step for MD is typically 1 fs, so that  $10^{12}$  iterations of the integration are required. Generally, the accessible time scale traced by the laboratory-level computer resources might be several hundreds of nanoseconds, which is far from the timescale for protein folding.

For this problem, We have recently proposed a series of methods as simple yet powerful conformational resampling methods [1]. In these methods, initial structures of the conformational resampling are selected as seeds by referring to several measures, and then short-time MD simulations from the selected

seeds with different initial velocities from a previous run are performed. Cycles of the above selection and resampling are repeated until convergence of predefined criteria is reached. For rare event searches, a key point is how to select appropriate seeds with sufficiently high potential to make structural transitions, where measures should be given *a priori* so as to characterize the structural transitions of interest. We further performed applications of our methods to several biological systems, such as domain motions of proteins with large-amplitude fluctuations, conformational transitions upon ligand binding, and protein-folding/refolding [2]. We have also proposed an automatic detection of relevant reaction coordinates for protein folding on the basis of the algorithm used in our method [3].

## References

- [1] R. Harada, T. Baba, Y. Takano, Y. Shigeta: *Phys. Chem. Chem. Phys.* **17** (2015) 6155.
- [2] R. Harada, T. Nakamura, Y. Takano, Y. Shigeta, *J. Comp. Chem.* **36** (2015) 763.
- [3] R. Harada, T. Nakamura, Y. Shigeta, *Chem. Phys. Lett.* **639** (2015) 269.

## Efficient Sampling Simulation of the Soft Modes Significantly Contribute to Protein Properties

Jacob SWADLING, Kazuhiro TAKEMURA, Yasutaka NISHIHARA,  
Hisham DOKAINISH, Duy TRAN, Chika SATO, and Akio KITAO  
*Institute of Molecular and Cellular Biosciences, University of Tokyo*

We will report our findings about hairpin loops using Replica Exchange Molecular Dynamics (REMD)<sup>1</sup> this year.

Hairpin loops are one of the most common secondary structural motifs found in RNA.<sup>2</sup> DNA hairpins, on the other hand, rarely occur in nature and as a consequence are far less studied. Our current work represents an in-depth computational comparison of the thermodynamics, structure formation and kinetics of these important secondary structures. We have used REMD to elucidate the free energy landscapes of single-stranded RNA and DNA, of sequence:

5'-UUUAACC(U)<sub>18</sub>GGUU-3'

5'-TTTAACC(T)<sub>18</sub>GGTT-3'

Each model consisted of 108 replicas of 32,522 atoms, simulated at temperatures ranging from 270 - 500 K for 1  $\mu$ s.

REMD is a state-of-the-art method for the study of protein and RNA folding. REMD consists of  $M$  noninteracting replicas of the original system in the canonical ensemble at  $M$  different temperatures  $T_m$  ( $m = 0, \dots, M$ ). The trajectory of each independent replica is computed using MD. Adjacent replicas exchange temperatures according to a Boltzmann probability distribution. REMD essentially runs  $N$  copies of the system, randomly initialised, at different temperatures. Then, on the basis of the Metropolis criterion, configurations are exchanged at different temperatures. The idea of

this method is to make configurations at higher temperatures available to the simulations at lower temperatures and vice versa. This results in a very robust ensemble that is able to sample both low- and high-energy configurations. REMD produces enhanced sampling over single trajectory MD because fixed-temperature conformations are much more easily trapped in local energy minima.

Our simulations have successfully reproduced many findings from single-molecule fluorescence experiments. Our simulations have added new insight and predictions to experiment, such as the complete structural distribution of folded, unfolded and misfolded conformations, that were previously unknown.

Melting temperatures visible in figure 1 show a difference of approximately 15 K between

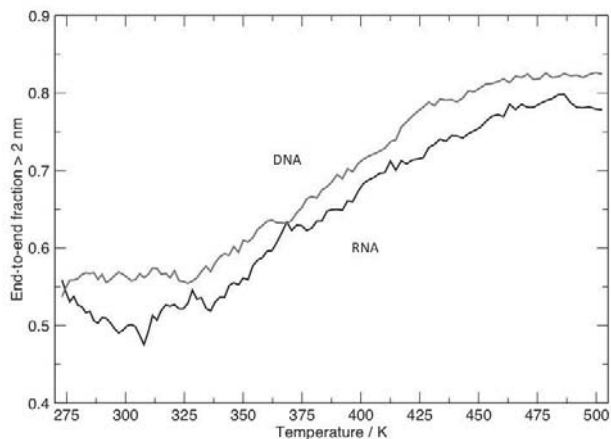


**Fig 1** Melting curves based on average fraction of end-to-end distances greater than 2 nm, for RNA and DNA.

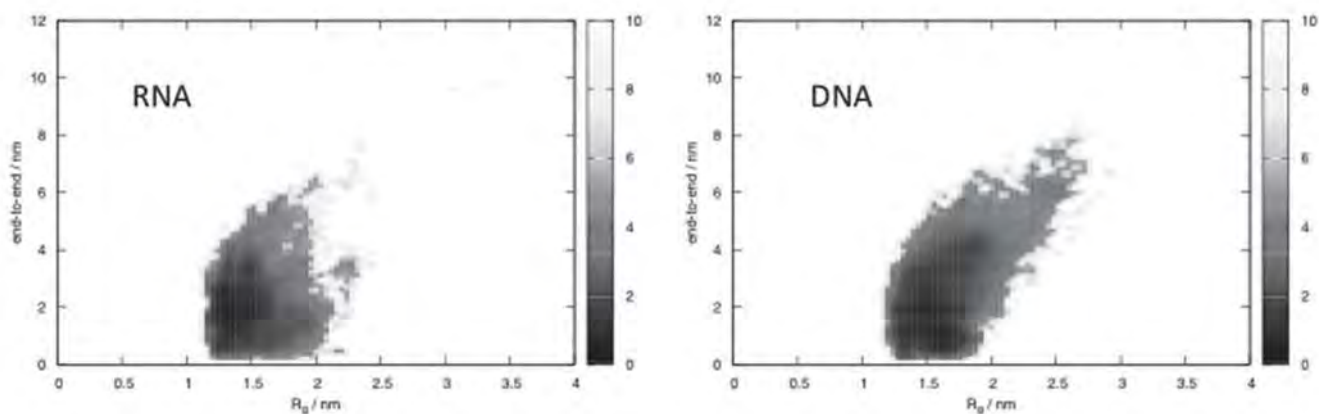


**Fig 2** Free energy surface for RNA and DNA, shown as radii of gyration and end-to-end distances. The shading shows the relative population of that area of conformational space, with the darker area being more populated.

RNA and DNA, which corroborates with the values taken from single-molecule fluorescence experiments.

The free energy surfaces shown in figure 2 show the different areas of conformational space that RNA and DNA occupy. RNA structures occupy a smaller area of conformational space than DNA, corresponding to structures that have shorter end-to-end distances and smaller radius of gyration – indicating that RNA favours a more compact folded conformation over DNA. In comparison DNA conformations display a broad distribution occupying more space in the unfolded regime.

The distribution of persistence lengths (a basic mechanical property quantifying the stiffness of a polymer) show DNA is much stiffer than RNA and occupies a narrower distribution of lengths. This data agrees with the accessible conformational space of the two nucleic acid strands. The stiffness of the sequence plays a significant role in differences between the melting temperatures of the two nucleic acid analogues.

Folded DNAs are much less studied than RNAs but have been found to play an important role in replication, transcription regulation, and recognition. More recently, they were shown to be used as recombination sites. The structural diversity

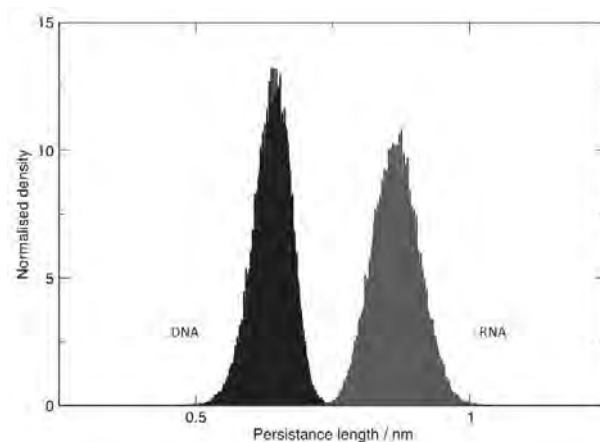


**Fig 3** Distribution of Persistence lengths for DNA and RNA at 300 K.

of RNA also contains information about biological processes that regulate biological functions.<sup>3</sup> Characterisation of the structural diversity and kinetics of folding will help our understanding of the fundamental role of RNA in biology. By comparing with a DNA analogue, we can realise the origins of unique RNA folding process.

## References

- [1] Y. Sugita and Y. Okamoto. *Chem. Phys. Lett.* 1999, 314, 141-151
- [2] Bernat, V., and Disney, D., *Neuron.* 2015, **87**, 28-46.
- [3] Donahue, C.P., Muratore, C., Wu, J.Y., Kosik, K.S., and Wolfe, M.S., *J. Biol. Chem.* 2006, **281**, 23302–23306.

# Tensor network calculation on two-dimensional quantum spin models

Kenji HARADA

*Graduate School of Informatics, Kyoto University, Kyoto 606-8501, Japan*

Recently, the development of tensor network algorithm is very active. However, if we use the tensor network for applying the interesting problem in the condensed matter physics, we need high computational resources. To resolve this issue, we need to develop the parallel library for general tensor network computations.

In this year, we mainly focus on building a library of parallel tensor computations for general tensor network algorithms. If we define two composite indices by splitting the tensor indices into two groups, we can always regard a tensor as a matrix. Thus, most operations of tensors can be rewritten as matrix computations temporarily derived from original tensors. For example, the basics calculation of tensors is a tensor contraction. It can be rewritten as a matrix multiplication of temporal matrices. Based on a transformation between tensor and matrix, we often use various matrix algorithms in a tensor network algorithm: singular value decomposition, QR decomposition, and so on. Therefore, we can build our parallel library of tensor calculations on a parallel computational library for large-scale matrix calculations.

ScaLAPACK[1] is a library of high-performance linear algebra routines for parallel distributed memory machines. There are many implementations on large-scale distributed-memory machines as the system B on ISSP. Thus, we choose ScaLAPACK as the basics parallel matrix library for our tensor library. In detail, ScaLAPACK is built on PBLAS (Parallel BLAS)[2] library for dis-

tributed matrices. We define a distributed tensor as a distributed matrix of PBLAS. To calculate a tensor contraction, we first prepare two distributed matrices by using data transformations based on MPI routines, and we call a PBLAS Level 3 routine to a matrix multiplication on a distributed-memory machine. Since PBLAS Level 3 routines are highly optimized by vendors of supercomputers, the performance except for data transformations is good. Even if we consider the data transformation time, the use of PBLAS Level 3 is a good solution.

We have a plan to open our library with APIs similar to NumPy library of Python language in near future.

## References

- [1] J. Choi, J. Dongarra, S. Ostrouchov, A. Petitet, D. Walker, and R. C. Whaley, in *Applied Parallel Computing Computations in Physics, Chemistry and Engineering Science*, edited by J. Dongarra, K. Madsen, and J. Waniewski (Springer Berlin Heidelberg, Berlin, Heidelberg, 1995), pp. 107–114.
- [2] J. Choi, J. Demmel, I. Dhillon, J. Dongarra, S. Ostrouchov, A. Petitet, K. Stanley, D. Walker, and R. C. Whaley, in *Applied Parallel Computing Computations in Physics, Chemistry and Engineering Science*, edited by J. Dongarra, K. Madsen, and J. Waniewski (Springer Berlin Heidelberg, Berlin, Heidelberg, 1995), pp. 95–106.

# Numerical study on low-energy states of quantum spin systems

Hiroki NAKANO

*Graduate School of Material Science, University of Hyogo  
3-2-1 Kouto, Kamigori-cho, Ako-gun, Hyogo 678-1297, Japan*

Since it is often difficult to estimate precisely physical quantities in systems of many-body problems in condensed matter physics, numerical approaches become more important. Under circumstances, computational studies have contributed much to our deeper understanding of such quantum systems. When quantum spin systems in spatial dimensions larger than one include frustrations, unfortunately, numerical studies are still difficult. The reason for this difficulty is that such systems cannot be treated by the density matrix renormalization group (DMRG) calculations and the quantum Monte Carlo simulations. Only the numerical diagonalization method based on the Lanczos algorithm is generally valid for such frustrated quantum spin systems in dimensions larger than one. This method, however, has a weak point. In this method, only very small system sizes can be treated. In order to overcome this disadvantage, we successfully developed a hybrid-type parallelized code of Lanczos diagonalization[1]. We study quantum spin systems using this Lanczos-diagonalization code we developed as a primary approach. Some quantum spin systems are examined from various points of view.

The primary study of this year in the present project examines the magnetization jump in the magnetization processes in the  $S = 1/2$  Heisenberg antiferromagnet on the square-kagome lattice with a distortion[2]. The magnetization jump was originally observed in the case without the distortion[3]. Within the study of [3] examining the finite-size systems up to 36 sites, however, the skip of the jump  $\delta M$  in a finite-size system is detected up to  $\delta M = 2$ . Only the skip  $\delta M = 2$  cannot deny

the possibility that this jump appears owing to the formation of the spin-nematic state because this state is a two-magnon bound state. Then, we attack calculations for a system with larger size of 42 sites and successfully obtain the magnetization processes of the cases without and with a distortion. Our result for the undistorted system of 42 sites shows the same skip of  $\delta M = 2$ . When we introduce small distortion into the square-kagome lattice, on the other hand, we successfully observe the skip of  $\delta M = 3$  in the 42-site system. This result indicates the exclusion of the possibility that this jump appears owing to the formation of a two-magnon bound state. This result also suggests that the magnetization jump is a macroscopic phenomenon which survives in the thermodynamic limit. The same behaviors of the jump are observed in the Heisenberg antiferromagnets on the Cairo-pentagon-lattice[4, 5], the  $\sqrt{3} \times \sqrt{3}$ -distorted kagome lattice[6, 7], and the *Shuriken*-bonded honeycomb lattice[6]. In these systems, however, only the finite-size jump of  $\delta M = 2$  are detected. Further studies by calculations of larger sizes on these lattices will be required to clarify the behavior of the magnetization jump in the thermodynamic limit. Such studies will contribute to our understandings of this magnetization jump and the nontrivial effect of frustration in magnetic materials.

## References

- [1] H. Nakano and A. Terai: J. Phys. Soc. Jpn. **78** (2009) 014003.
- [2] H. Nakano and T. Sakai: J. Phys. Soc. Jpn. **84** (2015) 063705.

- [3] H. Nakano and T. Sakai: J. Phys. Soc. Jpn. **82** (2013) 083709.
- [4] H. Nakano, M. Isoda, and T. Sakai: J. Phys. Soc. Jpn. **83** (2014) 053702.
- [5] M. Isoda, H. Nakano, and T. Sakai: J. Phys. Soc. Jpn. **83** (2014) 084710.
- [6] H. Nakano, Y. Hasegawa, and T. Sakai: J. Phys. Soc. Jpn. **83** (2014) 084709.
- [7] H. Nakano and T. Sakai: J. Phys. Soc. Jpn. **83** (2014) 104710.

## Numerical study of the low-lying excited state in low-dimensional frustrated magnetism

Tokuro SHIMOKAWA and Hikaru KAWAMURA

*Faculty of Science, Osaka University*

*Machikane-yama, Toyonaka Osaka 560-0043*

Recent theoretical studies have suggested that the effect of bond randomness could be the origin of the observed quantum spin liquid behaviors. Such a randomness-induced QSL is called “random-singlet (RS) state”. It has been reported that the RS state might be realized in the  $S=1/2$  random-bond antiferromagnetic (AF) Heisenberg models on the triangular and kagome lattices [1][2][3], and the possible importance of quenched randomness has been pointed out for understanding the observed QSL-like behaviors in herbertsmithite  $\text{ZnCu}_3(\text{OH})_6\text{Cl}_2$  and some organic salts such as  $\kappa\text{-(ET)}_2\text{Cu}_2(\text{C}_5\text{N})_3$  and  $\text{EtMe}_3\text{Sb}[\text{Pd}(\text{dmit})_2]_2$ .

In this study, we have investigated the low-lying excited properties from RS state by using thermal pure quantum (TPQ) state method [4]. This TPQ method enables us to treat larger finite-size clusters than those treated with the exact diagonalization (ED) method. More concretely, the total number of spins

$N$  we treated is  $N=18, 24, 30$ .

Previous ED calculation results [1][2] with small size ( $N \leq 18$ ) clusters exhibited the  $T$ -linear specific heat and gapless magnetic susceptibility with Curie like behavior in the RS state. In this study, we have computed the specific heat and magnetic susceptibility in larger size ( $N \geq 18$ ) systems. Figs. 1 show the calculation results of the specific heat (a) and the magnetic susceptibility (b) of the  $S=1/2$  random-bond AF Heisenberg model on the triangular lattice. Here,  $\Delta$  means the randomness parameter:  $\Delta=0$  and  $\Delta=1$  cases correspond to the regular and maximally random cases, respectively. (Details are shown ref. [1][2][3].) We can see clearly  $T$ -linear specific heat at low-temperature region and gapless magnetic susceptibility with Curie-like behavior in stronger randomness system even in  $N > 18$  size systems. We can also confirm these behaviors in Fig.2 (a) and Fig. 2 (b) exhibiting the numerical results of

$S=1/2$  random-bond AF Heisenberg model on kagome lattice.

Our TPQ calculations have been performed by using CPU and FAT nodes of system B. The parallel computing technique with OpenMP has been employed.

## References

- [1] K. Watanabe, H. Kawamura, H. Nakano, and T. Sakai: J. Phys. Soc. Jpn. **83** (2014) 034714.
- [2] H. Kawamura, K. Watanabe, and T. Shimokawa: J. Phys. Soc. Jpn. **83** (2014) 103704.
- [3] T. Shimokawa, K. Watanabe, and H. Kawamura: Phys. Rev. B **92** (2015) 134407.

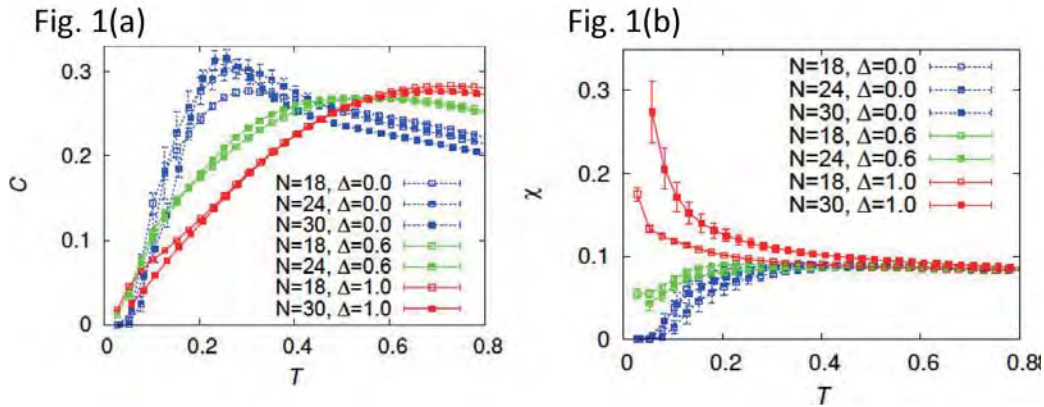


Figure 1: Temperature dependence of specific heat (a) and magnetic susceptibility (b) of the triangular-lattice Heisenberg antiferromagnet for several values of the randomness  $\Delta=0, 0.6, 1.0$ .

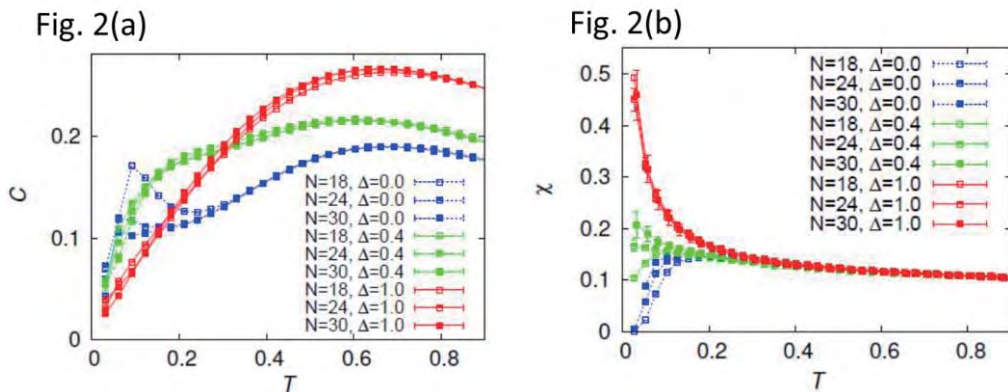


Figure 1: Temperature dependence of specific heat (a) and magnetic susceptibility (b) of the kagome-lattice Heisenberg antiferromagnet for several values of the randomness  $\Delta=0, 0.4, 1.0$ .

# Numerical study of the novel magnetic phenomenon on the honeycomb magnetism

Tokuro SHIMOKAWA, Hikaru KAWAMURA and Kazuki UEMATSU

*Faculty of Science, Osaka University  
Machikane-yama, Toyonaka Osaka 560-0043*

Motivated recent theoretical study [1] that the classical triangular-lattice Heisenberg model exhibit several types of multiple- $q$  states including the triple- $q$  state corresponding to skyrmion-lattice state, we here investigate the possibility of the realization of multiple- $q$  state in the  $J_1$ - $J_2$  classical honeycomb-lattice Heisenberg model.

The Hamiltonian of the honeycomb-lattice Heisenberg model is given by,

$$\begin{aligned} \mathcal{H} = & J_1 \sum_{\langle i,j \rangle} \mathbf{S}_i \cdot \mathbf{S}_j + J_2 \sum_{\langle\langle i,j \rangle\rangle} \mathbf{S}_i \cdot \mathbf{S}_j \\ & - H \sum_i S_i^z, \end{aligned} \quad (1)$$

where  $\sum_{\langle i,j \rangle}$  and  $\sum_{\langle\langle i,j \rangle\rangle}$  mean the sum over the nearest-neighbor and the second-neighbor pairs, respectively. Here,  $J_1$  and  $J_2$  are both antiferromagnetic interactions and  $H$  is the magnetic field intensity. By using monte carlo (MC) method based on the heat-bath method combined with the over-relaxation and replica exchange methods, we have revealed the realization of several multiple- $q$  orders on the honeycomb lattice under the magnetic field. In this study, we have focused on the region of  $1/6 < J_2/J_1 \leq 0.3$ .

In the case of  $J_2/J_1 = 0.3$ , we have confirmed clearly several types of mutiple- $q$  states including single- $q$ , double- $q$  and triple- $q$  states. We have found the appearance of two types of single- $q$  states characterized by different directions of  $q$ -vector. According to our calculation results of static spin structure factor, we have found that the direction of single- $q$  state ap-

pearing at lower (higher) magnetic field is the nearest (second-nearest) neighbor one. Previous study by the low-temperature expansion and monte carlo methods reported that the nearest neighbor direction is selected by thermal fluctuation under zero magnetic field in the case of  $J_2/J_1 = 0.3$  [2]. The direction of  $q$ -vector is switched from the nearest-neighbor direction to the second-nearest direction by the thermal fluctuation under the high magnetic field. This switching behavior could be understood qualitatively by our results of the low-temperature expansion under magnetic field.

In contrast to the result of triangular-lattice Heisenberg model, our triple- $q$  state in the honeycomb-lattice model does not correspond to the skyrmion state. The spin configuration of the triple- $q$  state in this honeycomb model forms meron-like structure. The difference between the honeycomb and triangular model are understood qualitatively within a mean-field analysis.

Our computational results were obtained by using CPU node of system B. Our MC code are executed in parallel by using OpenMP.

## References

- [1] T. Okubo, S. Chung, and H. Kawamura : Phys. Rev. Lett. **108** (2012) 017206.
- [2] S. Okumura, H. Kawamura, T. Okubo, and Y. Motome : J. Phys. Soc. Jpn. **79** (2010) 114705.

# Study of Quantum Phases in Triangular Kitaev-Heisenberg Model

Takami TOHYAMA

*Department of Applied Physics, Tokyo University of Science, Tokyo 125-8585*

The Kitaev-Heisenberg (KH) model on honeycomb lattice is suggested as an effective model for  $(\text{Na,Li})_2\text{IrO}_3$ . Not only honeycomb lattice but also triangular lattice has attracted much attention from both the theoretical and experimental viewpoints. From the experimental side,  $\text{Ba}_3\text{IrTi}_2\text{O}_9$  has been suggested as a possible candidate of a spin-liquid material with the triangular-lattice structure. Theoretically, because the KH model on the triangular lattice has both geometrical frustration and Kitaev-type frustration that breaks  $\text{SU}(2)$  spin symmetry, the quantum effect on the model is expected to be highly non-trivial and interesting.

Motivated by these, we examine the KH model on the triangular lattice by using the two-dimensional density-matrix renormalization group (2D-DMRG) method for a  $12 \times 6$ -site lattice [1]. We used the System B in the Supercomputer Center, the Institute for Solid State Physics, the University of Tokyo, and the K-computer. The 2D-DMRG code has been developed by our group. To perform DMRG, we map the original system to a snake-like one-dimensional chain, and combine the chain with long-range interactions. We keep 1300~1800 states in the DMRG block and performed more than 10 sweeps, resulting in a typical truncation error  $10^{-5}$  or smaller.

Calculating the ground-state energy and spin structure factors, we obtain the ground state phase diagram of the Kitaev-Heisenberg model. As suggested by previous studies, we find a  $120^\circ$  antiferromagnetic (AFM) phase,

a  $\text{Z}_2$ -vortex crystal phase, a nematic phase, a dual  $\text{Z}_2$ -vortex crystal phase (dual counterpart of  $\text{Z}_2$ -vortex crystal phase), a  $\text{Z}_6$  ferromagnetic phase, and a dual ferromagnetic phase (dual counterpart of  $\text{Z}_6$  ferromagnetic phase). Spin correlations discontinuously change at the phase boundaries because of first-order phase transitions. In the (dual)  $\text{Z}_6$  ferromagnetic phase, we find that the dominant spin component of the spin structure factors is different on either side of the  $\text{SU}(2)$  symmetric point, although there is no phase transition.

Furthermore, we study the relation among von Neumann entanglement entropy, entanglement spectrum, and phase transitions. As in the case of the spin structure factors, the entanglement entropy also discontinuously changes at all the phase boundaries. We find that the Schmidt gap defined by the energy difference between the ground state and the first-excited state in the entanglement Hamiltonian is much larger than the other gaps among entanglement levels. At the phase transition points, the Schmidt gap is closing. This is in contrast with the extended KH model on honeycomb lattice, where the Schmidt gap is not necessarily a measure of phase transition [2].

## References

- [1] K. Shinjo, S. Sota, S. Yunoki, K. Totsuka, and T. Tohyama: arXiv:1512.02334.
- [2] K. Shinjo, S. Sota, and T. Tohyama: Phys. Rev. B **91** 054401 (2015).

# Quantum Phase Transitions of One-Dimensional Spin Systems Coupling with Lattice Degrees of Freedom

Hidemaro SUWA

*Department of Physics, The University of Tokyo*

*7-3-1 Hongo, Bunkyo, Tokyo 113-0033*

The interplay between the spin and the lattice degrees of freedom can bring about a non-trivial structural phase transition and its criticality. In particular, the dimerization occurs when the energy decrease of the quantum spins exceeds the energy increase of the lattice. Many materials called the spin-Peierls system show the dimerization transition experimentally. The recently proposed quantum simulator of trapped ions can realize even the quantum spin-Peierls transition. In the meantime, the quantum nature of the lattice degrees of freedom has been often ignored in the theoretical analysis for the spin-Peierls systems. Such an approximation will be appropriate in the adiabatic limit where the energy scale of lattice is much smaller than the that of spins. However, the inorganic spin-Peierls material  $\text{CuGeO}_3$  has the comparable energy scales between the spin and the lattice. Then the quantum lattice fluctuation is expected to be important to the material and its phase transition. Nevertheless, the understanding of the quantum lattice effect has been lacking.

We have investigated the one-dimensional quantum spin system coupling the quantum phonons by means of the worldline quantum Monte Carlo method without any approximation [1]. The unbiased gap-estimation method is devised and the energy gaps are precisely calculated. While the adiabatic approximation concludes that the infinitesimal spin-lattice coupling drives the ground state into the dimer phase from the Tomonaga-Luttinger liquid phase, we have unambiguously shown that the Kosterlitz-Thouless-type quantum phase transition occurs between the dimer and liquid phases at a *finite*

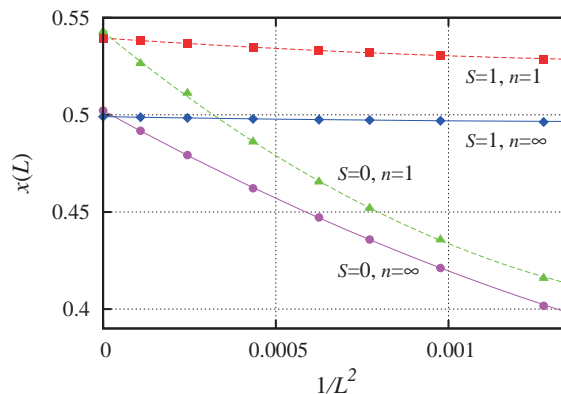


Figure 1: Scaling dimensions corresponding to the singlet and the triplet-exciting operators at the liquid-dimer transition point. The developed higher-order estimations successfully converges to  $1/2$ , which shows the transition point is described by the Wess-Zumino-Witten model, while the conventional second moment estimators ( $n = 1$ ) fails to converge to  $1/2$ . This figure was taken from Ref.[1]

spin-phonon coupling as a result of the quantum phonon effect (Fig. 1). We have established that the quantum lattice fluctuation is essential to the one-dimensional spin, or spinless fermion, system and the transition point is described by the  $k = 1$   $\text{SU}(2)$  Wess-Zumino-Witten model.

As for the computation, we used the system B as the class C (project ID:H27-Cb-0051). Independent worldline quantum Monte Carlo simulations with the worm (directed-loop) algorithm were efficiently run by the MPI parallelization.

## References

- [1] H. Suwa and S. Todo: Phys. Rev. Lett. **115** (2015) 080601

# Spectral Analysis of Quantum Phase Transition between Competitive Magnetic Order and Lattice Order Phases

Hidemaro SUWA

*Department of Physics, The University of Tokyo  
7-3-1 Hongo, Bunkyo, Tokyo 113-0033*

The Landau-Ginzburg-Wilson (LGW) paradigm is a powerful theoretical framework of general continuous phase transitions. The key concept of the paradigm is that the action of a physical system can be expanded in an order parameter and a phase transition can be described by the spontaneous symmetry breaking. Although this framework works very well in many phase transitions, it has been recently challenged by a new type of transition triggered by the so-called deconfined criticality [1]. As an example of the deconfinement, the phase transition between a spin-symmetry broken phase and a lattice-symmetry broken (and spin-symmetry unbroken) phase is predicted to be continuous, which must be first-order according to the LGW paradigm. The deconfined criticality is expected to appear in frustrated quantum spin systems, doped superconductors, heavy-fermion systems, and so on. Many of these systems, however, are not easy to study their phase transitions owing to the complex interaction and the sign problem. In the meantime, as a spin model amenable to the quantum Monte Carlo simulation, the  $J$ - $Q$  model was proposed [2] and extensively studied. Nevertheless, the criticality of the model has not been conclusive because of the unconventional finite-size effect. To understand the non-trivial physics of the deconfined criticality, the spectral analysis that could catch the deconfinement of the fractional (spinon) excitation is strongly needed.

We have calculated the excitation gaps of the SU(2)  $J$ - $Q$  model on the square lattice. The level-cross analysis was tested for locating the phase transition point between the Néel phase and the valence-bond-solid (VBS) phase. While the triplet at wavenumber  $(\pi, \pi)$  is the lowest excitation in the Néel phase for a finite-size system, the singlet at  $(\pi, 0)$  and  $(0, \pi)$  are the lowest excitation in the VBS phase. Then the crossing coupling between the two gaps should converge to the transition point in the thermodynamic limit. We have obtained the crossing coupling is remarkably well scaled in a power-law form. Combining the scaling of the crossing gap value, we have estimated the exponent relating to the spinon-deconfinement length. Also the triplet gap at  $(\pi, 0)$  was calculated, which must become zero if the phase transition is continuous. We have observed the gap approximately scales in  $1/L$ , and the system has the multiple gapless modes only at the critical point. A paper to sum up these results is under preparation.

As for the computation, we used the system B as the class C (project ID:H27-Ca-0090). Independent worldline quantum Monte Carlo simulations with the loop algorithm were efficiently run by the MPI parallelization.

## References

- [1] T. Senthil *et al.*, Science **303** (2004) 1490.
- [2] A.W. Sandvik, Phys. Rev. Lett. **98** (2007) 227202.

# Estimating Kinetic Equation from Bubble Dynamics

Hiroshi Watanabe

*Institute for Solid State Physics, University of Tokyo  
Kashiwa-no-ha, Kashiwa, Chiba 277-8581*

The coarsening phenomena can be described by the classical Lifshitz-Slyozov-Wagner (LSW) theory [2, 3]. The only input of the theory is the kinetic equation which describes the growth rate of a droplet. However, it was difficult to observe the kinetic equation directly. Therefore, one has to infer the kinetic equation from macroscopic behaviors, such as the power-law behavior of the average volume of the droplets. Recently, it was shown that the LSW theory works well for bubble coarsening [1]. Assuming that the dynamics is reaction-limited in low temperature and diffusion-limited in high temperature, the time evolution of the average volume of bubbles were well explained. However, the kinetic equation of bubbles are still in mystery. Therefore, we estimate the kinetic equation directly from the dynamics of bubbles [4]. We performed molecular dynamics simulation with the truncated Lennard-Jones (LJ) potential. The simulation involves up to 680 million atoms. From the snapshots of the simulation, we calculate the kinetic equation, *i.e.*, growth or shrinkage rates of bubbles. While confirmed that the form of the kinetic equation in low temperature is well described by the LSW theory assuming the reaction-limited dynamics, the kinetic equation were found to be multivalued function for higher temperature regime, and therefore, the mean-field like treatment may fail in this regime.

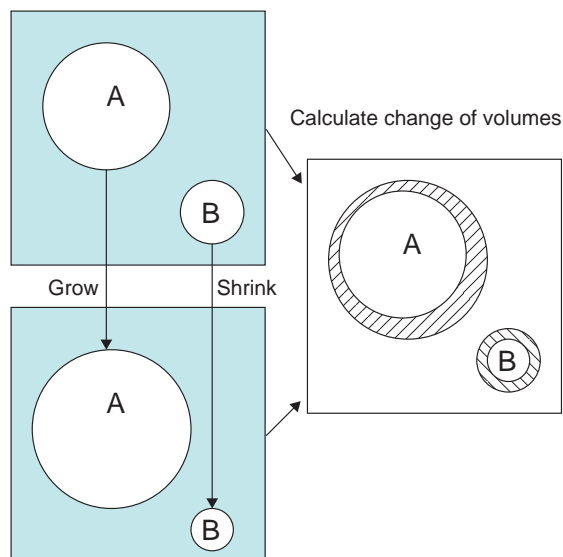


Figure 1: A schematic illustration of the calculation of the kinetic equation. We calculate the growth or shrinkage rates of bubbles from two successive snapshots.

## References

- [1] H. Watanabe, M. Suzuki, H. Inaoka, and N. Ito; *J. Chem. Phys.* **141**, 234703 (2014).
- [2] I. Lifshitz and V. Slyozov. *J. Phys. Chem. Solids*, 19:35–50, 1961.
- [3] C. Wagner. *Z. Elektrochem.*, 65:581 – 591, 1961.
- [4] H. Watanabe, H. Inaoka, and N. Ito; arXiv:1603.04181

# Improvement of dynamical scaling and accurate analysis of nonequilibrium relaxation data

Y. Ozeki

*Graduate School of Informatics and Engineering, The University of Electro-Communications*

We investigate the efficiency of the corrections to scaling to the dynamical scaling analysis in the nonequilibrium relaxation (NER) method [1] by the use of the Bayesian inference and the kernel method [2, 3]. Previously, we have applied the method to the 2D Ising model and obtained an improvement for the estimation of the transition temperature [4]. In the present study, we will check this improvement carefully by the use of the bootstrap method. Furthermore, we apply the method for the general  $S$  Ising model to check the accuracy of the estimated critical exponents.

In the dynamical scaling analysis for the NER method, a general scaling form is examined;

$$m(t, T) = \tau^{-\lambda} \Psi(t/\tau), \quad (1)$$

where  $m(t, T)$  is the relaxation of magnetization from the all aligned state.  $\tau(T)$  is the relaxation time, which is expected to diverge as

$$\tau(T) \sim |T - T_c|^{-z\nu}$$

in  $T > T_c$  or  $T < T_c$ . To estimate  $T_x$ , one may calculate  $m(t, T)$  for several values of  $T$ , and fit the data to the above formula. Recently, the corrections to scaling are included to the kernel method in the static case. [5] We apply this idea to the dynamical scaling analysis of NER data. The scaling form

$$m(t, T) = t^{-\lambda} \Psi(t/\tau, t^{-c}),$$

is applied instead of eq.(1).

Previously [4], we demonstrated the method for the data on the square lattice with  $1501 \times 1500$  up to 10000 MCS for 1024 samples in the temperature  $2.27 \leq T \leq 2.279$ . In the case without corrections, we had an estimation  $T_c = 2.2692301$ , while, in the present study, we obtained  $T_c = 2.2691851$ , which shows more accurate by comparing the exact value  $T_c = 2.2691853 \dots$ .

To obtain a precise estimation and a reliable error bar, here, we apply the bootstrap method. We perform multiple times dynamical scaling analysis for the data sampled at random, and take statistics. The relaxation data used in the above work is used. We prepare a sample by randomly choosing 100

points for each temperature identically along  $\log t$  axis, then perform the dynamical scaling for each sample. In the case without corrections, we had an estimation  $T_c = 2.269232(8)$ , while, with corrections to scaling, we obtained  $T_c = 2.269184(9)$ , which shows more accurate by Comparing with the exact value  $T_c = 2.2691853 \dots$ , we understand that the latter estimation gives a precise result with a reliable error bar, while the former shows a little deviation from it. Note that the estimated errors by the bootstrap method in the present study is not a confidential interval which is usually shown in the NER analysis, but a interval as highly reliable as one can estimate from the prepared data.

Next we check the efficiency for estimations of critical exponents. In the table, we show the result for the 2D Ising model with  $S = 1, 3/2, 5, 50$ , For each  $S$  case, estimations obtained with corrections give good values compared with the expected ones,  $z\nu \sim 2.15$  and  $\beta \sim 0.125$ .

	$z\nu$	$\beta$
$S = 1$ (no corrections)	2.0852	0.1261
$S = 1$ (with corrections)	2.1084	0.1246
$S = 3/2$ (no corrections)	2.0773	0.1279
$S = 3/2$ (with corrections)	2.1148	0.1253
$S = 5$ (no corrections)	2.0178	0.1306
$S = 5$ (with corrections)	2.1227	0.1214
$S = 50$ (no corrections)	2.0160	0.1371
$S = 50$ (with corrections)	2.1434	0.1236

[C class; 5000K (B), 0K (C)]

## References

- [1] Y. Ozeki and N. Ito, J. Phys. A: Math. Theor. **40** R149 (2007);
- [2] K. Harada, Phys. Rev. E **84** 056704 (2011).
- [3] Y. Ozeki and Y. Echinaka, Activity Report 2012 (Supercomputer Center, ISSP, 2013)
- [4] Y. Ozeki and Y. Echinaka, Activity Report 2013 (Supercomputer Center, ISSP, 2014)
- [5] K. Harada, cond-mat, stat-mech, arxiv: 1410.3622 (2014)

# Dynamical ordering of biomolecular systems by molecular dynamics simulations

Satoru G. Itoh and Hisashi Okumura

*Research Center for Computational Science,  
Institute for Molecular Science, Okazaki, Aichi 444-8585*

We are interested in amyloid fibrils, which are insoluble aggregates of misfolded fibrous proteins and associated with more than 30 human neurodegenerative diseases. For example, Alzheimer's disease is related to amyloid- $\beta$  ( $A\beta$ ) peptides. To overcome these diseases, it is essential to understand amyloid fibril formation. We have performed such molecular dynamics (MD) simulations of amyloid fibrils [1,2].

This year, we focused on dimerization process and conformations of  $A\beta(1-40)$ , which consist of 40 amino acids. For this purpose, we applied the Hamiltonian replica-permutation method [3], which is a better alternative to the Hamiltonian replica-exchange method, to two  $A\beta(1-40)$  molecules in explicit water solvent. The number of replicas is 18. We finished so far about 30ns per replica and about 550 ns in total.

At the first step of the dimerization process, two  $A\beta(1-40)$  molecules came close to each other and had intermolecular sidechain contacts. When two molecules had the intermolecular sidechain contacts, the  $A\beta(1-40)$  tended to have intramolecular secondary structures, especially  $\beta$ -hairpin structures as in Fig. 1. The two

molecules had intermolecular  $\beta$ -bridge structures by coming much closer at the second step of the dimerization process.

To obtain enough statistics, more MD simulations should be performed. We plan to continue the MD simulations and to analyze the data in more detail.

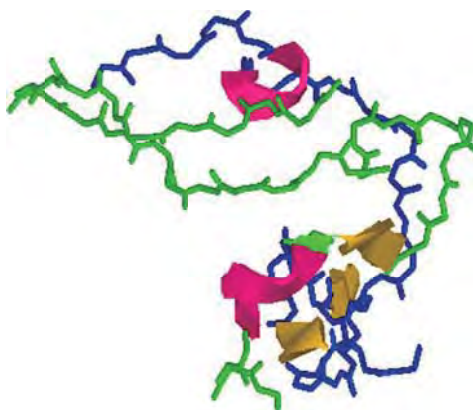


Fig. 1: Snapshot obtained by the Hamiltonian replica-permutation MD simulations.

## References

- [1] H. Okumura and S. G. Itoh: *J. Am. Chem. Soc.* **136** (2014) 10549.
- [2] S. G. Itoh and H. Okumura: *J. Phys. Chem. B* **118** (2014) 11428.
- [3] S. G. Itoh and H. Okumura: *J. Comput. Chem.* **34** (2013) 2493.

# Simulation studies of (i) the role of hydrodynamics on colloidal gelation and (ii) the essential difference in the dynamics between strong and fragile liquids

Akira Furukawa

*Institute of Industrial Science, University of Tokyo  
Komaba 4-6-1, Meguro-ku, Tokyo 153-8505*

(i) Using a fluid-particle dynamics (FPD) method [1], which is a hybrid simulation method for the dynamics of complex colloidal suspensions, we numerically studied the effects of hydrodynamic interactions on the collective gelation dynamics in model colloidal suspensions.

Colloidal gels are out-of-equilibrium structures, made up of a rarefied network of colloidal particles. With simulations which properly include hydrodynamics, we confirmed that hydrodynamic interactions suppress the formation of larger local equilibrium structures of closed shapes, and instead leads to the formation of highly anisotropic threads, which is crucial for making up the open gel network. We found a strong difference in the gelation dynamics between systems with and without hydrodynamics, quantifying the role of hydrodynamics [2].

(ii) Through molecular dynamics simulations, we revealed an essential difference in the dynamics between strong and fragile glass-formers [3]: In strong glass-formers, the relaxation dynamics of density fluctuations is non-conservative, whereas that of fragile glass-formers exhibits conservative (diffusive) behavior. We demonstrate that this distinction is a direct consequence of the fundamental difference in the underlying elementary process between these two dynamical classes of glass-

formers. For fragile glass-formers, a density-exchange process precedes the density relaxation, which locally takes place in normal states, but is increasingly cooperative and non-local as the temperature is lowered in supercooled states. On the other hand, in strong glass-formers such an exchange process is absent. Our finding provides a novel insight into the Angell's classification scheme from a hydrodynamic perspective.

These simulations (i) and (ii) were partially performed at the ISSP Supercomputer Center. The programs are parallelized with a combination of OpenMP and MPI techniques.

## References

- [1] H. Tanaka and T. Araki, Phys. Rev. Lett. **85**, 1338 (2000).
- [2] C. P. Royall, J. Eggers, A. Furukawa, and H. Tanaka, Phys. Rev. Lett. **114**, 258302 (2015).
- [3] A. Furukawa and H. Tanaka, submitted.

# Dynamical phase transitions under time dependent external fields

Seiji MIYASHITA

*Department of Physics, University of Tokyo  
7-3-1Hongo, Bunkyo-ku, Tokyo 113-0033*

We have studied various novel types of ordering processes, dynamics, and also related cooperative phenomena using massive computer simulations.

We developed Landau-Lifshitz-Gilbert equation for systems consisting of various amplitudes of spins at finite temperatures with stochastic noise. There we pointed out that within the condition of the fluctuation dissipation relation, there are several ways to realize the equilibrium states. We confirmed that the system reaches to the equilibrium state, but we pointed out that the relaxation depends on the choice largely. [1]

We have studied the effect of lattice distortion on the ordering processes of bistable systems. The distortion causes an effective long-range ferromagnetic interaction. Competition between the long-range ferromagnetic interaction and short range interaction of the system provides various new types of phase transition. In this fiscal year, we studied this competition in the Mekata model (triangular antiferromagnetic model with next nearest neighbor ferromagnetic interaction), and found the long-range ferromagnetic interaction causes a modification on the dual Kosterlitz-Thouless transition to be a new type of second order phase transition. [2]

In antiferromagnetic systems without frustration, the long-range ferromagnetic interaction does not relevant effect at zero magnetic field. However in finite magnetic field, we found a new type gas-liquid type phase

diagram.[3]

We have pointed out that high-spin low-spin transtion of an spin-crossover material SCO material  $[\text{Fe}^{\text{II}}\text{H}_2\text{L}^{2-\text{Me}}][\text{PF}_6]_2$  is well described by a modified ANNNI model.[4]

We have developed method to obtain ESR spectrum from microscopic Hamiltonian. In this fiscal year, we investigated time domain methods in which we study time evolution of autocorrelation function and obtain the spectrum by Fourier transform. Besides the method making use of the autocorrelation function (AC method), we introduced a new method by making use of the Wiener-Khinchin relation (WK method). We found the WK method is less suffered by the Gibbs oscillation, but we also found that the Gibbs oscillation is suppressed in large systems even in AC method. We obtain the spectrum up to 26 spin systems.[5]

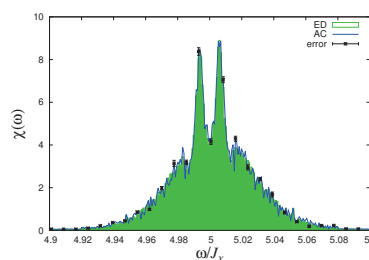


Figure 1: ESR Spectrum obtained by a new numerical method (Wiener-Khinchine method) of a XXZ chain. See the recerence [5]

We also studied collapse of metastable state in quantum systems. In particular, we inves-

tigated the quantum version of the Stoner-Wahlfarth model which consists of a single spin with uni-axial anisotropy in a magnetic field. The magnetization can stay in the opposite direction to the magnetic field due to the anisotropy. The metastable state disappears at a point which is a kind of spinodal point and is called Stoner-Wahlfarth point. We studied how a large  $S$  spin in quantum system behaves in this situation. We found that the energy gap distribution due to an quantum mixing term (in the present case the transverse field) has a singularity described by a classical spinodal decomposition. We also found that a nontrivial beating phenomena appears after the Stoner-Wahlfarth point.[6]

We have also studied mechanisms of coercive force in permanent magnets. In particular, we studied the nucleation and domain wall pinning at the grain boundary of magnets. In particular, we obtained the temperature dependence of the threshold field of the phenomena and we analyzed the dependence from the view point of temperature dependence of the anisotropy energy.[7]

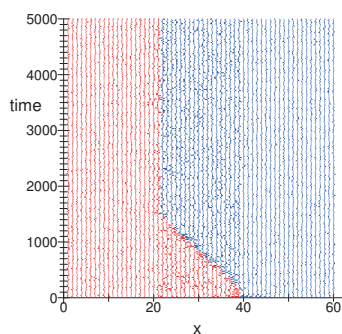


Figure 2: Domain-wall de-pinning. The horizontal axis denotes the space and the vertical axis denotes the time. The center part (20-40) is drain boundary consisting of a soft magnets. Initially, the right side of hard magnet is reversed. See the recerence [7]

## References

[1] M. Nishino and S. Miyashita, Realization of thermal equilibrium in inhomoge-

neous magnetic systems by the Landau-Lifshitz-Gilbert equation with stochastic noise, and its dynamical aspects, *Phys. Rev. B* 91, 134411(1-13) (2015).

- [2] M. Nishino, S. Miyashita, Termination of the Berezinskii-Kosterlitz-Thouless phase with a new critical universality in spin-crossover systems, *Phys. Rev. B* 92, 184404 (1-7) (2015).
- [3] P.A. Rikvold, G. Brown, S. Miyashita, C. Omand and M. Nishino, Equilibrium, metastability, and hysteresis in a model spin-crossover material with nearest-neighbor antiferromagnetic-like and long-range ferromagnetic-like interactions, *Phys. Rev. B* 93, 064109, (1-13) (2016).
- [4] H. Watanabe, K. Tanaka, N. Brefuel, H. Cailleau, J. F. Letard, S. Ravy, P. Fertey, M. Nishino, S. Miyashita and E. Collet, Ordering phenomena of high-spin/low-spin states in stepwise spin-crossover materials described by the ANNNI model, *Phys. Rev. B* 93, 014419, (1-12) (2016).
- [5] H. Ikeuchi, H. De Raedt, S. Bertaina, S. Miyashita, Computation of ESR spectra from the time evolution of the magnetization: Comparison of autocorrelation and Wiener-Khinchin-relation-based methods, *Phys. Rev. B* 92, 214431 (1-15) (2015).
- [6] T. Hatomura, B. Barbara and S. Miyashita, Quantum Stoner-Wohlfarth Model, *Phys. Rev. Lett.* 116, 037203, (1-5) (2016).
- [7] S. Mohakud, Sergio Andraus, M. Nishino, A. Sakuma and S. Miyashita, Temperature dependence of the threshold magnetic field for nucleation and domain wall propagation in an inhomogeneous structure with grain boundary, <http://arxiv.org/abs/1602.03285>.

# Scaling theory of disordered topological insulators

TOMI OHTSUKI<sup>1</sup>  
 TOHRU KAWARABAYASHI<sup>2</sup>  
 KEITH SLEVIN<sup>3</sup>  
 KOJI KOBAYASHI<sup>1</sup>

1) Dept. Phys., Sophia University, Chiyoda-ku, Tokyo 102-8554, Japan

2) Dept. Phys., Toho University, Miyama 2-2-1, Funabashi 274-8510, Japan

3) Dept. Phys., Osaka University, Toyonaka, Osaka 560-0043, Japan

Recent discoveries of two-dimensional quantum spin Hall states and three-dimensional (3D) topological insulators (TIs) have inspired extensive research for these novel materials. In the impurity free systems where the translational invariance exists, the topological insulator is characterized by the non-zero topological numbers, which are defined via integral over the Brillouin zone. This definition is no longer valid once the translational invariance is broken due to disorder. In this case, we usually use edge/surface states to characterize TIs.

Here we studied the transport properties of the thin disordered three-dimensional topological insulators [1]. We stacked  $N$  layers of two dimensional systems, and determined the TI and OI (ordinary insulator) phases, which subtly depends on  $N$ , but robust against certain amount of disorder. In addition, we have analyzed the density of states and the transport properties of bulk 3D TI's where only the surface of the systems are disordered [2].

Recently, we have proposed the density of state scaling for Dirac semi-metal phase and described the novel semi-metal to metal transitions [3]. We have extended this idea to the case of 3D Weyl semi-metals which is realized by stacking two dimensional Chern insulators. We have determined the phase diagram and analyzed the scaling of density of states as well as the conductivity scaling [3] via numerical and self-consistent Born calculation.

## References

1. K. Kobayashi, Y. Yoshimura, K.-I. Imura, T Ohtsuki: Physical Review B **92**, 235407 (2015)
2. V. Sacksteder, T. Ohtsuki, K. Kobayashi: Phys-

ical Review Applied **3**, 064006 (2015)

3. K. Kobayashi, T. Ohtsuki, K.-I. Imura, I. Herbut: PRL **112**, 016402 (2014)

4. S. Liu, T. Ohtsuki, R. Shindou: Physical Review Letters **116**, 066401 (2016)

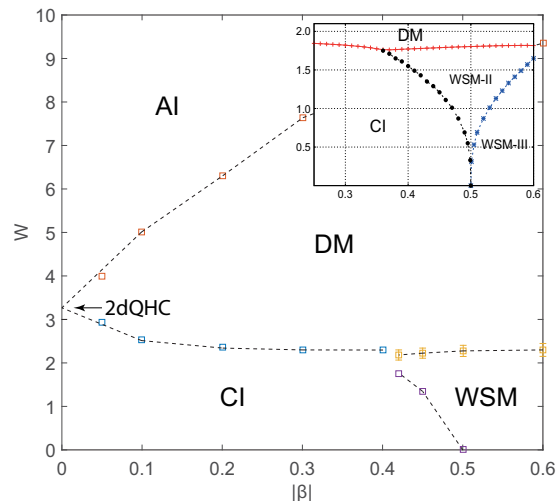


Figure 1: Phase diagram of layered Chern insulator subtended by disorder strength  $W$  and the interlayer coupling strength  $\beta$ . WSM, DM, CI, AI and 2dQHC stand for renormalized Weyl semimetal, diffusive metal, Chern insulator, ordinary Anderson insulator and 2D QH quantum critical point, respectively. (inset) Phase diagram obtained from the self-consistent Born analysis. The region-II WSM phase (WSM-II) has two pairs of the Weyl points, while the region-III WSM phase (WSM-III) has three pairs of the Weyl points.

# Developing microscopic simulation method of superconductors

Ryo IGARASHI

*Information Technology Center, The University of Tokyo  
Yayoi, Bunkyo, Tokyo 113-8658 JAPAN*

This project aims to account for physical properties and microscopic mechanism of various superconducting materials such as high-temperature cuprate superconductors and recently discovered iron pnictide superconductors. In this purpose, we need to develop highly accurate simulation method for quantum lattice model. The density matrix renormalization group (DMRG) method is widely used to obtain the ground state of large quantum lattice models. Since the DMRG method has been originally developed for one-dimensional models, we have implemented the direct extension DMRG (dex-DMRG) method as shown in Fig. 1 to simulate two-dimensional model using MPS framework. However, this extension re-

compare to the ALPS exact diagonalization [1]. We used the ISSP supercomputer system B and C for systematic comparison between the dex-DMRG method and the ALPS diagonalization.

## References

- [1] B. Bauer *et. al.* (ALPS collaboration): J. Stat. Mech. (2011) P05001.

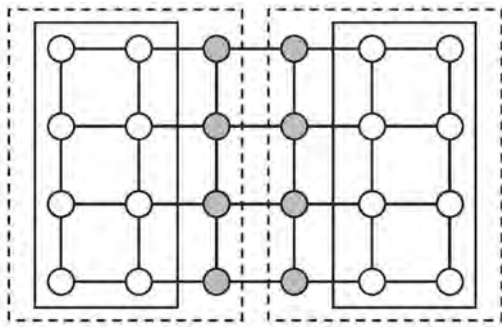


Figure 1: A schematic superblock configuration of direct extension DMRG method for a 4-leg model.

quires a large CPU time and a huge memory usage. Thus, we parallelized this method for massively parallel computer.

In order to check the validity of the dex-DMRG method further, we first decided to

# Dipolar Spin Systems on Kagomé Lattice

Yusuke TOMITA

*Shibaura Institute of Technology*

*307 Fukasaku, Minuma-ku, Saitama-City, Saitama 337-8570*

The effect of the dipolar interaction depends on a positional relation between interacting sites; it is ferroic when their moments are parallel to the displacement vector while it is anti-ferroic when they are perpendicular to the vector. The dependence on a positional relation brings about various order formations which depend on lattice forms, and their nontrivial ordered states and critical phenomena are attracting much interest from fundamental and applied sciences. Dipolar systems on kagomé lattice are fine instances which show nontrivial orders and critical phenomena. In the previous work, the author implied a part of moments on a kagomé lattice are disordered even in the ordered state [1], while recent studies advocate the order is a ferrimagnetic [2, 3]. Furthermore, Maksymenko and colleagues also studied the kagomé system with exchange interactions, and an unidentified ordered phase is found between the ferrimagnetic (Ferri) and an antiferromagnetic (AFM) phases.

The Hamiltonian of the dipolar systems are given by

$$\mathcal{H} = J \sum_{\langle i,j \rangle} \mathbf{S}_i \cdot \mathbf{S}_j + D \sum_{i < j} \left[ \frac{\mathbf{S}_i \cdot \mathbf{S}_j}{r_{ij}^3} - 3 \frac{(\mathbf{S}_i \cdot \mathbf{r}_{ij})(\mathbf{S}_j \cdot \mathbf{r}_{ij})}{r_{ij}^5} \right],$$

where  $\mathbf{S}_i$  represents a Heisenberg spin at site  $i$ . Coefficients  $J$  and  $D$  are parametrized by a single variable  $\theta$ ,

$$J = \sin \theta, \quad D = \cos \theta.$$

In order to update dipolar spins efficiently, I employed  $O(N)$  Monte Carlo method [4]. By observing the structure factor, the existence of the ferrimagnetic ground state is confirmed at the pure dipolar interaction point,  $\theta = 0$ , which has been pointed out by Maksymenko *et al.* and Holden *et al.* [2, 3]. When  $J$  is large enough, the antiferromagnetic order is observed at low temperatures. Using a finite-size scaling analysis, as Maksymenko *et al.* have reported, I confirmed that the universality class of the paramagnetic (P) to the AFM phase transition belongs to the two-dimensional ferromagnetic Ising model. In the intermediate re-

gion ( $1^\circ \leq \theta \leq 10^\circ$ ), three types of phase transitions, P-AFM, P-Ferri, and AFM-Ferri, are observed. In a region ( $5^\circ < \theta \leq 10^\circ$ ), successive phase transitions, P-AFM-Ferri, are observed. The P to AFM phase transition is continuous while the AFM to Ferri phase transition is discontinuous. Figure 1 shows the specific heat at  $\theta = 7.5^\circ$ . The specific heat data indicate the successive phase transition at  $T \sim 0.44$  and  $0.26$ . While I expect the triple point resides  $\theta \lesssim 5^\circ$ , a strong crossover from the first order transition line between the AFM and the Ferri phases hinders from determining the precise position. Further computational efforts are needed to identify the triple point and to clarify the critical phenomena at the triple point.

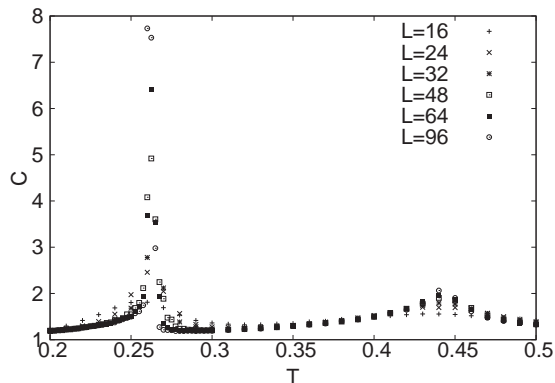


Figure 1: Specific heat at  $\theta = 7.5^\circ$ .

## References

- [1] Y. Tomita, *J. Phys. Soc. Jpn.* **78**, 114004 (2009).
- [2] M. Maksymenko, V. R. Chandra, and R. Moessner, *Phys. Rev. B* **91**, 184407 (2015).
- [3] M. S. Holden, M. L. Plumer, I. Saika-Voivod, and B. W. Southern, *Phys. Rev. B* **91**, 224425 (2015).
- [4] K. Fukui and S. Todo, *J. Comput. Phys.* **228**, 2629 (2009).

# Variety of bulk-edge correspondence by numerical methods

Y. Hatsugai

*Division of Physics*

*Faculty of Pure and Applied Sciences, University of Tsukuba*

*1-1-1 Tennodai, Tsukuba 305-8571, Ibaraki, Japan*

Topological phases are surely one of the recent focuses of the condensed matter society. Without relying on the symmetry breaking, many of the interesting phases have been identified as non trivial. The class includes the integer/fractional quantum Hall states, the quantized spin Hall states as the topological insulators, graphene and so on. The common feature is that there exist localized modes near the system boundaries or geometrically localized defects. This emergence of the edge states itself characterizes the bulk before making the boundary. Then the edge state is a sort of order parameter for the topological phases. This is a physical observable. Except this emergence of the edge states, the bulk is featureless for the topological state. Now we have many examples. Some of them are surface Dirac cones of the topological insulators, Majorana/Andreev bound states of unconventional superconductors and the Fujita state of zigzag boundary of graphene. Although the edge states characterize the bulk, the reverse is also true. The emergence of the edge states is predicted by bulk without making the boundary using topological invariants of the bulk. This topological invariant is usually hidden in the sense that the direct experimental measurement is difficult. As for a model hamiltonian, it is not the case and one may calculate the invariants/quantized quantities numerically. This is an advantage of the numerical works. These invariants are mostly constructed by the Berry connection of the quantum mechanical state as the quantized Berry phases and the Chern numbers.

This inter-relation is the bulk-edge correspondence. The bulk and the edges are closely related. In the project, we have tried to get another important realization of the bulk-edge correspondence to confirm its variety and universality using several numerical methods.

The validity of the bulk-edge correspondence is not limited to the quantum mechanics. It is also justified and quite productive for the photonic systems as a world governed by the classical Maxwell equation and even for the classical mechanics where the classical Newton equation determines everything. We have justified the bulk-edge correspondence for the mechanical graphene that is a spring-mass model on the honeycomb lattice[1](Fig.1). This bulk-edge correspondence is generically discussed by using the classic analogue of the Berry phase, that is, the Hannay angle[2]. Also more than the well established quantization of the Berry phase into  $\pi$ , anomalous/fractional quantization is also investigated in the project and used to identify several interesting phases in quantum spins in a magnetic field[3]. Another important result obtained in the project is that we have successfully reproduced the phase diagram of the Kane-Mele model that is a standard model of the topological insulator in 2D using the entanglement Chern number (EC)[4](Fig.2). The EC is a new topological tool proposed recently and here, in the project, we have demonstrated its validity.

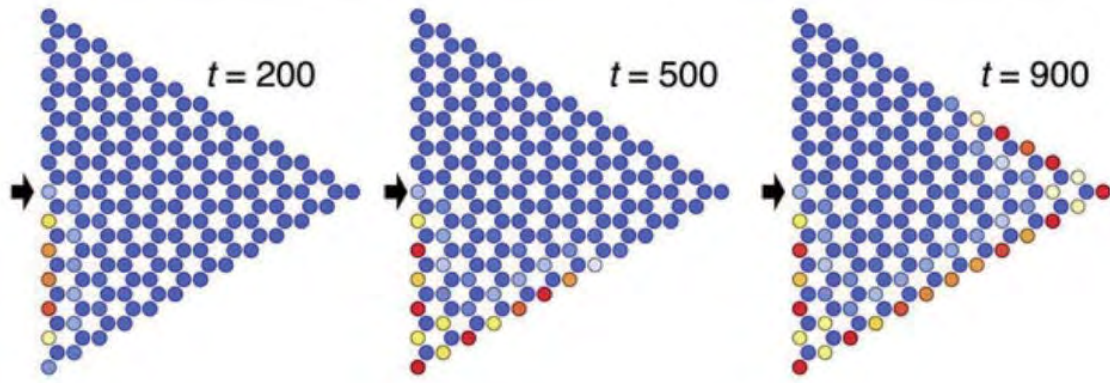


Figure 1: Classical analogue of the edge states: a localized chiral propagating mode of the Newton equation (a spring mass model) on a honeycomb lattice[1].

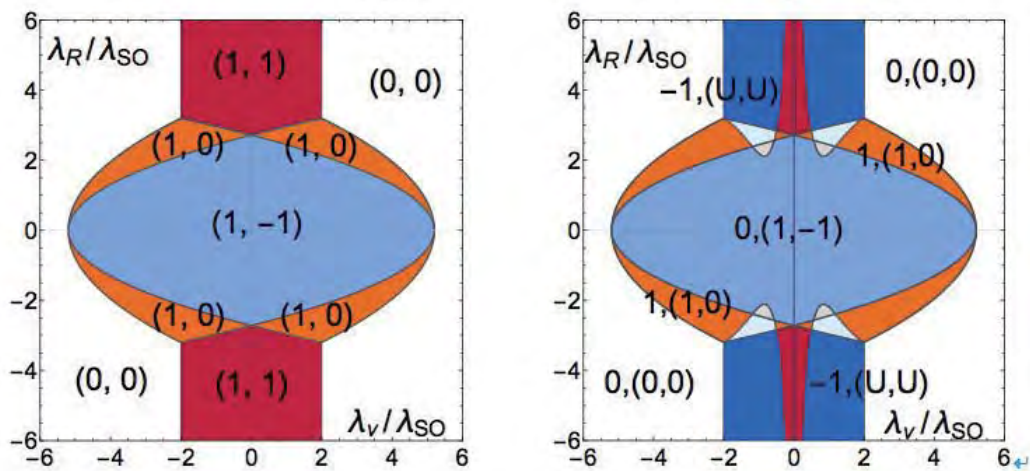


Figure 2: Various phases of the extended Kane-Mele model with the Zeeman term. (Entanglement) Chern numbers are effective to characterize the phases[4].

## References

- [1] "Manipulation of Dirac Cones in Mechanical Graphene", Toshikaze Kariyado, Yasuhiro Hatsugai, Scientific Reports **5**, 18107 (2015).
- [2] "Hannay Angle: Yet Another Symmetry-Protected Topological Order Parameter in Classical Mechanics", Toshikaze Kariyado, Yasuhiro Hatsugai, Journal of the Physical Society of Japan, **85**, 043001 (2016).
- [3] "Topological Order Parameters of the Spin-1/2 Dimerized Heisenberg Ladder in Magnetic Field", Toshikaze Kariyado, Yasuhiro Hatsugai, Phys. Rev. **B91** 214410 (2015).
- [4] "Entanglement Chern Number of the Kane-Mele Model with Ferromagnetism", Hiromu Araki, Toshikaze Kariyado, Takahiro Fukui, Yasuhiro Hatsugai, Journal of the Physical Society of Japan, **85**, 043706 (2016), selected as "Editor's choice".

## Characterization of thermal transport at nanostructure interface

Junichiro SHIOMI

*Department of Mechanical Engineering,*

*The University of Tokyo, 7-3-1, Hongo, Bunkyo-ku, Tokyo, 113-8656*

Desirable thermal boundary conductance (TBC), which is a measure of interfacial thermal transport, is dependent on thermal management applications. For instance, high TBC and low TBC are respectively demanded in thermal dissipation and thermal insulation devices. At the interface between two dissimilar semiconducting materials, TBC is mainly dominated by phonons (quanta of lattice vibration). Since the TBC is determined by not only spectral mismatch of phonons in two composed materials, but also an interfacial state (local atomic configuration, bond, etc.), in order to achieve high (low) TBC value, large (small) spectral mismatch between phonons in bulk and coherent (incoherent) atomic configuration at interface are required.

On the other hand, a manipulation of TBC value has been also required in thermoelectrics that is capable of converting wasted heat to electricity. Thermoelectric energy conversion efficiency is here determined by the figure of merit,  $Z$ , which is expressed as  $Z=S^2\sigma/\kappa$  in terms of electrical conductivity  $\sigma$ , Seebeck coefficient  $S$ , and thermal conductivity  $\kappa$  of material [1]. As seen, since the  $Z$  is inversely proportional to an inverse of  $\kappa$ , thermal conductivity reduction is one of effective approaches that enhance thermoelectric performance. Therefore several approaches including nanostructuring and alloying have been utilized in experiment.

Among several approaches, it has been demonstrated that poly-nanocrystalline can largely reduce thermal conductivity without significantly altering electrical properties of material [2]. The reduction of thermal conductivity by poly-nanocrystalline is mainly attributed to boundary scattering of phonons due to increment of specific interfacial area. However, the investigation to measure exact TBC value between nanoparticles in the poly-nanocrystal is limited due to the difficulty of measurement. Therefore we have recently proposed a new approach to isolate an actual nanoparticle-interface and measure its TBC value by means of time-domain thermoreflectance (TDTR)

technique (M. Sakata, *et al.* [3]).

In this method, we can measure the TBC at silicon-silicon smooth interface and also evaluate an influence of surface contamination and mirror index difference of sintered Si-Si interface to TBC value. These knowledge can lead to tailoring interfacial structure and manipulation of interfacial phonon transport.

In order to get insight into phonon transport at such well established interface structure, we have numerically calculated TBC value of same structure observed in experiment. In this calculation, firstly, by applying the image analysis technique to high-resolution TEM image, we have extracted atomic configurations at interface (Fig. 1(a)). Next we have performed molecular dynamics simulations to obtain the interface structure similar with TEM image (Fig. 1(b)). Finally, by performing independently non-equilibrium molecular dynamics and Green's function method, we have evaluated the correlation between actual interface structure and phonon-mode-dependent TBC (L. Feng, *et al.* [4]) (Fig. 1(c)).

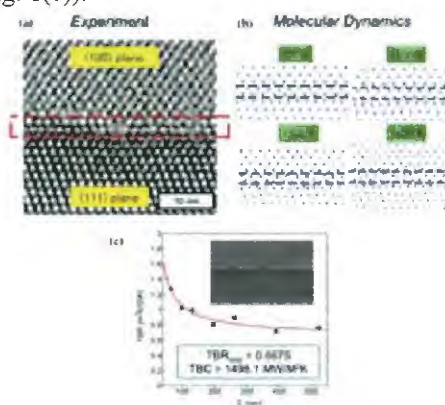


Fig. 1 (a) High-resolution transmission electron microscopy (TEM) image of Si(100)-Si(111) interface [3]. (b) Si(100)-Si(111) interfaces obtained by molecular dynamics simulations with different conditions. (c) Length-dependent thermal boundary

resistance (inverse of TBC) at 300 K [4].

As described above, in order to effectively suppress phonon conduction in material, structural manipulation by means of nanostructuring is effective. Here a key challenge to further reduce thermal conductivity and improve thermoelectric performance is to predict the relation between thermal conductivity reduction and the representative length scales of nanostructure, however, that requires the knowledge in mode-dependent contribution to thermal conductivity, i.e., thermal conductivity spectrum.

Here a difficulty arises: unlike electrical conductivity that can be attributed to electrons and holes around Fermi surface, distribution of phonons contributing to heat conduction is wide in energy space. For instance, in single-crystal silicon, phonons with frequency up to 16 THz and mean free paths (MFPs) up to 10  $\mu\text{m}$  noticeably contribute to heat conduction [5], which indicates that single kind nanostructure cannot cover with overall phonons contributing to heat conduction.

For the calculation of thermal conductivity spectrum of material, the first-principles-based anharmonic lattice dynamics (FP-ALD) method ([5], J. Shiomi, *et al.*, [6]) has recently become accessible, which enables us not only to quantitatively calculate thermal conductivity, but also to microscopically evaluate an influence of specific phonon-phonon scattering on heat conduction. Indeed, by performing the FP-ALD methods to several thermoelectric materials, we have revealed that large lattice anharmonicity yields intrinsically low thermal conductivity of lead chalcogenides (T. Shiga, *et al.*, [7]). Furthermore, by combining the FP-ALD method with first-principles-based molecular dynamics, we have succeeded in the thermal conductivity calculation of perovskite  $\text{SrTiO}_3$  that is the phase-transition material, and showed wide adoptability of FP-ALD scheme (L. Feng, *et al.*, [8]).

In principles, one can apply FP-ALD method to any materials. However, due to its high computational cost, it is hard to apply the FP-ALD method to numerous materials in order to obtain thermal conductivity spectrum. Therefore we have developed new empirical model that describes thermal conductivity spectrum of a crystal in terms only of harmonic phonon properties and bulk thermal conductivity.

In the model, while harmonic phonon properties (heat capacity and group velocity) are accurately calculated by first-principles-based (harmonic) lattice dynamics, relaxation time, which is caused by lattice anharmonicity, is modelled by the scattering phase space

(momentum-conserving two phonon density of states) and Klemens model at the classical model. By validating the model against the FP-ALD results, we have confirmed the current model reproduces the overall profiles of thermal conductivity spectra of several materials with different structural complexities and thermal conductivities (Fig. 2) (T. Shiga, *et al.*, [9]).

Since interfacial phonon transport depends on both bulk phonon property and interface structure, we have independently conducted atomistic simulations in order to calculate thermal boundary conductance (TBC) and phonon conduction in bulk. For the interfacial phonon transport, by performing molecular dynamics and Green's function method, we have calculated the TBC at Si-Si interface whose atomic configurations can be comparable with experimental ones. As for phonon transport in bulk material, we have proposed new empirical method that describes mode-dependent thermal conductivity in terms only of harmonic phonon properties and bulk thermal conductivity. Combination of these two approaches leads to comprehensive understanding of thermal transport at and around interface.

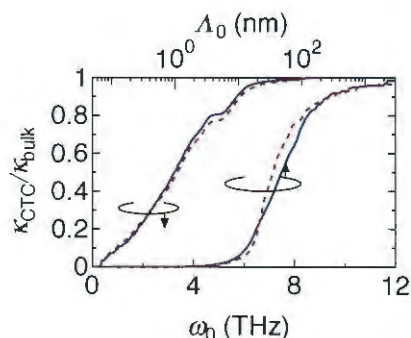


Fig. 2 Cumulative thermal conductivities of half-Heusler ZrCoSb at frequency and MFP spaces calculated from FP-ALD and the current model.

#### References

- [1] H. J. Goldsmid, *Introduction to Thermoelectricity* (2009).
- [2] B. Poudel, *et al.*, *Science* **320**, 634 (2008).
- [3] M. Sakata, T. Hori, T. Oyake, J. Maire, M. Nomura, J. Shiomi, *Nano energy, Rapid communication*, **13**, 601 (2015).
- [4] L. Feng, M. Ohnishi, T. Shiga, and J. Shiomi, **In preparing**.
- [5] K. Esfarjani, *et al.*, *Phys. Rev. B* **84**, 085204 (2011).
- [6] J. Shiomi, K. Esfarjani, G. Chen, *Phys. Rev. B* **84**, 104302 (2011).
- [7] T. Shiga, J. Shiomi, J. Ma, O. Delaire, T. Radzyunski, A. Lusakowski, K. Esfarjani, and G. Chen, *Phys. Rev. B* **85**, 155203 (2012).
- [8] L. Feng, T. Shiga, and J. Shiomi, *Appl. Phys. Express* **8**, 071501(2015).
- [9] T. Shiga, D. Aketo, L. Feng, and J. Shiomi, **submitted**

# Computational study of the mechanism of voltage sensing proteins

Yu TAKANO,<sup>1</sup> Yasushige YONEZAWA,<sup>2</sup> and Hiroko KONDO<sup>1</sup>

<sup>1</sup>*Graduate School of Information Sciences, Hiroshima City University, 3-4-1 Ozuka-Higashi, Asa-Minami-Ku, Hiroshima 731-3194*

<sup>2</sup>*High Pressure Protein Research Center, Institute of Advanced Technology, Kindai University, 930 Nishimitani Kinokawa, Wakayama 649-6493*

The voltage-gated proton channel, VSOP, [1,2] consisting of the four-transmembrane domain homologous to the voltage sensor in the voltage-gated potassium channel is activated by both the membrane potential and the pH gradient. Unlike other voltage-gated ion channels, the voltage-sensor domain of VSOP has a function as a pore. Though the X-ray crystallographic structure of VSOP with zinc ions in the resting state was obtained [3], the mechanism of proton permeation still remains unclear. Here we aim to clarify the effect of zinc ion on the activation of VSOP and a mechanism of proton permeation by using the molecular dynamics (MD) simulation.

We performed the simulations of wild-type (WT) VSOP with and without a zinc ion, and mutant proteins (E115S, D119S, and E115S/D119S) with a zinc ion. Zinc ions prevent the activation of VSOP, but the E115S/D119S mutant is known to be less sensitive to zinc ions. The differences in the tertiary structure and its fluctuation were

analyzed. We also created model structures of the activated state by using a homologous protein as a template, and performed the MD simulations for different protonation states. All simulations were carried out with GROMACS software package.

The results showed no large differences in the conformational fluctuations between WT and mutant proteins, suggesting that zinc ions physically prevent the conformational transition from the resting to the activated states. The simulations of model structures of the activated state also showed that two arginine residues formed salt-bridges with E115 and D119 that also interact with a zinc ion

## References

- [1] M. Sasaki et al., *Science* **312**, 589-592 (2006)
- [2] I. S. Ramsey et al., *Nature* **440**, 1213-1216 (2006)
- [3] K. Takeshita et al., *Nature Struct. Mol. Biol.* **21**, 352-357 (2014)

# Molecular Dynamics Simulation Study of Growth Promotion Mechanism of Ice Basal Plane by Antifreeze Protein

Hiroki NADA

*National Institute of Advanced Industrial Science and Technology (AIST)  
Onogawa16-1, Tsukuba, Ibaraki 305-8569*

Antifreeze proteins (AFPs), which are dissolved in the bodily fluids of organisms that lived in cold areas, function as inhibitors of ice crystal growth [1]. Studies on AFPs are important in regard to not only ice but also other materials. For example, elucidation of the mechanism of the ice crystal growth inhibition by AFPs provides insight into the control of crystal morphology and the design of functional composite materials in material technology.

In this project, we carried out a molecular dynamics (MD) simulation study on the mechanism of ice crystal growth in the presence of a winter flounder AFP. It is known that the AFP inhibits ice crystal growth on  $(20\bar{2}1)$  pyramidal planes and, therefore, the growth shape of ice crystals in the presence of the AFP is hexagonal bipyramid containing 12 equivalent flat  $(20\bar{2}1)$  planes [2].

Interestingly, when the hexagonal bipyramidal ice crystals are grown in the presence of the AFP, ice crystal growth on  $(0001)$  basal planes is "promoted". However, the mechanism of ice crystal growth promotion has not yet been elucidated. Therefore, in this project, we specially focused on the mechanism of ice crystal growth promotion on the basal plane in the presence of the AFP.

MD simulations were performed using a rectangular-parallelepiped system in which an ice crystal was sandwiched by two liquid water phases. The number of  $\text{H}_2\text{O}$  molecules in the

system was 9720. A six-site model of  $\text{H}_2\text{O}$  [3] was used to estimate the intermolecular interaction between a pair of  $\text{H}_2\text{O}$  molecules. Temperature and pressure were maintained at 270 K and 1 atm, respectively.

Owing to the facilities of ISSP supercomputer center (system B), slow ice crystal growth on the basal plane due to the growth mechanism of a layer-by-layer mode in real systems was successfully reproduced. MD simulations in the presence of the AFP have also been performed. The AFP did not bind to the basal plane stably. This result is consistent with the fact that ice crystal growth inhibition does not occur on the basal plane. Further simulations with a much longer run than in this study are needed to elucidate the mechanism of ice crystal growth promotion on the basal plane.

## References

- [1] H. Nada and Y. Furukawa: *Polym. J.* **44** (2012) 690.
- [2] H. Nada and Y. Furukawa: *J. Phys. Chem. B* **112** (2008) 7111.
- [3] H. Nada and J.P.J.M. van der Eerden, *J. Chem. Phys.*, **118** (2003) 7401.

# Simulation of collective migrations induced by the cell-cell adhesion and the cell polarity

Katsuyoshi Matsushita  
*Cybermedia Center, Osaka University*  
*Machikaneyama, Toyonaka 560-0043*

We have investigated the collective cell migration of *Dictyostelium discoideum* (Dicty). Here, collective cell migration is a collective motion of cells, in which the cells mechanically contact with each other and they form an order state in cell polarity related to their motion [1]. The collective migration is indispensable for the development of the fruiting body formation of Dicty.

In collective cell migration, Dicty exhibits various styles of intercellular contact when the effect of an adhesion molecule is inhibited. Therefore, the style of intercellular contact strongly reflects intercellular interaction through cell-cell adhesion with adhesion molecule. The style of side-by-side contact is observed in the case of inhibition of DdCad1 [2]. Here side-by-side contact is intercellular contact in the direction perpendicular to the cell polarity as shown in Fig. 1(a). Since this protein is known to have high concentration in the direction of cell polarity, we can expect that the intercellular contact in the direction of the cell polarity as shown in Fig. 1(b). Thus, the formation of side-by-side contact is seemingly peculiar observation.

The clarification of the relation between the style of intercellular contact in collective cell migration and cell-cell adhesion is important to promote our understanding of collective cell migration. To clarify this, we carried out a simulation using cellular Potts model [3] where the concentration of cell-cell adhesion protein is correlated with the direction of cell polarity.

Through this simulation, although the concentration is in the direction of cell polarity, we observe the formation of side-by-side contact. Namely, we show that the concentration of DdCad1 is consistent with the experimental observation of side-by-side contact [4]. This result implies that the side-by-side contact is a cooperation effect between the cell-cell adhesion and cell motility.

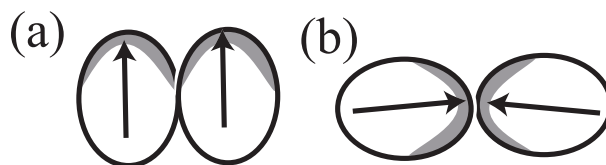


Figure 1: (a) side-by-side contact and (b) expected contact on the basis of the concentration of adhesion protein. Gray region indicates the high concentration of adhesion protein. Arrow indicates the direction of cell polarity.

## References

- [1] M. H. Köpf, *Phys. Rev. E* 91, 012712 (2015).
- [2] H. Beug, F. E. Katz, and G. Gerisch, *J. Cell Biol.* 56,
- [3] F. Graner and J. A. Glazier, *Phys. Rev. Lett.* 69, 2013 (1992).
- [4] K. Matsushita, submitted.

# Heat Transfer Characteristics of Condensate Film Flow along Vertical Plates with Microscopic Grooves

Takahiro ADACHI

*Department of Mechanical Engineering, Akita University  
Tegata-Gakuen 1-1, Akita, Akita 010-8502*

The characteristics of thin, falling liquid films due to condensation along a vertical plate have been of interest to engineers, for example, in plate-type absorber, plate-type condenser and so on. In order to enhance the heat transfer, fluted parts along the streamwise direction have been established on the plate. This is because the liquid film spreads as thinly as possible over the plate surface since strong surface tension aids in the removal of film from the top to bottom of the fluted parts, thereby producing a very thin liquid film. This is called a drainage effect[1].

On the other hand, little research was done on the film flow along a plate with a grooved part setting perpendicular to the streamwise direction due to some mathematical difficulties. Therefore, our objective in this study is to clarify how the grooved part affects the flow patterns and heat transfer.

We consider a liquid film flow along a plate with a rectangular groove setting perpendicular to the stream-wise direction on its surface. Figure 1 shows a geometry of the problem and the coordinate system. The  $x$ -axis is taken to be parallel to the vertical direction and the  $y$ -axis to be perpendicular to it. Nondimensional parameters to characterize the plate configuration, height  $h$  of the groove, width of the groove  $w_b$ , inlet length  $w_i$  and outlet length  $w_o$  are, using  $\delta_0^*$  at the inlet as a characteristic length, defined as

$$h = \frac{h^*}{\delta_0^*}, \quad w_b = \frac{w_b^*}{\delta_0^*}, \quad w_i = \frac{w_i^*}{\delta_0^*}, \quad w_o = \frac{w_o^*}{\delta_0^*} \quad (1)$$

where we represent physical quantities with their dimensions by attaching a superscript \* to them, and the total plate length is  $L =$

$w_i + w_b + w_o$ . The characteristic length  $\delta_0^*$  can be derived from Nusselt's film theory such as

$$\delta_0^* = \left( \frac{3\nu_l^* Q^*}{g^*} \right)^{1/3}, \quad (2)$$

where  $\nu_l^*$ ,  $g^*$  and  $Q^*$  are dynamic viscosity of the fluid, gravitational acceleration and flow rate, respectively.

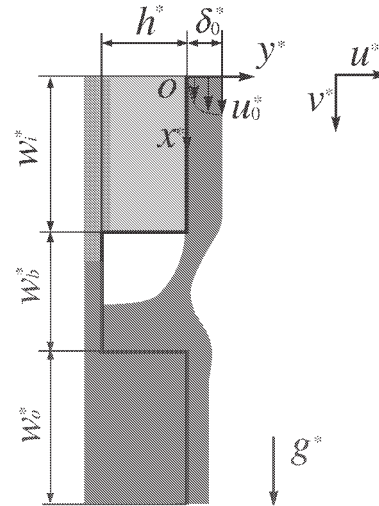


Fig.1 Geometry and coordinates.

We assume that the flow is two-dimensional because the film flow is thin and the depth in the spanwise direction of plate is large enough. Moreover, the fluid is assumed to be incompressible and the shear stress from the gas phase side can be negligible. Then we make non-dimensional the following quantities, by using characteristic length  $\delta_0^*$  and surface velocity at the reference point as  $u_0^* = \rho_l^* g^* \delta_0^{*2} / (2\mu_l^*)$  which is also derive from Nusselt's film theory, as

$$\mathbf{x} = \frac{\mathbf{x}}{\delta_0^*}, \quad \mathbf{u} = \frac{\mathbf{u}}{u_0^*}, \quad t = \frac{t^* u_0^*}{\delta_0^*}, \quad p = \frac{p^*}{\rho_l^* u_0^{*2}},$$

$$\rho = \frac{\rho^*}{\rho_l^*}, \quad \mu = \frac{\mu^*}{\mu_l^*}. \quad (3)$$

This time, we proceed our calculations not only for liquid phase but also for gas phase. Then, the governing equations for the velocities and pressure are written in non-dimensional forms as

$$\nabla \cdot \mathbf{u} = 0, \quad (4)$$

$$\rho \left\{ \frac{\partial \mathbf{u}}{\partial t} + (\mathbf{u} \cdot \nabla) \mathbf{u} \right\} = \rho Fr \mathbf{e}_x - \nabla p - \frac{Fr}{Bo} \kappa \nabla H + \frac{1}{Re} \nabla \left[ \mu \{ \nabla \cdot \mathbf{u} + (\nabla \cdot \mathbf{u})^T \} \right], \quad (5)$$

Nondimensional parameters in the equations are the Reynolds number, Flude number and Bond number respectively defined as

$$Re = \frac{u_0^* \delta_0^*}{\nu^*}, \quad Fr = \frac{\delta_0^* g^*}{u_0^{*2}}, \quad Bo = \frac{\delta_0^{*2} \rho^* g^*}{\sigma^*}. \quad (6)$$

First, we solve the governing equations Eq. (4) and (5) for velocity and pressure fields numerically by Highly Simplified Marker and Cell (HSMAC) method using staggered grid system. In addition to HSMAC method for the velocity and pressure fields, we have used a Coupled Level-Set and Volume Of Fluid (CLSVOF) method[2,3] to determine the free surface between gas and liquid phases, where we have been dealing with a new approach to impose surface tension effect and discontinuous changes of physical quantities between liquid and gas phases. Namely, Ghost Fluid Method(GFM)[4] are examined as well as CLSVOF Mmethod in our program.

Before, we used CSF(Continuum Surface Force) model proposed by Brackbill et al.[5] in order to express the surface tension effect.

In such model, a continuous Heaviside function was used. However in this study, we have used a discontinuous Heaviside function in the Ghost Fluid method defined as

$$\begin{aligned} H(\phi) &= 1, & \text{if } \phi \geq 0, \\ &= 0, & \text{if } \phi \leq 0. \end{aligned} \quad (7)$$

Therefore, we can express the discontinuous changes of density and viscosity between the liquid and gas phased as

$$\rho = \frac{\rho_g^*}{\rho_l^*} (1 - H(\phi)) + H(\phi), \quad (8)$$

$$\mu = \frac{\mu_g^*}{\mu_l^*} (1 - H(\phi)) + H(\phi). \quad (9)$$

This leads to the more realistic calculation results in our study.

However, the treatment of condensation is very difficult. In addition, iteration process in HSMAC spends much time of about 80% to total time in our code. So we are now trying to parallelize the part by using MPI.

## References

- [1] R. Gregorig, Z. Angew. Math. Phys., Vol. 5, (1954) 36.
- [2] M. Sussman, E. G. Puckett. J. Comput. Phys., Vol. 162, (200) 301.
- [3] G. Son, and N, Hur. Numer. Heat Transf., Part B, Vol. 42, (2002) 523.
- [4] G. Son, and V. K. Dhir. Numer. Heat Transf., PArt B, Vol. 52, (2007) 153.
- [5] U. J. Brackbill, D. B. Kothe, and C. Zemach. J. Comput. Phys., Vol. 100, (1992) 335.

# Study on numerical method to solve $n$ -beam Takagi-Taupin equation for not coplanar $n$ -beam cases.

Kouhei OKITSU

*Institute of Engineering Innovation, University of Tokyo  
2-11-16 Yayoi, Bunkyo-ku, Tokyo 113-8656*

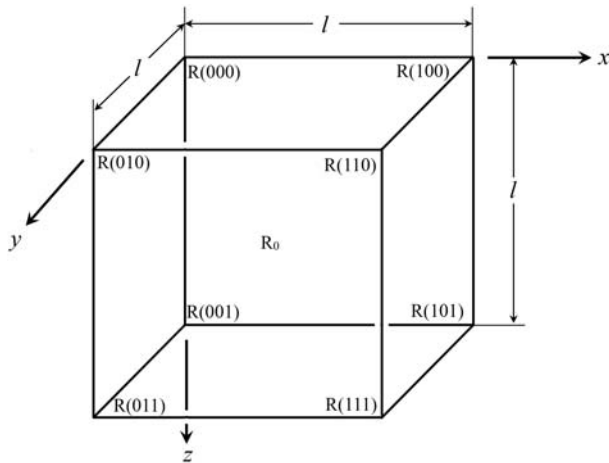


Figure 1: A small cube whose center is  $R_0$  and corners are  $R(n_x n_y n_z)$ , where  $n_x, n_y, n_z \in \{0, 1\}$ .

The present author has derived  $n$ -beam Takagi-Taupin equation that describes X-ray wavefields when  $n$  X-ray beams ( $n \in \{3, 4, 5, 6, 8, 12\}$ ) are simultaneously strong [1, 2] and has verified it by comparing experimentally obtained pinhole topograph images and computer-simulated ones obtained by numerically solving the equation. Excellent agreements were found between them [3, 4, 5]. This equation can be applied for coplanar  $n$ -beam cases in which  $n$  reciprocal lattice nodes are on a circle in reciprocal space.

However, the ultimate purpose of the study on  $n$ -beam cases is solving the phase problem of protein crystal structure analysis. In

cases of proteins, many ( $>12$ ) reciprocal lattice nodes always exist in the vicinity of surface of the Ewald sphere since reciprocal lattice node density is extremely large as compared with cases of small molecular-weight crystals. Therefore, an  $n$ -beam equation applicable for not coplanar  $n$ -beam cases is necessary. The equation that the present author derived is given by

$$\begin{aligned} \frac{\partial}{\partial s_i} D_i^{(l)}(\mathbf{r}) + \frac{i}{4\pi K} \nabla^2 D_i^{(l)}(\mathbf{r}) \\ = -i2\pi K \sum_{m=0}^1 S_{i,0}^{(m)} \gamma_i^{(m)} D_i^{(l)}(\mathbf{r}) \\ - i\pi K \sum_{j=0}^{n-1} \sum_{m=0}^1 C_{i,j}^{(l,m)} \chi_{h_i-h_j} D_j^{(m)}(\mathbf{r}), \quad (1) \end{aligned}$$

where  $i, j \in \{0, 1, \dots, n-1\}$ ,

$$l, m \in \{0, 1\}.$$

Here,  $\partial/\partial s_i$  is  $\mathbf{s}_i \cdot \text{grad}$ ,  $D$  is X-ray amplitude,  $i$  and  $j$  ( $i, j \in \{0, 1, 2, \dots, n-1\}$ ;  $n$  is number of waves) are ordinal number of the X-ray beams,  $l$  and  $m$  ( $l, m \in \{0, 1\}$ ) are polarization states and  $K$  is wavenumber ( $1/\lambda$ ) of X-rays in vacuum.  $S_{i,0}^{(m)}$  and  $C_{i,0}^{(l,m)}$  are polarization factors defined such that  $\mathbf{e}_j = S_{i,j}^{(m)} \mathbf{s}_i + C_{i,j}^{(0,m)} \mathbf{e}_i^{(0)} + C_{i,j}^{(1,m)} \mathbf{e}_i^{(1)}$ . Here,  $\mathbf{s}_i$  is a unit vector parallel to the wavevector of the  $i$ th X-ray beam and  $\mathbf{e}_i^{(0)}$  and  $\mathbf{e}_i^{(1)}$  are unit vectors taken such that  $\mathbf{s}_i$ ,  $\mathbf{e}_i^{(0)}$  and  $\mathbf{e}_i^{(1)}$  construct a right-handed orthogonal system.  $\gamma_i^{(m)}$  is angular deviation in the direction of  $\mathbf{e}_i^{(m)}$  of the  $i$ th

numbered Laue point  $La_i$  from 0th numbered Laue point  $La_0$ .

When dealing with a lattice displacement field  $\mathbf{u}(\mathbf{r})$ ,  $\chi_{h_i-h_j}$  can be replaced with  $\chi_{h_i-h_j} \exp [i2\pi(\mathbf{h}_i - \mathbf{h}_j) \cdot \mathbf{u}(\mathbf{r})]$ . Except for the case of grazing incidence, the second term of the left-hand side of (1)  $\nabla^2 D_i^{(l)}(\mathbf{r})$  is negligible small.

A method that the present author recently developed numerically to solve (1) is as follows, which can be read by referring to Fig. 1. At first,  $\partial/\partial s_i$  can also be described as follows,

$$\frac{\partial}{\partial s_i} = s_{i_x} \frac{\partial}{\partial x} + s_{i_y} \frac{\partial}{\partial y} + s_{i_z} \frac{\partial}{\partial z}. \quad (2)$$

Here,  $s_{i_x}$ ,  $s_{i_y}$  and  $s_{i_z}$  are  $x$ -,  $y$ - and  $z$ -components of  $\mathbf{s}_i$ , respectively. In Fig. 1, when the size of the cube  $l$  is sufficiently small,  $\partial D_i^{(l)}(\mathbf{R}_0)/\partial x$  at the center of cube  $\mathbf{R}_0$  can be approximated in the following two ways,

$$\begin{aligned} \frac{\partial D_i^{(l)}(\mathbf{R}_0)}{\partial x} &= D_i^{(l)}(\mathbf{R}(100))/2l \\ &\quad - D_i^{(l)}(\mathbf{R}(000))/2l \\ &\quad + D_i^{(l)}(\mathbf{R}(111))/2l \\ &\quad - D_i^{(l)}(\mathbf{R}(011))/2l. \end{aligned} \quad (3)$$

$$\begin{aligned} \frac{\partial D_i^{(l)}(\mathbf{R}_0)}{\partial x} &= D_i^{(l)}(\mathbf{R}(110))/2l \\ &\quad - D_i^{(l)}(\mathbf{R}(010))/2l \\ &\quad + D_i^{(l)}(\mathbf{R}(101))/2l \\ &\quad - D_i^{(l)}(\mathbf{R}(001))/2l. \end{aligned} \quad (4)$$

$\partial D_i^{(l)}(\mathbf{R}_0)/\partial y$  and  $\partial D_i^{(l)}(\mathbf{R}_0)/\partial z$  can also be approximated in two ways, respectively, similarly to (3) and (4). Therefore, there are eight independent equations to approximate  $\partial D_i^{(l)}(\mathbf{R}_0)/\partial s_i$ . On the other hand,  $D_i^{(l)}(\mathbf{R}_0)$  can be approximated in one way as follows,

$$D_i^{(l)}(\mathbf{R}_0) = \sum_{n_x=0}^1 \sum_{n_y=0}^1 \sum_{n_z=0}^1 D_i^{(l)}[R(n_x n_y n_z)]/8. \quad (5)$$

Therefore, there are  $16n$  independent difference equations described with  $D_i^{(l)}(R_{n_x} R_{n_y} R_{n_z})$  and  $D_j^{(m)}(R_{n_x} R_{n_y} R_{n_z})$  ( $i, j \in \{0, 1, 2, \dots, n-1\}$ ,  $l, m \in \{0, 1\}$ ,  $n_x, n_y, n_z \in \{0, 1\}$ ) that approximate (1).

When a crystal is divided by orthogonal  $N_m$  meshes whose size is sufficiently small, X-ray amplitudes at nodes whose number is less than  $16 \times n \times N_m$  can be obtained by solving  $16 \times n \times N_m$  simultaneous linear equations by least-square fitting.

This problem turns out to be a least square problem that can be solved by using for example lapack routine 'ZGels'. The present author is now coding a program to solve (1) based on the method described above.

## References

- [1] K. Okitsu: Acta Cryst A **59** (2003) 235-244.
- [2] K. Okitsu, Y. Yoda, Y. Imai, Y. Ueji, Y. Urano and X.-W. Zhang: Acta Cryst A **62** (2006) 237-247.
- [3] K. Okitsu, Y. Imai, Y. Ueji and Y. Yoda: Acta Cryst A **59** (2003) 311-316.
- [4] K. Okitsu, Y. Yoda, Y. Imai and Y. Ueji: Acta Cryst A **67** (2011) 557-558.
- [5] K. Okitsu, Y. Imai and Y. Yoda: In-Tech *Recent Advances in Crystallography* (2012) 67-86 [Invited].

# Some trials of predicting thermodynamic properties using the modified Lennard-Jones system

Kazuhiro Fuchizaki, Kazuma Okamoto, and Takahiro Sakagami  
*Department of Physics, Ehime University, Matsuyama 790-8577*

Yuta Asano

*Department of Applied Chemistry, Nagoya University, Nagoya, 464-8603*

We have been trying to “standardize” the modified Lennard-Jones (mLJ) system as a substitute for the ordinary LJ system [1]. In FY 2015, we used the mLJ system to discuss melting. The melting curve of the mLJ system could be satisfactorily predicted from the melting equation. The condition for Simon’s equation to be valid was identified in the course of derivation. This aspect is sketched in the following. We are now trying to find the equilibrium melting point using a one-phase approach, which is mentioned subsequently. The third topic concerns a recent trial for predicting density of a liquid mLJ system from its structural information. In the following all the quantities are expressed in reduced units, which are standard for the (m)LJ system.

## *Melting curve of the mLJ system*

With the one-phase approach, a melting curve is then given by the solution to the following thermodynamic identity.

$$\frac{d \ln T_m}{dp} = \frac{\Gamma_m}{K_m}, \quad (1)$$

where  $K_m$  is the bulk modulus at the melting point  $T_m$  for a pressure  $p$ , and  $\Gamma_m$  is defined by

$$\Gamma_m = -\frac{d \ln T_m}{d \ln v_m}. \quad (2)$$

Note here that  $T_m$  represents not the equilibrium melting point but rather a stability limit of solid state.  $v_m$  is the specific volume at  $T_m$ . An important step in the derivation of the melting curve was the evaluation of  $\Gamma_m$ ,

defined by Eq. (2), and  $K_m$  separately as functions of  $p$ . Various solutions, including Simon’s and Kechin’s curves, are obtainable depending on the degree of “Padé’s approximation” on the RHS of Eq. (1).

Our strategy in solving Eq. (1) does not take any versions of Lindemann’s law into account, but does reexpress Eq. (2) as

$$\Gamma_m = \frac{d \ln T_m / dp}{-d \ln v_m / dp}, \quad (2')$$

noting that  $p$  is the only independent variable along a melting curve.

Isothermal–isobaric molecular simulation for the mLJ system with 6912 particles was extensively carried out to establish the equation of state (EOS) of the solid phase. A preliminary result was described in 2014 activity report. The accurate EOS was reported in Ref. [2], and was assumed to be valid until melting. The EOS then could give  $K_m$  and its first pressure derivative at the reference state. Our simulation data allowed us to evaluate the  $p$ -dependence of  $\ln T_m$  and  $\ln v_m$  in Eq. (2’), from which  $\Gamma_m$  and its first pressure derivative at the reference state could be obtained. The Padé series converged at an intermediate stage to give Simon’s melting curve

$$T_m = T_{m0} \left( 1 + \frac{\Delta p}{\pi_0} \right)^{1/c_s}, \quad (3)$$

where  $\Delta p = p - p_0$  with  $p_0 = 2.417 \times 10^{-3}$  and  $T_{m0} = T_m|_{p_0} = 0.752$ , as the solution to

Eq. (1). The predicted values for the parameters were  $\pi_0 = 6.50(8)$  and  $c_S = 1.44(20)$ , which are almost comparable with those obtained by the direct fit of the melting points to Eq. (3). We have explicitly shown that Simon's equation becomes exact when  $\Gamma'_m|_{p_0} = 0$  [3]. This criterion was found to be fulfilled for the melting curve of the mLJ solid. We have thus arrived at the significant conclusion that the melting curve of the mLJ solid is exactly captured by Simon's equation [4].

#### *A trial implementation of the nonequilibrium relaxation (NER) method*

The equilibrium solid–liquid phase boundary of the mLJ system has been already reported [5]. The boundary was determined using a costly two-phase approach. The situation motivated us to look for a costless method to determine the boundary with comparative accuracy. The NER was employed to this end.

Two mLJ systems, one is in solid state and the other in liquid state, with different densities were combined together to form a rectangular parallelepiped composite system, in which the solid–liquid boundary is to be moved freely under isobaric and isothermal conditions. The Parrinello–Rahman barostat and Nosé–Hoover thermostat were used to control pressure and temperature, respectively. The shape of the combined system was kept unchanged. Figure 1 shows time variations in density of the composite system consisting of 20512 particles (in which 6912 particles were initially on the solid side) at temperatures indicated under  $p = 1.0$ . The density approaches that of the solid phase at  $T = 0.71$  whereas it approaches the liquid density at  $T = 0.72$ , implying that the melting point is located between the two temperatures. However, the expecting  $T_m \simeq 0.715$  is somewhat higher than the accurate result of 0.693. Examining the difference is now in progress.

#### *A new approach for estimating the density of noncrystalline substances*

A new trial for estimation of density from

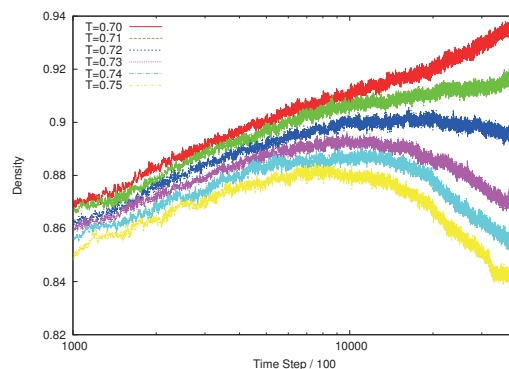


Figure 1: Time variation in density of the combined system kept at temperature indicated under  $p = 1.0$ .

structure factors of noncrystalline systems was examined based on the working ansatz: noncrystalline substances would be structurally similar provided that they are under thermodynamically similar circumstances. By rescaling the length of the reference structure with the known density, the structures expected to be realized at nearby thermodynamic conditions were simulated, thereby allowing us to compare the actual density of the realized state with the predicted density. The ansatz was inspected by simulating the structures along an isothermal or an isobaric path emanating from the reference state. We thus arrived at a conjecture that a liquid takes a more similar structure when varied along rather than away from the melting curve [6].

#### References

- [1] K. Fuchizaki: Read at 4th CCMS, ISSP, November 12–14, 2014.
- [2] K. Fuchizaki, K. Okamoto, and S. Doi: *J. Phys. Soc. Jpn.* **84** (2015) 085002.
- [3] K. Fuchizaki and Y. Asano: *J. Phys. Soc. Jpn.* **84** (2015) 064601.
- [4] K. Fuchizaki and K. Okamoto: *Phys. Lett. A* **380** (2016) 293.
- [5] Y. Asano and K. Fuchizaki: *J. Chem. Phys.* **137** (2012) 174502.
- [6] T. Sakagami, K. Fuchizaki, and K. Ohara: submitted to *J. Phys.: Condens. Matter*.

## Ground-State Phase Diagram of an Anisotropic $S=1/2$ Two-Leg Ladder with Different Leg Interactions

Takashi Tonegawa

*Professor Emeritus, Kobe Univ. and Visiting Professor, Osaka Prefecture Univ.*

The purpose of this report is to explore the ground-state phase diagram of an anisotropic  $S=1/2$  two-leg ladder with different leg interactions by using mainly numerical methods. We express the Hamiltonian which describes this system as

$$\begin{aligned} \mathcal{H} = & J_{\text{leg},a} \sum_{j=1}^L \vec{S}_{j,a} \cdot \vec{S}_{j+1,a} \\ & + J_{\text{leg},b} \sum_{j=1}^L \vec{S}_{j,b} \cdot \vec{S}_{j+1,b} \\ & + J_{\text{rung}} \sum_{j=1}^L [\vec{S}_{j,a}, \vec{S}_{j,b}]_{\Delta} \end{aligned} \quad (1)$$

with

$$[\vec{S}_{j,a}, \vec{S}_{j,b}]_{\Delta} \equiv S_{j,a}^x S_{j,b}^x + S_{j,a}^y S_{j,b}^y + \Delta S_{j,a}^z S_{j,b}^z. \quad (2)$$

Here,  $\vec{S}_{j,\ell} = (S_{j,\ell}^x, S_{j,\ell}^y, S_{j,\ell}^z)$  is the  $S=1/2$  operator acting at the  $(j, \ell)$  site assigned by rung  $j$  and leg  $\ell (= a \text{ or } b)$ ;  $J_{\text{leg},a}$  and  $J_{\text{leg},b}$  denote, respectively, the magnitudes of the isotropic leg  $a$  and leg  $b$  interactions;  $J_{\text{rung}}$  denotes that of the anisotropic rung interaction, the  $XXZ$ -type anisotropy being controlled by the parameter  $\Delta$ ;  $L$  is the total number of rungs, which is assumed to be even. It should be noted that this system has a frustration when  $J_{\text{leg},a} J_{\text{leg},b} < 0$  irrespective of the sign of  $J_{\text{rung}}$  [1].

The most striking feature of the present system is the fact that, if the condition  $J_{\text{leg},a} + J_{\text{leg},b} = 0$  is satisfied, the following three states are the *exact eigenstates* of the Hamiltonian (1) [2]:

- 1) The state in which all rungs form the singlet-dimer  $((\alpha_{j,a}\beta_{j,b} - \beta_{j,a}\alpha_{j,b})/\sqrt{2})$  pair. This state is the direct-product singlet-dimer state.
- 2) The state in which all rungs form the triplet-dimer  $((\alpha_{j,a}\beta_{j,b} + \beta_{j,a}\alpha_{j,b})/\sqrt{2})$  pair. This state is the direct-product triplet-dimer state.
- 3) The state in which all rungs are in the state given by a linear combination of two ferromagnetic states,  $\cos\phi\alpha_{j,a}\alpha_{j,b} + \sin\phi\beta_{j,a}\beta_{j,b}$ , where  $\phi$  is an arbitrary phase. This state is the nematic state with  $\phi$ .

Here,  $\alpha_{j,\ell}$  denotes the  $S_{j,\ell}^z = +1/2$  state and  $\beta_{j,\ell}$  the  $S_{j,\ell}^z = -1/2$  state. Furthermore, it can be analytically shown that, when  $J_{\text{leg},a} + J_{\text{leg},b} = 0$ ,  $J_{\text{rung}} < 0$ , and the  $XY$ -type anisotropy of rung interactions is

sufficiently strong  $(1 - \frac{2|J_{\text{leg},a}|}{|J_{\text{rung}}|} \gg \Delta \geq 0)$ , the direct-product triplet-dimer state is the *exact ground state* of the system, and that, when  $J_{\text{leg},a} + J_{\text{leg},b} = 0$  and  $J_{\text{rung}} (> 0)$  is sufficiently large, the direct-product singlet-dimer state is the *exact ground state* of the system. It is noted that the above result concerning with the direct-product singlet-dimer state has been already shown by Tsukano and Takahashi [3]. We also note that all of the above results including the nematic state with  $\phi$  as well as the direct-product triplet-dimer and singlet-dimer states are applicable to systems in higher dimensions, in which units of two  $S=1/2$  spins form lattices [2].

When  $J_{\text{rung}} < 0$  and  $|J_{\text{leg},\ell}| \ll |J_{\text{rung}}|$ , by the use of the degenerate perturbation theory, we can map the present spin-1/2 ladder onto the one-dimensional spin-1 chain governed by the effective Hamiltonian  $\mathcal{H}_{\text{eff}}$ ; in the lowest-order of  $|J_{\text{leg},\ell}|/|J_{\text{rung}}|$ , it is given by

$$\mathcal{H}_{\text{eff}} = \sum_{j=1}^L \left\{ J_{\text{eff}} \vec{T}_j \cdot \vec{T}_{j+1} + D_{\text{eff}} (T_j^z)^2 \right\} \quad (3)$$

with

$$J_{\text{eff}} = \frac{1}{4}(J_{\text{leg},a} + J_{\text{leg},b}), \quad D_{\text{eff}} = \frac{1}{2}J_{\text{rung}}(\Delta - 1), \quad (4)$$

where  $\vec{T}_j$  is the pseudo  $S=1$  operator at the  $j$ th site, and  $T_j^z$  is its  $z$ -component. It is apparent that the above  $\mathcal{H}_{\text{eff}}$  is not applicable to the frustrated region of the original Hamiltonian (1), which includes the case where  $J_{\text{leg},a} + J_{\text{leg},b} = 0$ . In order to improve this point, higher-order perturbation calculations are indispensable. Chen *et al.* [4] have determined the ground-state phase diagram of this spin-1 chain, and showed, for example, that when  $J_{\text{eff}} = -1$ , the phase transition from the  $XY$  phase to the large- $D$  phase takes place at  $D_{\text{eff}} \simeq 1$ , as the value of  $D_{\text{eff}}$  increases from zero. From this result, we may conclude that in our spin-1/2 ladder with  $J_{\text{rung}} = -1$ , the phase transition between the  $XY$  phase and the triplet-dimer phase occurs at  $J_{\text{leg},a} + J_{\text{leg},b} \simeq 2(\Delta - 1)$  when  $J_{\text{leg},a} + J_{\text{leg},b} < 0$  (or, equivalently, when  $\Delta < 1$ ). It is noted that the large- $D$  phase in the spin-1 chain corresponds to the triplet-dimer phase in the present spin-1/2 ladder.

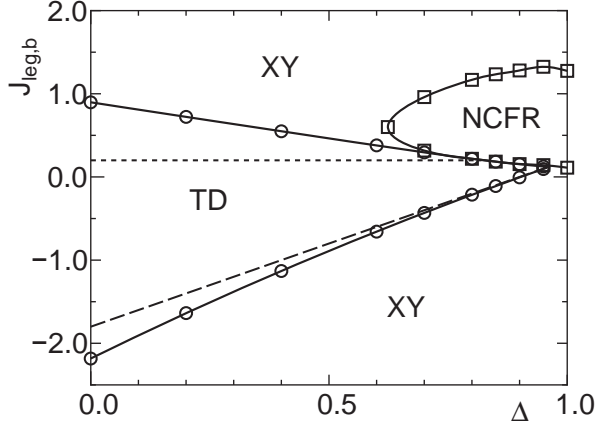


Figure 1: Ground-state phase diagram on the  $\Delta$  versus  $J_{\text{leg},b}$  plane for  $J_{\text{leg},a} = -0.2$  and  $J_{\text{rung}} = -1$ . Here, TD and NCFR stand, respectively, for triplet-dimer and the non-collinear ferrimagnet.

Choosing the values of  $J_{\text{leg},a}$  and  $J_{\text{rung}}$  as  $J_{\text{leg},a} = -0.2$  and  $J_{\text{rung}} = -1$ , respectively, we have numerically determined the ground-state phase diagram on the  $\Delta$  versus  $J_{\text{leg},b}$  plane, where  $0 \leq \Delta \leq 1$ . The obtained result is shown in Fig.1. This phase diagram consists of the triplet-dimer (TD) phase, the XY phase and the non-collinear ferrimagnetic (NCFR) phase [3,5] which has an incommensurate character. The solid lines with open circles shows the TD-XY transition lines, while that with open squares the NCFR-XY or the NCFR-TD transition line. On the broken line, where  $J_{\text{leg},b} = 0.2 (= -J_{\text{leg},a})$ , the direct-product TD state is the *exact ground state*. Furthermore, the dashed line shows the result of the degenerate perturbation calculation for the TD-XY transition line; it is in excellent agreement with the numerical result at least when  $|J_{\text{leg},b}|$  is not too large.

Since the phase transition between the TD and XY phases is of the Berezinskii-Kosterlitz-Thouless type [6], the phase transition line can be very accurately estimated by using the level spectroscopy method developed by Nomura and Kitazawa [7] in the following way. First, we calculate the finite-size critical value  $J_{\text{leg},b}^{(\text{cr})}(L)$  of  $J_{\text{leg},b}$  for given  $\Delta$  by solving numerically the equation,

$$E_0^{(\text{pb}c)}(L, 2) = E_0^{(\text{tb}c)}(L, 0, +1). \quad (5)$$

Here,  $E_0^{(\text{pb}c)}(L, M)$  is the lowest energy eigenvalue of the Hamiltonian (1) under periodic boundary conditions within the subspace characterized by both  $L$  and the total magnetization  $M$  defined by  $M = \sum_{j=1}^L (S_{j,a}^z + S_{j,b}^z)$ , and  $E_0^{(\text{tb}c)}(L, M, P)$  is that under twisted boundary conditions within the subspace characterized by  $L$ ,  $M$  and  $P (= +1$  or  $-1)$  which is the eigenvalue of the space inver-

sion operator with respect to the twisted bond. Then, we estimate the phase transition point  $J_{\text{leg},b}^{(\text{cr})}$  of the infinite system by extrapolating  $J_{\text{leg},b}^{(\text{cr})}(L)$  to  $L \rightarrow \infty$ . In practical calculations, we have extrapolated  $J_{\text{leg},b}^{(\text{cr})}(L)$ 's for  $L = 8, 10, 12$ , and  $14$  to  $L \rightarrow \infty$  by assuming that  $J_{\text{leg},b}^{(\text{cr})}(L)$  is a quadratic function of  $(1/L)^2$ . The results of the least-square fitting, for example, for  $\Delta = 0.6$  are given by  $J_{\text{leg},b}^{(\text{cr})} = -0.6570(1)$  and  $0.3787(1)$ .

In order to estimate the phase transition line between the NCFR phase and one of the XY and TD phases, we have calculated, for various values of  $J_{\text{leg},b}$  and  $\Delta$ , the ground-state magnetization  $M_g$  by performing density-matrix renormalization-group (DMRG) calculations mainly for the finite-size system with  $2L = 72$  spins. (In a few cases, we have made sure that the results obtained for  $2L = 96$  and  $120$  agree with those for  $2L = 72$  within the numerical error.) In the NCFR region  $M_g$  is finite, while  $M_g = 0$  in the TD and XY regions; for example, the phase transition points for  $\Delta = 0.8$  are  $J_{\text{leg},b}^{(\text{cr})} = 0.2185(5)$  and  $1.1675(5)$ . The value of  $M_g$  depends on  $\Delta$  and  $J_{\text{leg},b}$  in the NCFR region. It is difficult, however, to clarify the order of this transition only by the DMRG method. We have also calculated the ground-state site-magnetization  $m_{j,a,g}$  by the DMRG method, and shown that the NCFR state has an incommensurate character by examining the Fourier transform of this quantity.

This work has been done in collaboration with T. Hikihara, K. Okamoto and T. Sakai.

[1] Vert recently, we [T. Tonegawa, K. Okamoto, T. Hikihara and T. Sakai: J. Phys.: Conf. Series **683** (2016) 012039] have discussed the ground-state phase diagram of an anisotropic  $S = 1/2$  ladder, in which leg interactions are antiferromagnetically uniform and isotropic, while rung interactions are ferromagnetically-antiferromagnetically alternating and have a common Ising-type anisotropy. This system is another example of the frustrated  $S = 1/2$  two-leg ladder.

[2] T. Hikihara, T. Tonegawa, K. Okamoto, T. Sakai and T. Momoi: in preparation.

[3] M. Tsukano and M. Takahashi: J. Phys. Soc. Jpn. **66** (1997) 1153.

[4] W. Chen, K. Hida and B. C. Sanctuary: Phys. Rev. B **67** (2003) 104401.

[5] S. Yoshikawa and S. Miyashita: J. Phys. Soc. Jpn. **74** (2005) Suppl. 71.

[6] Z. L. Berezinskii: Sov. Phys.-JETP **34** (1971) 610; J. M. Kosterlitz and D. J. Thouless: J. Phys. C: Solid State Phys. **6** (1973) 1181.

[7] K. Nomura and A. Kitazawa: J. Phys. A: Math. Gen. **31** (1998) 7341.

# Molecular Dynamics Simulation of Ferroelectrics Using a Shell Model

T. Hashimoto

*Research Center for Computational Design of Advanced Functional Materials (CD-FMat),  
National Institute of Advanced Industrial Science and Technology (AIST),  
Tsukuba Central 2, 1-1-1 Umezono, Tsukuba, Ibaraki 305-8568, Japan*

KNbO<sub>3</sub> is an ABO<sub>3</sub> type perovskite whose solid solution with other A site atoms could be a potential candidate for Pb free piezoelectric materials. KNbO<sub>3</sub> undergoes phase transitions among, listing from high temperature to low temperature, cubic (C), tetragonal (T), orthorhombic (O), and rhombohedral (R) phases. Despite its importance, the number of the experimental reports on the piezoelectric constants of KNbO<sub>3</sub> is small due to experimental difficulties. Molecular dynamics (MD) simulations using a shell model were performed that focus on room temperature piezoelectric properties of Li<sub>x</sub>K<sub>1-x</sub>NbO<sub>3</sub>[1]. In this study, we also performed MD simulations using the shell model[2, 3, 4], but we focused on the temperature dependence of the piezoelectric properties of the mother material KNbO<sub>3</sub>[5].

The piezoelectric constants were calculated by[6]  $d_{kij} = \frac{1}{k_B T} \langle \Delta M_k \Delta \eta_{ij} \rangle$ . Here,  $\eta_{ij} = \frac{1}{2} (H_0^{t-1} G H_0^{-1} - 1)$  is the strain tensor, where  $G = H^t H$  with  $H = \{\mathbf{a}, \mathbf{b}, \mathbf{c}\}$  representing the MD cell, and  $H_0$  is the reference state of  $H$ .  $\mathbf{M}$  is the total dipole moment of the MD cell.  $\Delta X$  represents  $X - \langle X \rangle$ , where  $X$  is  $M_k$  or  $\eta_{ij}$ .

The temperature dependences of piezoelectric constants were similar to those obtained by the Landau-Ginzburg-Devonshire (LGD) theory[7, 8]. The shear and some of the longitudinal piezoelectric constants changed by 200–300 % depending on the temperature. This arises from the temperature dependence of the dipole moment and the strain fluctua-

tions. We also calculated the temperature dependences of the longitudinal piezoelectric surface  $d_{33}^*$  of KNbO<sub>3</sub>. Due to the large temperature dependence of the piezoelectric constants, the  $d_{33 \text{ max}}^*$  surface changes significantly with temperatures[5].

## References

- [1] R. Machado, M. Sepiarsky, and M. G. Stachiotti, *Appl. Phys. Lett.* **103** (2013) 242901.
- [2] M. Sepiarsky, S. R. Phillpot, D. Wolf, M. G. Stachiotti, and R. L. Migoni, *Appl. Phys. Lett.* **76** (2000) 3986.
- [3] T. Hashimoto and H. Moriwake, *Mol. Simul.* **41** (2015) 1074.
- [4] T. Hashimoto and H. Moriwake, *Physica B* **485** (2016) 110.
- [5] T. Hashimoto and H. Moriwake, *J. Phys. Soc. Jpn.* **85** (2016) 034702.
- [6] A. García and D. Vanderbilt, *Appl. Phys. Lett.* **72** (1998) 2981.
- [7] M. Budimir, D. Damjanovic, and N. Setter, *J. Appl. Phys.* **94** (2003) 6753.
- [8] L. Liang, Y. L. Li, S. Y. Hu, L.-Q. Chen, and G.-H. Lu, *J. Appl. Phys.* **108** (2010) 094111.

# Large-scale simulations of semiconductor nanocrystals

Takamichi TERAO

*Department of Electrical, Electronic and Computer Engineering,*

*Gifu University, Yanagido 1-1, Gifu 501-1193*

Recently, glassy dynamics in interacting electron systems with geometrical frustration have attracted much attention. For example, an organic conductor with a triangular lattice was experimentally studied, and it was observed that the electronic system in the clean organic conductors freezes on cooling and a charge-cluster glass is formed [1]. Despite these studies, the behavior of electronic systems with geometrical frustration is still not fully understood, requiring further investigations of this problem.

It has been pointed out that these frustrated electron systems may show a non-equilibrium relaxation behavior similar to that found in Coulomb glass systems where both many-body electron–electron interactions and randomness of the system are present. The relaxational dynamics of the Coulomb glass model were investigated, and a transition from stationary to non-stationary dynamics at the equilibrium glass transition temperature of the system was observed. At low temperatures, the system exhibits glassy dynamics, and the two-time autocorrelation function shows aging owing to the lack of time translation invariance. The behavior of electronic systems with geometrical frustration is still not fully understood, requiring further investigations of this problem, and it is interesting to clarify their glassy behavior.

In this study, the hopping electron model on the Kagome lattice was investigated by kinetic

Monte Carlo simulations and the non-equilibrium nature of the system has been elucidated. We have numerically confirmed the presence of aging phenomena in the autocorrelation function  $C(t, t_w)$  obtained in the electron system of the geometrically frustrated lattice without any disorder. We have also studied the waiting-time distribution  $p(\tau)$  of hopping electrons of the system, and it was confirmed that the  $p(\tau)$  profile at lower temperatures obeys the power-law behavior. The power law dependence is a characteristic feature of the continuous time random walk (CTRW) behavior of the electrons in different systems such as the system on the Kagome lattice and that of the Coulomb glass, while the obtained  $p(\tau)$  profiles at higher temperatures differ between these two systems.

[1] T. Sato *et al.*, J. Phys. Soc. Jpn. 83, 083602 (2014).

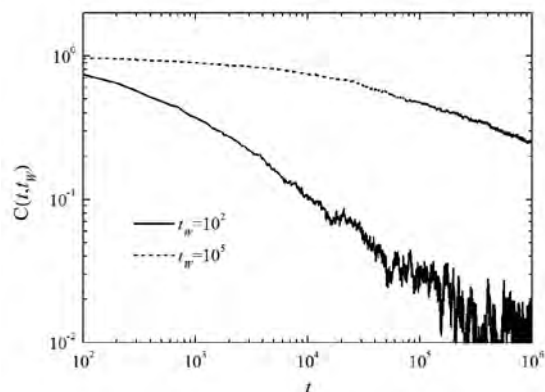


Fig. 1: Autocorrelation function  $C(t, t_w)$  on Kagome lattice

# Spin dynamics of frustrated quantum spin chain in magnetic field

Hiroaki ONISHI

*Advanced Science Research Center, Japan Atomic Energy Agency,  
Tokai, Ibaraki 319-1195*

The spin nematic state, which is a quantum spin analogue of the nematic liquid crystal, has been of great interest as a novel spin state. In this project, we have studied the spin nematic state in a spin- $\frac{1}{2}$  frustrated  $J_1$ - $J_2$  chain with ferromagnetic  $J_1$  and antiferromagnetic  $J_2$  in a magnetic field [1, 2, 3]. In the  $J_1$ - $J_2$  chain, a spin nematic state occurs at high fields, while a vector chiral state appears at low fields [4]. Here, we investigate the influence of an added Dzyaloshinskii-Moriya (DM) interaction.

To clarify the properties of the spin nematic state from the dynamical aspect, we analyze the dynamical spin structure factor,  $S^\alpha(q, \omega)$ , at zero temperature by exploiting a dynamical DMRG method [5]. Note that we calculate the spectral weight at  $q$  and  $\omega$  after one DMRG run with fixed  $q$  and  $\omega$ , so that we need to perform many runs according to the number of meshes to obtain a full spectrum in a wide range of the  $q$ - $\omega$  space. The computations are accelerated by parallel simulations utilizing the system B of the ISSP supercomputer.

In Fig. 1, we show results of  $S^-(q, \omega)$  in the spin nematic regime. We find a lowest-energy peak around  $q=\pi/2$  at a finite energy, which corresponds to the binding energy of a magnon pair. The overall spectral shape looks similar even if we consider the DM interaction, but the peak position shifts toward low energy, i.e., the gap decreases, indicating that the spin nematic state is suppressed due to the DM interaction, since it induces a helical spin state. Detailed analyses will be reported elsewhere [3].

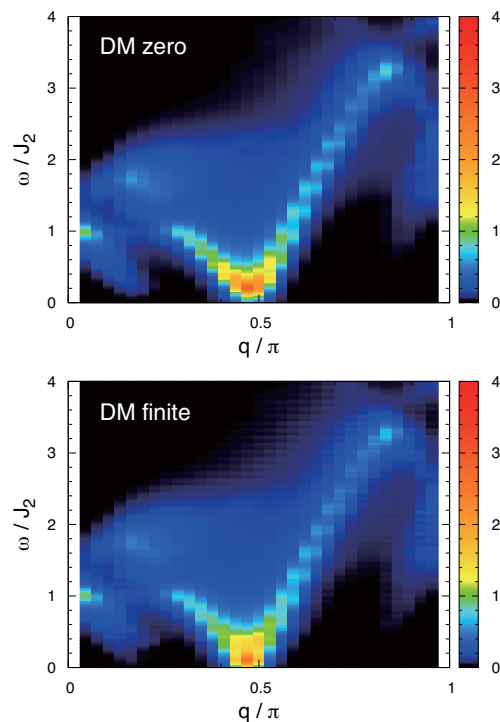


Figure 1:  $S^-(q, \omega)$  without and with the DM interaction.

## References

- [1] H. Onishi, J. Phys.: Conf. Ser. **592**, 012109 (2015).
- [2] H. Onishi, J. Phys.Soc. Jpn. **84**, 083702 (2015).
- [3] H. Onishi, in preparation.
- [4] T. Hikihara, L. Kecke, T. Momoi, and A. Furusaki, Phys. Rev. B **78**, 144404 (2008).
- [5] E. Jeckelmann, Phys. Rev. B **66**, 045114 (2002).

# Simulation of quantum response of graphene quantum devices

Koichi KUSAKABE

*Graduate School of Engineering Science, Osaka University*

*1-3 Machikaneyama, Toyonaka, Osaka 560-8531*

## 1. Introduction

The topological zero mode is known to appear at a tri-hydrogenated vacancy of graphene,  $V_{111}$ . [1, 2] Since one-body hybridization between the zero-energy eigen mode and Dirac modes is cut, relevant hybridization between the zero mode and Dirac modes of graphene is given by two-body interactions, which is given by super processes. [3] We have shown that the Coulomb interaction chooses the singlet ground state, which causes various characteristic low-energy phenomena including the Kondo effect. [4]

## 2. A new approach to nanographene molecular device

For a proof of the singlet ground state, the vacancy-centered armchair-edged nanographene [5] provides us a firm ground. On this network, when we consider a Hubbard model of the  $\pi$  electrons, the singlet ground state is exactly concluded. The degenerate single-particle levels of the quasi-localized zero mode (QLZM) and the  $\sqrt{3} \times \sqrt{3}$  zero mode (S3ZM) have vanishing first-order perturbation by the on-site Hubbard interaction letting the higher-order anti-ferromagnetic exchange relevant. There are various derivatives of VANG, where the edge states may appear at edge boundaries of the molecule. Thus, quantum dynamics may be designed to show correlation of QLZM and the edge states in their response to external electro-magnetic fields.

## 3. Kondo screening in graphene as a zero-gap-insulator

The VANG molecules may have a large size limit, where the inter-level spacing  $\Delta$  vanishes faster than the on-site effective interaction  $U_0$  in QLZM. This picture defined by VANG provides us a novel Kondo effect, where low-lying modes in the Dirac cone screen the  $s=1/2$  spin of QLZM. This may be a prototype of the zero-gap Kondo effect.

## 4. Hydrogen reaction processes relevant for hydrogen storage devices

The  $V_{111}$  structure and relating several hydrogenated vacancy structures of graphene can be used to strengthen chemical functions of graphene drastically. After providing control methods of charge transfer rates at various atomic sites of hydrogenated graphene, [6] we evaluated potential energy surfaces relevant for hydrogenation processes of a graphene vacancy. [7] The result strongly suggests a possible enhancement method of hydrogen storage ability of graphene by creation of the vacancy.

- [1] M. Ziatodinov, *et al.*: Phys. Rev. B **89** (2014) 155405. [2] S. Fujii, *et al.*: Faraday Discuss., **173** (2014) 10. [3] K. Kusakabe and I. Maruyama: Japanese patent No. 5447674. [4] N. Morishita, *et al.*: arXiv:1412.8589. [5] N. Morishita, *et al.*: arXiv:1604.06841. [6] G.K. Sunnardianto, *et al.*: J. Comput. Thero. Nanosci., in print. [7] G.K. Sunnardianto, *et al.*: J. Adv. Sci. Eng. Med., in print.

## Novel properties of low-dimensional electron systems at solid surfaces and finite electron systems in nanoparticles

Takeshi INAOKA

*Department of Physics and Earth Sciences, Faculty of Science,  
University of the Ryukyus, 1 Senbaru, Nishihara, Okinawa 903-0213*

Strain engineering is expected to achieve higher operation performance of Si devices through modification of the band structure, since the conventional downsizing approach is showing its limitations. We investigated the strain effect on electronic structure of the Si(001) surface and on bulk electronic structure of Ge.

Graphene (GPN) is a promising candidate for high speed electronic devices owing to its extremely high electron mobility. However, to realize effective switching performance, we need to introduce a band gap at the Dirac point. On the other hand, hexagonal boron nitride (h-BN) is a suitable template for creating an atomic-layer structure with GPN. We examined the gap opening in atomic-layer systems of GPN and h-BN.

To perform the above calculations, we used the program package 'Vienna ab initio Simulation Package' (VASP) [1,2] on the systems B and C.

### (1) Tensile strain effect on the electronic structure of the Si(001)-2x1 surface [3]

By forming a Si layer on a  $\text{Si}_{1-x}\text{Ge}_x$  buffer layer, we can apply biaxial tensile strain to the Si layer. We analyzed the electronic structure of the Si(001)-2x1 surface under biaxial tensile strain. No normal stress is a reasonable condition for the Si layer extended biaxially on the buffer layer. We assume a slab system of 30 atomic layers, and terminate dangling bonds on the other side by H atoms. Our thick slab enables us to identify the surface-resonance states extending into a deeper region. We employ the generalized gradient approximation (GGA). By minimizing the total energy, we optimize the structure in a unit cell under the condition of given biaxial extension of the unit cell.

Figure 1 shows the valence-band

dispersion on the  $\bar{\Gamma}-\bar{J}'$  line under (a) no strain and (b) 1.1 % biaxial tensility. This surface has an asymmetric surface dimer due to stabilization. The band S is the lower one of the surface-band pair that has its electron density concentrated on the up atom of the dimer. We can locate the surface states and the surface-resonance states by analyzing the electron-density distribution of each eigenstate. These states are indicated by squares in this figure. In the absence of

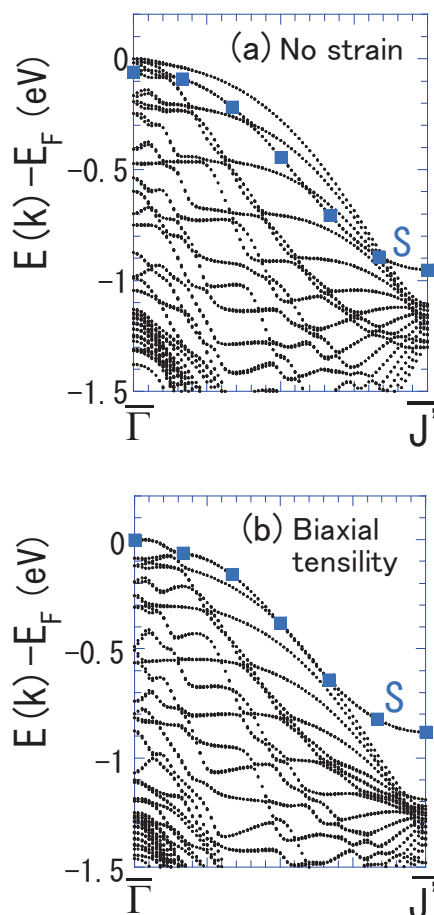


**Fig. 1** Valence-band dispersion of the Si(001)-2x1 surface under (a) no strain and (b) 1.1% biaxial tensile strain. As for details, see the text.

strain, these states lie below the upper boundary of the valence band of the semi-infinite system (thick slab in this calculation) except near the  $\bar{J}'$  point. However, when biaxial tensile strain is applied, these states shift to the upper boundary of the valence band. To be exact, tensile strain lowers energies of the surface or surface-resonance states less effectively than those of the valence-band states. Though we can expect that the surface-localized states are more sensitive to biaxial tensility, we can recognize that the in-plane tensile strain increases the apex angle of backbonds of the up atom of the dimer, and therefore, we can ascribe the above smaller energy fall of the surface-localized states under strain to weakening of the buckling stabilization.

## (2) Strain effect on the valence band of bulk Ge [4]

By means of combination of the hybrid density functional method and the first-principles-optimized  $\mathbf{k} \cdot \mathbf{p}$  method, we started to examine the strain effect on the valence band of bulk Ge. Assuming no normal stress and minimizing the total energy, we determined the normal and internal strain for each applied strain. The internal strain means the relative displacement of two atoms in a primitive unit cell. We considered [111] uniaxial and (111) biaxial strain, and paid special attention to the angle dependence of the hole effective-mass ratio  $m^*/m_e$ . Here, the angle was varied from the [111] direction to the  $[11\bar{2}]$  direction.

In 1% [111] uniaxial compression, the ratio  $m^*/m_e$  takes the smallest value 0.032 in the [111] direction, while, in 1% [111] uniaxial tensility, this value assumes the lowest value 0.038 in the  $[11\bar{2}]$  direction.

In (111) biaxial tensility, the ratio  $m^*/m_e$  takes the smallest value 0.022 in the [111] direction, while, in 1% (111) biaxial compression, this value assumes the lowest value 0.052 in the  $[11\bar{2}]$  direction.

We can obtain remarkably small effective masses in the strain direction of uniaxial compression, and in the normal direction to the biaxial tensility plane.

## (3) Electronic structure of atomic-layer systems of GPN and h-BN [5]

By means of the GGA combined with a recent revised version of the van-der-Waals (vdW) density functional (rev-vdW-DF2) [6], we examined the electronic structure of atomic-layer systems of GPN and h-BN.

First, we considered a GPN layer adsorbed on the h-BN substrate (6 layer slab). We took a  $\Gamma$ -centered  $16 \times 16 \times 1$   $k$ -point grid and a cutoff energy of 1200 eV. As the LDA calculation predicted [7], the most stable stacking type is the one where one of the two C atoms in a primitive unit cell of GPN sits just above a B atom and the other of the two C atoms above the center of a hexagonal BN ring. The binding energy per unit cell of the GPN layer with the BN substrate was found to be 125 meV, which is significantly larger than the LDA value of 62 meV. This difference originates from the vdW interaction included in our calculation. We obtained a band gap of 51 meV at the Dirac point.

Next, we considered a periodic arrangement of one GPN layer and three h-BN layers with the above stacking type. We chose a  $16 \times 16 \times 8$   $k$ -point mesh. Our calculation indicated that a gap opens along the dispersion line from the K to the H point in the Brillouin zone. The gap energy varies only slightly from 97 to 103 meV as we move from the K to the H point. This gap is about twice that of the above adsorbed GPN layer.

## References

- [1] G. Kresse and J. Hafner. Phys. Rev. B **47** (1993) 558-561.
- [2] G. Kresse and J. Furthmüller. Comput. Mat. Sci. **6** (1996) 15-50.
- [3] T. Inaoka, S. N. Takeda, and T. Shirasawa: to be prepared.
- [4] T. Inaoka, T. Tsuda, and S. Yanagisawa: unpublished.
- [5] T. Inaoka, M. Kaminuma, and S. Yanagisawa: unpublished.
- [6] I. Hamada: Phys. Rev. B **89** (2014) 121103 (R).
- [7] G. Giovannetti et al.: Phys. Rev. B **76** (2007) 073103.

# Development of parallelized codes for tensor network methods

Satoshi MORITA

*Institute for Solid State Physics, The University of Tokyo,  
Kashiwa-no-ha, Kashiwa, Chiba 277-8581*

Tensor network method is one of numerical methods for quantum and classical many-body systems. To achieve high accuracy simulation for interesting problems, one needs to increase bond dimensions of tensors. Unfortunately, the computational cost and the amount of necessary memory rapidly increase. Therefore we need to develop parallelized codes for tensor network methods.

The main operations in tensor network methods are “contraction” and “decomposition”. The former operation, which combines some tensors into one tensor, can be implemented using matrix-matrix product. With GPGPU porting support by ISSP, we developed MPI-parallelized CUDA codes of matrix-matrix product routines, pdgemm and pzgemm, in ScaLAPACK[1]. Our code of pdgemm[2] is 4.3 times faster than the original one for  $65536 \times 65536$  matrices on 72 nodes with 144 GPUs in ISSP supercomputer System B.

For the latter operation, singular value decomposition (SVD) and QR decomposition are typical. In the most case, however, the exact

decomposition is not necessary. For example, one 4-rank tensor with bond dimension  $\chi$  is decomposed into two 3-rank tensors connected by a  $\chi$ -dim bond, in which only  $O(\chi)$  singular values are necessary. For such a problem, we developed parallelized codes of the randomized algorithms for the low-rank approximation, which was recently proposed[3]. Its computational cost is  $O(\chi^5)$  for the previous example in contrast to the  $O(\chi^6)$  cost of the exact decomposition. We applied the randomized algorithm to the Tensor Network Renormalization method (TNR), and succeeded in reducing its computational cost from  $O(\chi^6)$  to  $O(\chi^5)$  by avoiding a creation of 4-rank tensors.

## References

- [1] <http://www.netlib.org/scalapack/>
- [2] <https://github.com/smorita/cuscalapack/>
- [3] N. Halko, P. G. Martinsonn, J. A. Tropp, SIAM Review **53**, 217 (2011).

# Numerical research of many-body effects on phonon transport by a quantum Monte Carlo method

Takeo KATO

*Institute for Solid State Physics, University of Tokyo  
Kashiwa-no-ha, Kashiwa, Chiba 277-8581*

Heat and electric transport have several similarities as well as dissimilarities. For example, ballistic transport of electrons leads to the quantization of conductance, whereas ballistic transport of phonons to the quantization of thermal conductance. Recently, the signature of the Kondo effect, which is a typical many-body effect in electronic transport via a quantum dot, has been discussed theoretically in heat transport via a local two-state system coupled with ohmic reservoirs [1].

In order to obtain the whole feature in heat transport via a local two-state system, we have studied heat transport via a local two-state system coupled with *non-ohmic* reservoirs. We have expressed a thermal conductance by a correlation function of the two-state system based on the linear response theory. The correlation function has been evaluated along the imaginary time by a Monte Carlo calculation using a mapping to a Ising model with a long-range exchange interaction. To obtain the real-frequency correlation function, we have performed analytic continuation from data of the imaginary-frequency correlation function. To obtain reasonable results, one has to calculate the correlation function very accurately. We have employed the Wolff algorithm, and have performed typically 50,000,000 Monte Carlo steps for one parameter set.

In Figure 1, we show a calculated thermal conductance for the super-ohmic case of  $s = 2$ , where  $s$  is an exponent of the spectral function ( $s = 1$  corresponds to the ohmic case). The

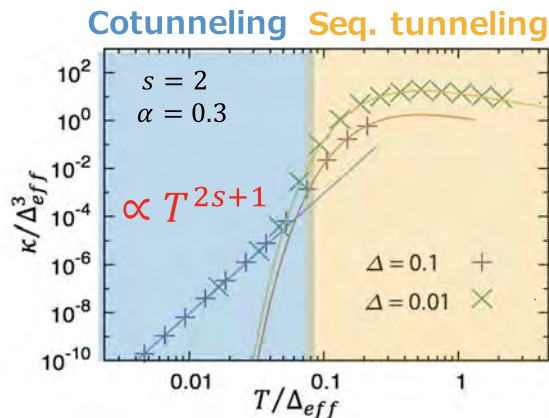


Figure 1: A calculated thermal conductance as a function of a temperature.

solid curves show analytic results for sequential tunneling and cotunneling. At high temperatures, the calculated conductance agrees with the result of the sequential tunneling, whereas at low temperatures, it agrees with the one of the cotunneling. We have shown that the thermal conductance is proportional to  $T^{2s+1}$  by using the generalized Shiba relation. We have also studied the sub-ohmic case, and found a drastic change at low temperatures due to a quantum phase transition [2].

## References

- [1] K. Saito and T. Kato, Phys. Rev. Lett. **111**, 214301 (2013).
- [2] M. Kato, T. Kato, and K. Saito, in preparation.

# Study of Heisenberg-Kitaev model by exact diagonalization package “Rokko”

Tatsuya Sakashita

*Institute for Solid State Physics, University of Tokyo  
7-1-26-R501 Port Island South, Kobe 650-0047*

To establish universal exact diagonalization package for quantum lattice models including the Heisenberg-Kitaev model, we focused on developing integrated interfaces for eigensolvers, “Rokko”[1].

In Rokko, we implemented the integrated interfaces for the following types:

- Serial solvers for dense matrices (Eigen3, LAPACK)
- MPI parallelized solvers for dense matrices (EigenExa[2], ELPA[3], Elemental[4], ScaLAPACK)
- MPI parallelized solvers for sparse matrices (Anasazi in Trilinos[5], SLEPc[6]) to cover matrix representations below:
  - CRS (Compressed Row Storage)
  - Matrix-free method (the method to give matrix-vector product routines to solvers)

Rokko has the following features:

- Integrated interfaces for eigensolvers and matrices, independent of individual eigensolver libraries
- Rokko’s interfaces are implemented by utilizing factory. It enables the user to dynamically select a solver.
- C, Fortran, and Python bindings of Rokko
- Automatically detecting libraries by using CMake in building Rokko
- The install scripts of eigensolvers for various architectures

We prepare a paper to report design policy, software structure, and usage examples of Rokko.

## References

- [1] T. Sakashita, R. Igarashi, Y. Motoyama, T. Okubo, and S. Todo. Repository of Rokko. <https://github.com/t-sakashita/rokko.git>, 2012.
- [2] T. Imamura, T. Hirota, and T. Fukaya. EigenExa web page. [http://www.aics.riken.jp/labs/lpncntrt/EigenExa\\_e.html](http://www.aics.riken.jp/labs/lpncntrt/EigenExa_e.html), 2013.
- [3] ELPA Consortium. ELPA (Eigenvalue solvers for Petaflop Applications web page). <http://elpa.rzg.mpg.de>, 2013.
- [4] J. Poulson, M. Petschow, and P. Bientinesi. Distributed-memory dense linear algebra Elemental web page. <http://libelemental.org/>, 2013.
- [5] M. A. Heroux, R. A. Bartlett, V. E. Howle, R. J. Hoekstra, J. J. Hu, T. G. Kolda, R. B. Lehoucq, K. R. Long, R. P. Pawlowski, E. T. Phipps, A. G. Salinger, H. K. Thornquist, R. S. Tuminaro, J. M. Willenbring, A. Williams, and K. S. Stanley. Trilinos Project web page. <http://trilinos.org>, 2003.
- [6] V. Hernandez, J. E. Roman, and V. Vidal. SLEPc web page. <http://www.grycap.upv.es/slepc/>, 2002.

# Search of close packing states of multicomponent hard-sphere systems by the parallelized Wang-Landau sampling

Tomoaki NOGAWA

*Faculty of Medicine, Toho University*

*5-21-16, Omori-Nishi, Ota-ku, Tokyo, 143-8540*

We have been studied a numerical method to search the densest packing of hardcore particle. We use the Wang-Landau sampling [1] for grandcanonical ensemble which is expected to be efficient because it leads to frequent global reconfiguration of particles owing to the repeat of packing and thinning. It have been found, however, that the conversion of the learning step of the Wang-Landau sampling cannot be achieved even in very small size systems if we include the densest packing state. It seems to be an essential difficulty for the optimization of the systems with continuous variable. In this work, we employ a system with discrete variables and take the continuous limit. For simplicity we treat one dimensional system: hardcore particles which occupy serial  $D$  lattice point of one dimensional chain.

When we aim to realize the flat probability distribution with respect to a single state variable, that is the number of particle  $N$ , it is actually impossible to visit the all possible value of the state variable. The number of the state which has not been visited decreases slower than any power-law decaying function of time, i.e., Monte-Carlo step. By employing two state variables,  $N$  and the number of contacts of two particles  $C$ , we obtain exponential decay of the unvisited states. However, the characteristic time of the decay grows as an exponential function of particle length  $D$  to diverge in the continuous limit.

Such a slowing down of convergence is pre-

sumably due to the bottle neck effect; most of the trial of state change toward higher density state is forbidden in the high density region of state-variable space. We next try to improve the efficiency by using the method proposed by Jaster [2] that is rejection free in the case that  $N$  is fixed and  $C$  is not observed. Even though we change  $N$  and observe  $C$ , it actually reduced the bottle-neck. Furthermore, we also modify the method of adding a particle. When we randomly choose the place of setting particle, the place is occupied by another particle with large probability. We integrate the moving and adding of particles. After one particle moves by the Jaster's method, we add a particle so that it contacts on the back of the particle moved. It also raises the acceptance probability of particle adding. The total performance is, however, not improved as we expected. Unfortunately, we have not been able to find the reason, but inverse process to decrease  $N$  becomes the next bottleneck. Now we consider the possibility of a state variable, instead the contact number, which avoid the divergence of convergence time in the continuous limit.

## References

- [1] D. P. Landau, Shan-Ho Tsai and M. Exler: *Am. J. Phys.* **72** (2004) 1294.
- [2] Jaster, *Physica A* **264** (1999) 134.

# Self-propelled motion of a Janus particle in periodically phase separating mixtures

Takeaki ARAKI and Shintaro FUKAI

*Department of Physics, Kyoto University*

*Kitashirakawa-oiwake-cho, Sakyo-ku, Kyoto 606-8502*

Recently, the developments of science and technology enabled us to product high performance particles such as Janus particles. Janus particles are a kind of colloidal particles whose surface is divided into two hemispheres having different chemical and physical properties. The asymmetry of Janus particles causes a variety of phenomena which do not appear in normal colloidal systems. For example, strange properties are observed in their aggregated structures and electrical field responses. Also, self-propelled motions of Janus particles have been attracting attention of many researchers studying biological and non-equilibrium physics. The mechanism of the self-propelled motion of Janus particles is very interesting. Even when Janus particles are in symmetrical environments, they make asymmetry in their neighboring environment to move by themselves.

In this study, we investigated the dynamics of amphiphilic Janus particles in binary liquid (oil-water) system with numerical simulations. We used fluid particle dynamics simulation method. In this scheme, we treat a colloidal particle as a fluid particle of high viscosity to deal with hydrodynamic interactions efficiently. We have focused on two cases. In the first case, we studied many-particles dynamics in phase-separating mixtures and their aggregated structures. Through the phase separation dynamics, the particles behave as surfactant and the resultant phase-separated pattern depends on the particle concentration. In

an equilibrium state, the particles' positions and directions are fixed at interfaces between the two phases (see Fig. 1). In the second case, we studied the self-propelled motion of a single particle in binary mixtures where the temperature is repeatedly changed around the phase transition temperature. The temporal change in the temperature leads to a cycle of phase separation and mixing in the water and oil mixtures. We observed some patterns of self-propelled motions which depend on the volume fraction of the binary mixture and the frequency of the temperature change. Roles of hydrodynamic interaction are asymmetric in the periods of the phase separation and mixing. This asymmetry causes a directional motion of the Janus particle. We propose an optimum condition of the self-propelled motion.[1]

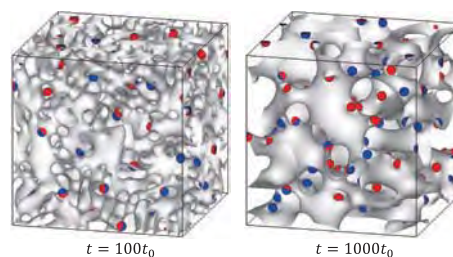


Figure 1: Snapshots of Janus particles in a phase-separated binary mixture. At  $t = 0$ , the system is quenched from a mixing state to a two-phase state.

## References

- [1] T. Araki and S. Fukai: *Soft Matter* **11** (2015), 3470.

# Spin-lattice coupling effects in Heisenberg antiferromagnets on pyrochlore lattices

Kazushi AOYAMA

*Department of Earth and Space Science, Graduate School of Science, Osaka University  
Machikaneyama-cho, Toyonaka-shi, Osaka 560-0043*

## 1 Introduction

Geometrical frustration plays an important role in magnetism. One typical example of frustrated systems is antiferromagnets on a pyrochlore lattice which is a three dimensional network of corner-sharing tetrahedra. With the nearest-neighbor (NN) antiferromagnetic interaction alone, classical Heisenberg spins on the tetrahedra do not order at any finite temperatures.

The spinel oxides  $\text{ACr}_2\text{O}_4$  ( $A=\text{Zn}, \text{Cd}, \text{Hg}, \text{Mg}$ ) are well-known pyrochlore antiferromagnets with spin-3/2. The common feature of  $\text{ACr}_2\text{O}_4$  is that the system undergoes a first order Neel transition together with a simultaneous structural transition, which suggests strong spin-lattice coupling (SLC) in this class of antiferromagnets. Similar magnetostructural orderings have been also observed in the antiferromagnets on "breathing pyrochlore" lattices consisting of alternating array of small and large tetrahedra,  $\text{LiInCr}_4\text{O}_4$  and  $\text{LiGaCr}_4\text{O}_4$ . In spite of the SLC commonly seen in the chromium oxides, ordering patterns of the Neel states vary material to material, and the origin of the long-range magnetic orders has not been well understood. In view of such a situation, we theoretically investigate SLC effects on the spin ordering in the antiferromagnetic classical Heisenberg model on the pyrochlore lattice. This year, we examined effects of *local* lattice distortions based on the so-called site-phonon model.

## 2 Model and numerical method

The effective spin Hamiltonian in the site-phonon model has been derived elsewhere and is given by  $\mathcal{H}_{\text{eff}} = \mathcal{H}_0 + \mathcal{H}_{\text{SL}}$ ,

$$\begin{aligned}\mathcal{H}_0 &= J \sum_{\langle i,j \rangle_s} \mathbf{S}_i \cdot \mathbf{S}_j, \\ \mathcal{H}_{\text{SL}} &= -Jb \sum_{\langle i,j \rangle} (\mathbf{S}_i \cdot \mathbf{S}_j)^2 \\ &\quad - \frac{Jb}{2} \sum_i \sum_{j \neq k \in N(i)} \mathbf{e}_{ij} \cdot \mathbf{e}_{ik} (\mathbf{S}_i \cdot \mathbf{S}_j)(\mathbf{S}_i \cdot \mathbf{S}_k),\end{aligned}$$

where  $J$  is the antiferromagnetic exchange interaction between NN classical Heisenberg spins  $\mathbf{S}_i$  and  $\mathbf{S}_j$ , the parameter  $b$  measures the strength of the SLC, and  $\mathbf{e}_{ij}$  is a unit vector connecting NN sites  $i$  and  $j$ . In  $\mathcal{H}_{\text{SL}}$ , the first term favors collinear spin state and the second term includes effective further neighbor interactions. In a collinear spin state, due to the effective further neighbor interactions, three neighboring spins on a straight line cannot be up-up-up nor down-down-down. This local constraint in the collinear state is called "bending rule". The question is whether or not these inter-tetrahedral interactions may drive a long-range spin order, and if so, what type.

In this work, we determined a zero-field phase diagram of the site phonon model based on Monte Carlo (MC) simulations. In our MC simulation, we perform  $10^6$  Metropolis sweeps under periodic boundary conditions at each temperature, where the first half is discarded

for thermalization. Our single spin flip at each site consists of the conventional local update and a successive over-relaxation process in which we try to rotate a spin by the angle  $\pi$  around the local mean field. Observations are done in every 5 MC steps and the statistical average is taken over 8 – 10 independent runs. Since the cubic unit cell includes 16 sites, a total number of spins  $N$  is  $N = 16L^3$  for a system size  $L$ . In this study, we take  $L = 4$  and 8. In the present model, the transitions into ordered phases are of first order and a large hysteresis can be seen. The results shown below are obtained in warming runs. We note that on cooling, the first order transition temperatures at  $b = 0.2$  and  $b = 0.35$  are lower than the corresponding warming results by 10% and 20%, respectively, but the low-temperature spin structures themselves are basically unchanged.

### 3 Result and Discussion

Our results are shown in Fig.1. We find two different types of collinear long-range magnetic orders, each accompanied by periodic local lattice distortions. For stronger SLC (larger  $b$ ), the ordered phase is made of  $\uparrow\uparrow\downarrow\downarrow$  spin chains running along all the six  $[110]$  directions showing the multiple Bragg peaks at the  $(\frac{1}{2}, \frac{1}{2}, \frac{1}{2})$  family in the spin structure factor (see Fig.1(c)). This spin state and the associated local lattice distortion are cubic-symmetric. For weaker SLC (smaller  $b$ ), the ordered state consists of the  $\uparrow\downarrow\uparrow\downarrow$  and  $\uparrow\uparrow\downarrow\downarrow$  spin chains running along the two facing tetrahedral bonds and the rest four, respectively (see Fig.1(b)). This spin configuration is tetragonal-symmetric characterized by the  $(1, 1, 0)$ -type magnetic Bragg reflections and the associated local lattice distortion is two dimensional [1].

From neutron diffraction experiments, it has been known that the ordered states in most of the spinel chromium oxides basically involve the  $(1, 1, 0)$  magnetic patterns as observed in

the weak SLC regime in the present model. The  $(\frac{1}{2}, \frac{1}{2}, \frac{1}{2})$  Bragg reflections observed in the strong SLC regime in the site phonon model have been reported as a magnetic domain in  $\text{ZnCr}_2\text{O}_4$ , although the experimentally proposed spin structure looks different from ours. These results suggest that the SLC originating from the site phonons may be relevant to the magnetic ordering in these materials.

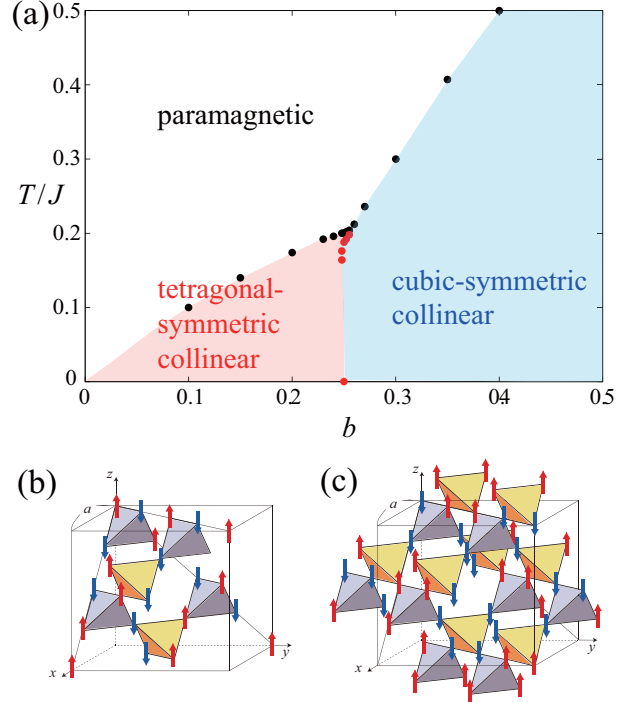


Figure 1: (a) The  $b$ - $T$  phase diagram of pyrochlore antiferromagnets with local lattice distortions. (b) and (c) Real space spin configurations for the weaker and stronger SLC, respectively. A box represents the cubic unit cell.

### References

- [1] K. Aoyama and H. Kawamura, submitted.

# Molecular Simulation Study of Micellar Shape Transition in Amphiphilic Solution

Susumu FUJIWARA

*Graduate School of Science and Technology, Kyoto Institute of Technology*

*Matsugasaki, Sakyo-ku, Kyoto 606-8585*

Amphiphilic molecules such as lipids and surfactants comprise both a hydrophilic group and a hydrophobic group. In solutions, they spontaneously self-assemble into various structures such as micelles, lamellar structures, and bicontinuous structures [1-3]. Self-assembling properties of amphiphilic molecules have been intensively studied because they are of great importance in many biological and industrial processes. Although several computer simulations have been performed on the micelle formation, few simulation studies have been conducted on the micellar shape transition. The purpose of this study is to determine the effect of hydrophilicity on the micellar shapes in amphiphilic solutions. With a view to investigating the micellar shape transition in amphiphilic solutions at the molecular level, we perform the molecular dynamics (MD) simulations of coarse-grained rigid amphiphilic molecules with explicit solvent molecules and analyze the micellar shape transitions.

The computational model used is the same as that used in the previous work [4]. An amphiphilic molecule is modeled as a rigid rod

which is composed of one hydrophilic head particle and two hydrophobic tail particles. A solvent molecule is modeled as a hydrophilic particle. These particles interact via the non-bonded potentials. The interaction between a hydrophilic particle and a hydrophobic particle is modeled by a repulsive soft core potential and all other interactions are modeled by a Lennard-Jones (LJ) potential. Let me note that the LJ interaction parameter  $\epsilon_{hs}^*$  between the hydrophilic head particles and the solvent particles represents the intensity of the hydrophilic interaction.

The equations of motion for all particles are solved numerically using the leap-frog algorithm at constant temperature with a time step of  $\Delta t^* = 0.0025$  and the temperature is controlled at every 10 time steps by *ad hoc* velocity scaling [5]. We apply periodic boundary conditions and the number density  $\rho^*$  is set to  $\rho^* = 0.75$ . Initially, we prepare an isolated micelle of 97 amphiphilic molecules with  $\epsilon_{hs}^* = 1.0$  in solutions. The number of solvent particles is 5541, which leads to the amphiphilic concentration of 0.05. The

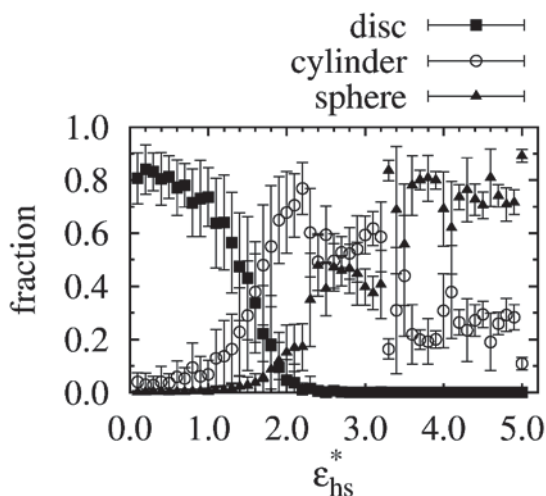


Fig. 1: The fraction of various micellar shapes versus the intensity of the hydrophilic interaction  $\varepsilon_{hs}^*$ .

intensity of the hydrophilic interaction  $\varepsilon_{hs}^*$  is then varied ( $0.1 \leq \varepsilon_{hs}^* \leq 5.0$ ) and MD simulations of  $t^* = 2.0 \times 10^4$  ( $8.0 \times 10^6$  time steps) are carried out for each simulation run.

Figure 1 shows the fraction of various micellar shapes as a function of the intensity of the hydrophilic interaction  $\varepsilon_{hs}^*$ . We use the orientational order parameters along three principal axes of inertia of the micelle as indices to characterize the micellar shapes [4]. This figure tells us that the dominant micellar shape is disc-like for  $\varepsilon_{hs}^* < 1.6$ , cylindrical for  $1.6 < \varepsilon_{hs}^* \leq 2.2$ , and spherical for  $\varepsilon_{hs}^* \geq 3.3$ . It is also ascertained that there exists a wide coexistence region in the intensity of the

hydrophilic interaction between the cylinder and the sphere for  $2.3 \leq \varepsilon_{hs}^* \leq 3.2$ . In contrast, there exists a narrow coexistence region between the cylinder and the disc, which is located around  $\varepsilon_{hs}^* \approx 1.6$ . It is worth noting that the micellar shapes are clearly distinguishable even in the coexistence region, that is, two types of micellar shapes (cylindrical and spherical, or cylindrical and disc-like) coexist dynamically.

## References

- [1] J. N. Israelachvili: *Intermolecular and Surface Forces*, 2nd ed. (Academic Press, London, 1992).
- [2] *Micelles, Membranes, Microemulsions, and Monolayers*, edited by W. M. Gelbart, A. Ben-Shaul and D. Roux (Springer-Verlag, New York, 1994), pp. 1-104.
- [3] I. W. Hamley: *Introduction to Soft Matter*, Rev. ed. (J. Wiley, Chichester, 2007).
- [4] S. Fujiwara, T. Itoh, M. Hashimoto and R. Horiuchi: *J. Chem. Phys.* **130** (2009) 144901.
- [5] M. P. Allen and D. J. Tildesley: *Computer Simulation of Liquids*, 2nd ed. (Clarendon, Oxford, 1987).

# Analysis of deterministic Monte Carlo algorithms

Hideyuki SUZUKI and Takaaki MIMURA

*Graduate School of Information Science and Technology, University of Tokyo  
Hongo, Bunkyo-ku, Tokyo 113-8656*

In the fields of statistical physics and machine learning, efficient sampling from spin systems is crucial for achieving better analysis of a model and better learning of data. Recently, deterministic Monte Carlo algorithms such as chaotic Boltzmann machines [1–3] and herded Gibbs sampling [4] have been proposed. These algorithms can generate samples from spin systems without any use of random numbers. Furthermore, such algorithms may possibly exhibit better performance than conventional (stochastic) Monte Carlo algorithms.

Although it has been shown [2] that chaotic Boltzmann machines can be applied to estimate statistics of spin systems, dynamical behavior of deterministic Monte Carlo algorithms has not been investigated well.

Therefore, in this project, we focused on dynamical aspects of deterministic Monte Carlo algorithms when applied to spin systems. More specifically, we estimated dynamical critical exponents of deterministic algorithms. We also developed cluster algorithms for chaotic Boltzmann machines and analyzed their correlation time.

**(1) Dynamical critical exponents.** The dynamical critical exponent  $z$  of a sampling algorithm characterizes its dynamical behavior at the critical temperature. In this experiment, we employed four Monte Carlo sampling algorithms: Gibbs sampling, the Sakaguchi model [5], the chaotic Boltzmann machine, and herded Gibbs sampling. We applied these algorithms to the Ising model on two-dimensional square lattices, and estimated dynamical critical exponents. First, we confirmed that the results for Gibbs sampling and the Sakaguchi model are consistent with the previous study [6]. Then, we obtained the following estimates for dy-

namical critical exponents of deterministic algorithms:  $2.01 \pm 0.05$  (chaotic Boltzmann machine) and  $1.90 \pm 0.03$  (herded Gibbs).

**(2) Cluster algorithms for chaotic Boltzmann machines.** We developed two types of cluster algorithms for chaotic Boltzmann machines. One is multi-grid chaotic Boltzmann machines, in which multi-grid algorithm [7] and chaotic Boltzmann machines are combined. The other is parallelized chaotic Boltzmann machines, in which chaotic Boltzmann machines for multiple layers run in parallel. We applied these algorithms to  $XY$  model on two-dimensional square lattices and showed that correlation time is reduced significantly.

Throughout this project, a massive amount of samples are required to obtain reliable estimates of correlation time, for which the ISSP supercomputer system played an important role.

## References

- [1] H. Suzuki, J. Imura, Y. Horio, and K. Aihara: *Sci. Rep.* **3** (2013) 1610.
- [2] H. Suzuki: *Phys. Rev. E* **88** (2013) 052144.
- [3] H. Suzuki: arXiv:1501.07039 (2015).
- [4] L. Bornn, Y. Chen, N. de Freitas, M. Eskelein, J. Fang, and M. Welling: arXiv:1301.4168 (2013).
- [5] H. Sakaguchi: *Prog. Theor. Phys.* **80** (1988) 7.
- [6] P. Marcq and H. Chaté: *Phys. Rev. E* **57** (1998) 1591.
- [7] J. Goodman and A. D. Sokal: *Phys. Rev. D* **40** (1989) 2035.

## Absorbing phase transition and viscoelasticity of Non-Brownian suspension in Low Reynolds number fluid

Masaki Sano, Kotaro Otomura

*Department of Physics, Graduate School of Science,  
The University of Tokyo, 7-3-1 Hongo, Bunkyo-ku, Tokyo, 113-033*

We have studied about the rheology of the non Brownian suspension, composed of low Reynolds number fluid and athermal particles. Such suspensions typically exhibit elasticity and change of viscosity, which is expected to have something to do with absorbing phase transition.

The numerical simulation method adopted in this thesis is Smoothed Profile Method, which is a optimized method for computational fluid dynamics of suspensions[1]. In this method, the boundaries of particles are not solid but diffusive, which enable us to reduce the meshing cost drastically. Using this method, it is investigated that the relevance of rheology and internal structure of suspensions numerically and theoretically, finding that internal structure of suspension develops into various type of structure by shear induced diffusion under a large amplitude oscillatory shear.

In addition, both linear and nonlinear rheological properties have been changed

by development of the structure.

In detail, qualitative behaviors are drastically changed by volume fraction of suspension. It is found that shear induced diffusion causes elasticity and strain thickening with relatively low volume fraction, and their typical nonlinearity evaluated by Chebyshev rheology are strain-softening and shear-thickening. In this case, internal structure tends to be organized with moderate strain amplitudes, but eventually broken down with large strain amplitude with anisotropy in shear plane. A phenomenological model to describe rheology of suspensions with relatively low volume fraction is proposed, based on these results. This model provides us how short ranged interparticle interaction contributes to the rheology. In particular, it is in agreement with numerical results in elasticity and strain thickening, which indicates their source is interparticle interaction.

Increase of volume fraction suppresses shear induced diffusion even with large

strain amplitude.

Suppression of shear induced diffusion leads to slow down of development of structure, which causes the locally organized structure. As a result, suspension becomes much stiffer compared with fully organized structure since confinement of particles motion. However, once after fully organized structure is created, such structure becomes quite robust, and the suspension exhibits strain softening in elasticity and quasi Newtonian behavior in viscosity.

These results provide us many insights about the relationship between rheology, structure, and dynamics of suspensions. It is indicated that the contribution of short ranged interparticle interaction to

them is significant, which was not fully investigated quantitatively. Especially the phenomenological proposed in this thesis is the first minimal model to describe the contribution of short ranged interparticle interaction to bulk rheology of non Brownian suspension with low Reynolds number fluid[2].

## References

- [1] J. Molina, K. Otomura, H. Shiba, M. Sano, and R. Yamamoto. *JFM*, **792** (2016) 590.
- [2] K. Otomura: Doctoral Thesis (2016)

# Phase Transition in Quantum Spin Systems Coupled to Lattice Degrees of Freedom

Chitoshi YASUDA and Shota MIYARA

*Department of Physics and Earth Sciences, Faculty of Science,  
University of the Ryukyus, Nishihara, Okinawa 903-0213, Japan*

In the spin-Peierls (SP) compound  $\text{CuGeO}_3$ , positions of magnetic atoms are distorted alternately at low temperatures and two nearest magnetic atoms form a spin singlet state. An antiferromagnetic long-range ordered phase is induced when nonmagnetic impurities are doped in the SP compound. The mechanism is understood in terms of effective spins near impurities [1]. By substituting a magnetic atom of a singlet pair for a nonmagnetic atom, an effective spin is induced around the other magnetic atom. Since the effective spins interact through a sea of spin-singlet pairs, the antiferromagnetic long-range order is induced. However, an experimental result contradictory to this interpretation has been reported: the effective spins are not induced near diluted sites. We need to take into account of the lattice degrees of freedom to investigate positions of effective spins induced.

In the present work, we investigated bond-randomness effects of a ground state of low-dimensional systems with the lattice degrees of freedom, and how position of effective spins change depending on parameters. A spin interaction coupled to adiabatic lattice displacements is written as a Hamiltonian  $H_{\text{sl}} = J \sum_i (1 + \Delta_i) \mathbf{S}_i \cdot \mathbf{S}_{i+1}$ . In order to numerically calculate a stable spin configuration and a stable lattice displacement, we use Lanczos diagonalizations and the quantum Monte Carlo simulations with the continuous-imaginary-time loop algorithm. An iterative procedure is used to determine the displacements  $\{\Delta_i\}$  by solving a set of coupled nonlinear equations. At first,

we select an initial set of the lattice displacements and calculate spin correlation functions under the fixed lattice displacement. Next, we solve a set of coupled nonlinear equations described by the spin correlation functions and obtain a next set of the lattice displacements. By performing the iterative procedure, we can obtain solutions within a certain accuracy. There is one problem with this method: poor accuracy of correlation functions leads to an incorrect solution depending on the initial set. In order to avoid this problem, we performed the procedure under various initial sets and compared the energies.

As the result, it is found that there are two types of the lattice displacement. One is the bond-alternating displacement with strong and weak bonds (type A). The lattice displacement of type A is always realized in pure systems. The other is the strong-bond displacement with strong bonds near impurities (type B). In the case of type B, the effective spins are not induced near impurities. We performed simulations in two-dimensional systems in addition to one-dimensional systems. In impure systems, the type B is realized in wide regions of parameters. On account of difficulty of the iterative procedure, however, we have not done calculations for small concentration of impurities. It is a future problem.

## References

- [1] C. Yasuda, *et al.*: Phys. Rev. B **64** (2001) 092405; J. Phys. Soc. Jpn. **75** (2006) 124704.

## Phase transition on scale-free networks 2

Masanori SHIRO

*HTRI, National Institute of Advanced Industrial Science and Technology  
Umezono1-1-1 Central 2, Tsukuba, Ibaraki 305-8568*

A purposes of our project is to clarify the phase transition temperature of the ising model on some types of scale-free network by using Monte Carlo method.

Pure ising model is based on grid network, which express a strong proximal interaction and well studied. But changes of transitions on a scall-free network of it, are not well known. We checked it on this project.

In the solid stat physics, these conditions express time evolutionary systems as growth of a para-crystal. Or some types of heavy fermions included long-term interaction may be related to the system.

Example of results is as follows. Fig. 1 shows the specific heat on normal ising model. Fig.2 shows the specific heat on B-A model.

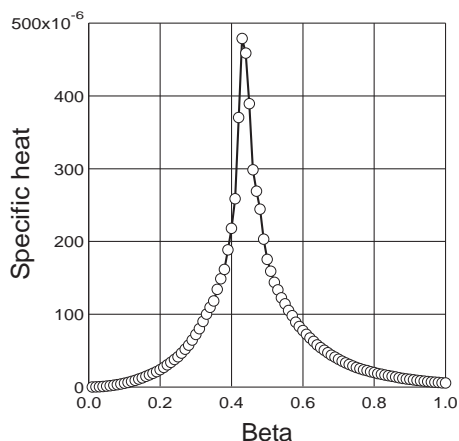


Fig.1 Pure ising model transition

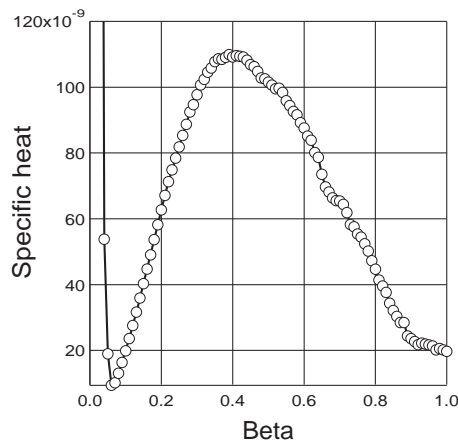


Fig.2 B-A model transition

In Figs, connection rate is assumed 0.2 and 1000 nodes, network topology is B-A model. Program is written in C++ and used Boost libraries. Results of larger scaled network are under analysis now.

The most important of facts is that proximal interactions are important for phase transition because the long range interactions homogenize the system. Hence in the B-A model, transition curve is doodling and we cannot find peak.

# Nonequilibrium phase transition in the large scale dense hard sphere molecular dynamics simulation

Masaharu ISOBE

*Nagoya Institute of Technology*

*Gokiso-cho, Showa-ku, Nagoya, 466-8555*

The hard disk/sphere systems are one of the crucial models to investigate fundamental problems in the field of both equilibrium and non-equilibrium statistical physics. In this project, we investigated non-equilibrium phase transition in the hard disk/sphere model system with modern algorithms, especially for Event-Chain Monte Carlo (ECMC) [1] and Event-Driven Molecular Dynamics (EDMD) [2], where we propose the “Hybrid Scheme”, namely, ECMC for equilibration and EDMD for calculation of dynamical properties [3, 4].

(i) *Hard-sphere melting and crystallization with Event-Chain Monte Carlo*: Crystallization and melting have been investigated as central subjects in statistical physics. The hard-sphere system is simple to describe, however, equilibration in the whole particle systems is a quite slow due to the large activation free energy for crystallization. Timescales are also quite long especially in the fluid-solid coexistence regime due to the surface tension between coexisting phases. In this study, we simulate crystallization and melting with three algorithms, local Monte Carlo (LMC), ECMC [1], and with EDMD [2], in systems with up to one million three-dimensional hard spheres. We confirmed that our implementations of the three algorithms rigorously coincide in their equilibrium properties. We then study nucleation from the fcc crystal into the homogeneous liquid phase and from the liquid into the homogeneous crystal. We concluded

that both ECMC and EDMD approached equilibrium orders of magnitude faster than LMC. ECMC is also notably faster than EDMD, especially for the equilibration into a crystal from an initially disordered condition at high density [5].

(ii) *Dynamic Facilitation in Binary Hard Disk Systems*: In a couple of decades, it has been highly debated to describe the theoretical approaches regarding relaxational dynamics of glass formers such as supercooled liquids. Dynamic facilitation (DF) theory [6, 7, 8] provides one of perspective which is constructed on the idealized kinetically constrained models (KCMs). The central predictions of the DF approach are as follows: (i) In the supercooled regime, relaxation originates from localized excitation distributed randomly with an equilibrium concentration which decreases exponentially with inverse temperature. The kinetics of localized excitation is facilitated such that the relaxation of excitations occurs in the vicinity of excitations, which cause heterogeneous dynamics. (ii) Relaxation is “hierarchical” cause the increasing relaxation time as a “parabolic” law with no finite temperature singularity. The super-Arrhenius behavior is distinct from the empirical Vögel-Fulcher-Tammann (VFT) law. (iii) The origin of glassy slowing down is a non-equilibrium “space-time” transition, i.e. a transition in the space of trajectories between a dynamically active equilibrium liquid phase and a dynamically inactive non-equilibrium glass phase. In

this study, we investigate numerically the applicability of DF theory for glass-forming binary hard disk systems where supercompression is controlled by “pressure”. The modern, efficient algorithms [1, 2, 3] for hard disks generate successfully the regions of the supercompressed equilibrium states with the model of the additive non-equimolar binary mixture, where micro-crystallization and size segregation do not emerge at the highly packing fraction. Above the onset pressure, the kinetically constraint facilitated and hierarchical collective motion, a parabolic form of structural relaxation, the exponential decay of excitation concentration and logarithmic growth of excitation-free energy emerge as in the soft sphere system below onset temperature. These observations are fairly consistent with the predictions of DF generalized to systems controlled by pressure instead of inverse temperature [9].

[9] M. Isobe, A. S. Keys, J. P. Garrahan, and D. Chandler: arXiv:1604.02621.

## References

- [1] E. P. Bernard, W. Krauth, and D. B. Wilson: Phys. Rev. E **80** (2009) 056704.
- [2] M. Isobe: Int. J. Mod. Phys. C **10** (1999) 1281.
- [3] M. Isobe: Mol. Sim. (2016) in press.
- [4] M. Isobe: Proceedings Book of Berni Alder’s 90th Birthday Symposium. (2016) in press.
- [5] M. Isobe and W. Krauth: J. Chem. Phys. **143** (2015) 084509.
- [6] D. Chandler and J. P. Garrahan, Annu. Rev. Phys. Chem. **61** (2010) 191
- [7] L. O. Hedges, R. L. Jack, J. P. Garrahan and D. Chandler, Science **323** (2009) 1309.
- [8] A. S. Keys, L. O. Hedges, J. P. Garrahan, S. C. Glotzer, and D. Chandler, Phys. Rev. X, **1** (2011) 021013.

# Numerical Study of One Dimensional Frustrated Quantum Spin Systems

Kazuo HIDA and Hiroshi SHINAOKA

*Division of Material Science, Graduate School of Science and Engineering  
Saitama, Saitama 338-8570*

## 1 Topological Phases in Zigzag Heisenberg Ladder with Ferromagnetic Legs

Ground-state phases of the spin-1/2 zigzag ladder with unequal ferromagnetic legs

$$\mathcal{H} = \sum_{l=1}^L [J_F \mathbf{S}_{2l-1} \mathbf{S}_{2l} + J_A \mathbf{S}_{2l} \mathbf{S}_{2l+1} + J_L(1+\delta) \mathbf{S}_{2l-1} \mathbf{S}_{2l+1} + J_L(1-\delta) \mathbf{S}_{2l} \mathbf{S}_{2l+2}] \quad (1)$$

are investigated based on the iDMRG calculation of the entanglement spectrum (ES). We consider the case of  $J_L < 0$ ,  $J_F < 0$ ,  $J_A > 0$ ,  $0 \leq \delta \leq 1$ . This model tends to the spin-1 chain in the limit of  $J_F \rightarrow -\infty$ .

For  $\delta = 0$ , a series of topologically distinct spin-gap phases have been found from the analysis of the edge spin[1, 2]. For  $\delta = 1$ , this model reduces to the  $\Delta$ -chain with ferromagnetic main chain. Although similar series of spin-gap phases are known in this model[3], their nature remained unclarified so far. However, the phase diagram obtained in [3] redrawn with the present parametrization turned out to be almost identical with that for  $\delta = 0$ . We carried out the iDMRG calculation of the ES with divisions A and B depicted in Fig. 1 for  $\delta = 0, 0.5$  and 1 with  $J_L/J_A = -2.5$ . It is found that the behaviors of ES are insensitive to  $\delta$  as shown in Fig. 2.

The results are consistent with the exact solution on the ferromagnetic-nonmagnetic phase boundary[4] and the nonlinear sigma

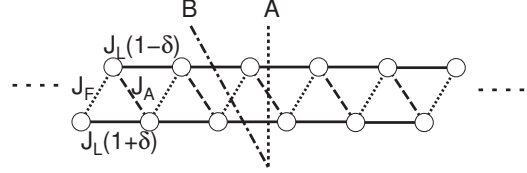


Figure 1: Lattice structure of the present system. Two types of divisions for the calculation of ES are also shown.

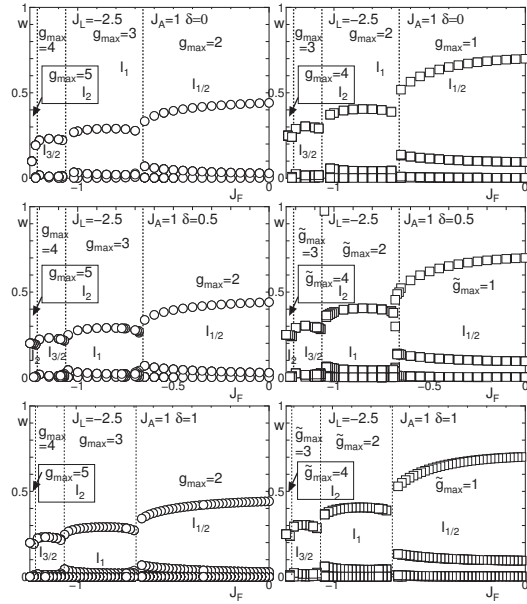


Figure 2:  $J_F$ -dependence of ES. The degeneracy of largest eigenvalues are  $g_{\max}$  for division A and  $\tilde{g}_{\max}$  for division B.

model analysis[5] for large  $J_L$ .

This work is supported by KAKENHI (C) (No. 25400389) from JSPS.

## 2 Finite-temperature phase diagram of the single-band Hubbard model on the pyrochlore lattice

Itinerant electronic systems on the pyrochlore lattice are one of the most frustrated three-dimensional systems. Such models may be relevant for understanding the electronic and magnetic properties of pyrochlore oxides and spinel oxides where transition metal atoms comprise the pyrochlore lattice.

In the recent years, extensive numerical studies have been carried for two-dimensional frustrated itinerant systems such as the Hubbard model on the triangular lattice. In particular, the dynamical mean-field theory (DMFT) and its cluster extensions have been used to investigate finite-temperature properties of the models. However, so far, no DMFT studies have been reported for the pyrochlore Hubbard model, which may be due to a severe sign problem coming from the geometrical frustration in solving an impurity problem by continuous-time quantum Monte Carlo (QMC) methods.

Recently, we systematically investigated the dependence of the sign problem on the single-particle basis [6]. We explored both the hybridization-expansion and the interaction-expansion variants of continuous-time QMC for three-site and four-site impurity models with baths that are diagonal in the orbital degrees of freedom. We found that the sign problem in these models can be substantially reduced by using a non-trivial single-particle basis.

In this study, we applied this non-trivial single-particle basis “dimer basis” to four-site cluster DMFT calculations to map out its finite-temperature phase diagram. We consider the single-band Hubbard model only with nearest-neighbor hopping ( $t = 1$ ) at half filling. We employed the interaction-expansion QMC algorithm. We plot the quasi-particle weight

computed at  $\beta = 20$  in Fig. 3. We used a metallic solution or an insulating solution as the initial state of the DMFT self-consistent procedure. We assumed paramagnetic solutions. There is hysteric behavior around  $U/t \simeq 9$ , indicating the existence of a first-order transition. The critical value  $U/t \simeq 9$  is almost twice larger than the estimate by the unrestricted Hartree-Fock approximation [7].

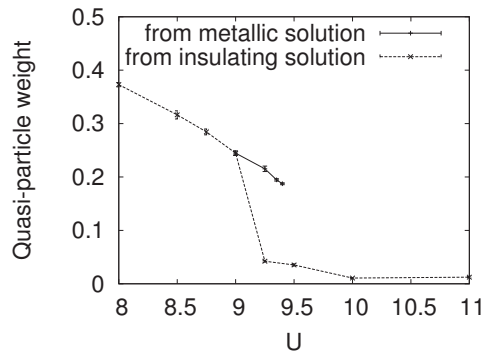


Figure 3:  $U$  dependence of the quasi-particle weight. We used a metallic solution or an insulating solution as the initial state of the DMFT self-consistent procedure. The data of the self-consistent solutions are shown by the solid line (from metallic initial state) and the broken line (from insulating initial state), respectively.

This work was done in collaboration with Yusuke Nomura.

## References

- [1] K. Hida, K. Takano and H. Suzuki : J. Phys. Soc. Jpn. **82** 064703 (2013).
- [2] K. Hida : J. Phys. Soc. Jpn. **85** 024705 (2015).
- [3] K. Hida : J. Phys. Soc. Jpn. **77** 044707 (2008), [Errata **79** 028001 (2010)].
- [4] H. Suzuki and K. Takano: J. Phys. Soc. Jpn. **77** 113701(2008).
- [5] S. C. Furuya : private communication.
- [6] H. Shinaoka, Y. Nomura, S. Biermann, M. Troyer, P. Werner, Phys. Rev. B **92**, 195125 (2015).
- [7] N. Swain, R. Tiwari and P. Majumdar, arXiv:1505.03502v1.